Report No. FAA-RD-77-87

RD
77
87

COPY 1

NAFEC LIBRARY
OCT 1977

# Project Report

ATC-77

A. R. Paradis

# L-Band Air-to-Air Multipath Measurements

6 September 1977

Prepared for the Federal Aviation Administration by

Lincoln Laboratory

MASSACHUSETTS INSTITUTE OF TECHNOLOGY

LEXINGTON, MASSACHUSETTS

Document is available to the public through
the National Technical Information Service,
Springfield, Virginia 22151.

This document is disseminated under the sponsorship of the Department of Transportation in the interest of information exchange. The United States Government assumes no liability for its contents or use thereof.

Technical Report Documentation Page

| 1. Report No. | 2. Government Accession No. | 3. Recipient's Catalog No. |
|---|---|---|
| FAA-RD-77-87 | | |

| 4. Title and Subtitle | 5. Report Date |
|---|---|
| L-Band Air-to-Air Multipath Measurements | 6 September 1977 |
| | 6. Performing Organization Code |
| 7. Author(s) | 8. Performing Organization Report No. |
| A.R. Paradis | ATC-77 |
| 9. Performing Organization Name and Address | 10. Work Unit No. |
| Massachusetts Institute of Technology<br>Lincoln Laboratory<br>P.O. Box 73<br>Lexington, MA 02173 | Proj. No. 034-241-012 |
| | 11. Contract or Grant No. DOT-FA77-WAI-727 |
| 12. Sponsoring Agency Name and Address | 13. Type of Report and Period Covered |
| Department of Transportation<br>Federal Aviation Administration<br>Systems Research and Development Service<br>Washington, DC 20591 | Project Report |
| | 14. Sponsoring Agency Code |

15. Supplementary Notes

The work reported in this document was performed at Lincoln Laboratory, a center for research operated by Massachusetts Institute of Technology under Air Force Contract F19628-76-C-0002.

16. Abstract


A series of air-to-air earth-scattered L-Band multipath measurements are described and experimental results presented. During these measurements RF pulses were transmitted between two instrumented general aviation aircraft flying coaltitude, diverging paths over a variety of terrain and water surfaces. Multipath data was collected over grazing angles ranging from ~5° to ~75°. The objectives of these measurements were the:

1. Characterization of the multipath environment in which beacon based airborne collision avoidance (BCAS) equipment would operate.
2. Investigation of the merits and limitations of various degrees of antenna diversity in the rejection of multipath.


| 17. Key Words | 18. Distribution Statement |
|---|---|
| antenna diversity<br>grazing angle<br>multipath<br>Rayleigh distribution<br>scattering | Document is available to the public through the National Technical Information Service, Springfield, Virginia 22151. |

| 19. Security Classif. (of this report) | 20. Security Classif. (of this page) | 21. No. of Pages |
|---|---|---|
| Unclassified | Unclassified | 100 |

Form DOT F 1700.7 (8-72) Reproduction of completed page authorized

ILLUSTRATIONS


| Figure | | Page |
|---|---|---|
| 2.1 | Multipath-to-Signal Ratio Variation With Terrain. | 5 |
| 4.1 | Effect of Antenna Diversity on Ocean Scattered Multipath (Log-Video Photographs). | 15 |
| 4.2 | Effect of Antenna Diversity on Land Scattered Multipath (Log-Video Photographs). | 16 |
| 4.3 | Comparison of Land and Water Scattered Multipath (Log-Video Photographs With Long Time Scale). | 17 |
| 4.4 | Airborne Measurement Facility (AMF). | 20 |
| 4.5 | Data Acquisition Crosslink Signals. | 22 |
| 4.6 | Multipath Experiment Pulse Data Dump. | 25 |
| 5.1 | Ocean Scattered Multipath (Log-Video Photographs). | 29 |
| 5.2 | Ocean (Sea State 1) Multipath Time-Raster. | 31 |
| 5.3 | Multipath Delay. | 33 |
| 5.4 | Ocean (Sea State 1) Multipath Instantaneous Signal Strength. | 35 |
| 5.5 | Normalized Autocovariance (Ocean Sea State 1). | 36 |
| 5.6 | Signal-to-Multipath Ratio Cumulative Distribution (Ocean Sea State 1). | 37 |
| 5.7(a-b) | Ocean (Sea State 1) Multipath Average Signal Strength. | 39 |
| 5.7(c) | Ocean (Sea State 1) Multipath Average Signal Strength (Top-To-Bottom Link). | 40 |
| 5.8 | Signal-to-Multipath Ratio, Antenna Gain, and Total Scattering Loss (Ocean Sea State 1). | 42 |
| 5.9 | Signal-to-Multipath Ratio Distribution Variations (Ocean Sea State 1). | 44 |
| 5.10 | Altitude Variations in Signal-to-Multipath Ratio (Ocean Sea State 1). | |

ILLUSTRATIONS (CON'T)


| Figure | | Page |
|---|---|---|
| 5.11 | Geometrical Dependence of Signal-to-Multipath Ratio (Ocean Sea State 1). | 49 |
| 5.12 | Signal-to-Multipath Ratio Cumulative Distribution (Ocean Sea State 2). | 52 |
| 5.13 | Ocean (Sea State 2) Multipath Average Signal Strength. | 54 |
| 5.14 | Signal-to-Multipath Ratio, Antenna Gain, and Total Scattering Loss (Ocean Sea State 2). | 55 |
| 5.15 | Signal-to-Multipath Ratio Distribution Variations (Ocean Sea State 2). | 57 |
| 5.16 | Altitude Variations in Signal-to-Multipath Ratio (Ocean Sea State 2). | 58 |
| 5.17 | Geometrical Dependence of Signal-to-Multipath Ratio (Ocean Sea State 2). | 60 |
| 5.18 | Frozen Lake (High Grazing Angle) Multipath Instantaneous Signal Strength. | 61 |
| 5.19 | Normalized Autocovariance (Frozen Lake). | 62 |
| 5.20 | Frozen Lake (Low Grazing Angle) Multipath Instantaneous Signal Strength. | 63 |
| 5.21 | Frozen Lake (Low Altitude) Multipath Average Signal Strength. | 64 |
| 5.22 | Frozen Lake (High Altitude) Multipath Average Signal Strength. | 67 |
| 5.23 | Calm Lake Multipath Instantaneous Signal Strength. | 69 |
| 5.24 | Desert Multipath Time-Raster. | 70 |
| 5.25 | Desert Multipath Average Signal Strength. | 71 |

ILLUSTRATIONS (CON'T)


| Figure | | Page |
|---|---|---|
| 5.26 | Signal-to-Multipath Ratio, Antenna Gain, and Total Scattering Loss (Desert). | 73 |
| 5.27 | Signal-to-Multipath Ratio Distribution Variations (Desert, High Grazing Angles). | 75 |
| 5.28 | Signal-to-Multipath Ratio Distribution Variations (Desert, Low Grazing Angles). | 76 |
| 5.29 | Altitude Variations in Signal-to-Multipath Ratio (Desert). | 77 |
| 5.30 | Flat Plain Multipath Average Signal Strength. | 78 |
| 5.31 | Normalized Autocovariance (Smooth Land). | 80 |
| 5.32 | Geometrical Dependence of Signal-to-Multipath Ratio (Desert). | 81 |
| 5.33 | Geometrical Dependence of Signal-to-Multipath Ratio (Flat Plain). | 82 |
| 5.34 | Rough Land Multipath Time-Raster. | 83 |
| 5.35 | Signal-to-Multipath Ratio Distribution Variation (Rough Land). | 85 |
| 5.36 | Rough Land Multipath Average Signal Strength. | 86 |
| 5.37 | Snow Covered Rough Land Multipath Average Signal Strength. | 87 |
| 5.38 | Forested Mountain Multipath Average Signal Strength. | 88 |
| 5.39 | Multipath Sensitivity to Banking. | 90 |

TABLES


| Table No. | | Page |
|---|---|---|
| 2.1 | Summary of Multipath Data | 4 |
| 4.1 | Scattering Surfaces Investigated | 12 |

# PART 1: OVERVIEW AND SUMMARY

# 1. OVERVIEW

An airborne collision avoidance system employing Air Traffic Control (ATC) beacon transponders is under development by the Federal Aviation Administration. This system (called BCAS for Beacon Collision Avoidance System) will be capable of operating with the present Air Traffic Control Radar Beacon System (ATCRBS) transponders as well as those of the future Discrete Address Beacon System (DABS).

The occurrence of terrain induced multipath on the air-to-air link is of considerable interest in the design of the BCAS system. Previously published multipath data was judged inadequate to support the BCAS design due to incorrect geometry or incomplete documentation. For this reason, Lincoln Laboratory performed a study of air-to-air multipath based on actual field measurements using a pair of instrumented general aviation aircraft. Aircraft geometries, RF frequency, scattering surfaces, and antenna configuration were all selected to have maximum relevance to the BCAS design effort.

A summary of the key findings of this study is presented in Chapters 2 and 3. Details of the experimental data collection and results are provided in Chapters 4 and 5.

## 2. SUMMARY OF MULTIPATH DATA

Detectable multipath echos were observed from all reflection surfaces over which measurements were conducted. Observations were made as to the multipath delay, waveform, short-term variability, power levels, dependence on geometry, dependence on reflecting surface, and the performances of various antenna configurations in rejecting multipath. Data collected over similar surfaces on different days, separated by as much as a year, exhibited striking consistency with regard to each multipath parameter.

The data presented refers to the direct and multipath receptions including the effects of the aircraft antenna patterns. The primary results are summarized in Table 2-1, Fig. 2-1, and in the following paragraphs.

Delay. When compared with the "signal" (namely the received pulse which traveled the direct path from transmitter to receiver), the echo was in every case delayed by an amount which agrees with the simple geometrical formula

$$\text{Delay} = R(\text{secant } G - 1)/c$$

where R is the air-to-air range, c is the speed of light, and grazing angle G is

$$G = \text{Tan}^{-1}((A_1 + A_2)/R)$$

in terms of the altitudes $A_1$ and $A_2$ of the two aircraft above the level of the reflecting surface.

Multipath Waveform. The waveform of the multipath echo is determined primarily by the roughness of the scattering surface. When observed at the output of a log-video amplifier, the waveform may be described as consisting

TABLE 2.1

SUMMARY OF MULTIPATH DATA

| Multipath Property | Reflecting Surface | | | |
|---|---|---|---|---|
| | Ocean | Frozen Lake | Smooth Land (Desert, Flat Plain) | Rough Land (sub. areas, Mtns.) |
| Multipath Waveform Resulting from 0.5 μs RF Pulse | Pulselike | | | Low Noise Level of Long Duration (~35 μs) |
| Delay Time | Closely Follows Theoretical Curve: R(secant(G)-1)/c** | | | |
| Short Term Variability* (10% to 90%) | ~13dB | ~2dB | ~13dB | |
| Correlation* Time | <50 msec | ~1 sec | <50 msec | |
| Multipath to Signal Ratio (Bottom-to-Bottom Antennas, Median Value, Grazing Angle = 30°) | As high as ~0dB less severe for rough ocean | ~-5dB | ~-15dB | ~-20dB |
| Signal to Multipath Ratio Improvement Due to single top Antenna Link*** | Significant (~15 dB for grazing angles >20°) less improvement at lower grazing angles | | | |

*Defined in more detail in the text.
**R = range
G = grazing angle
c = speed of light
*** The improvement is greater for the top-to-top link.

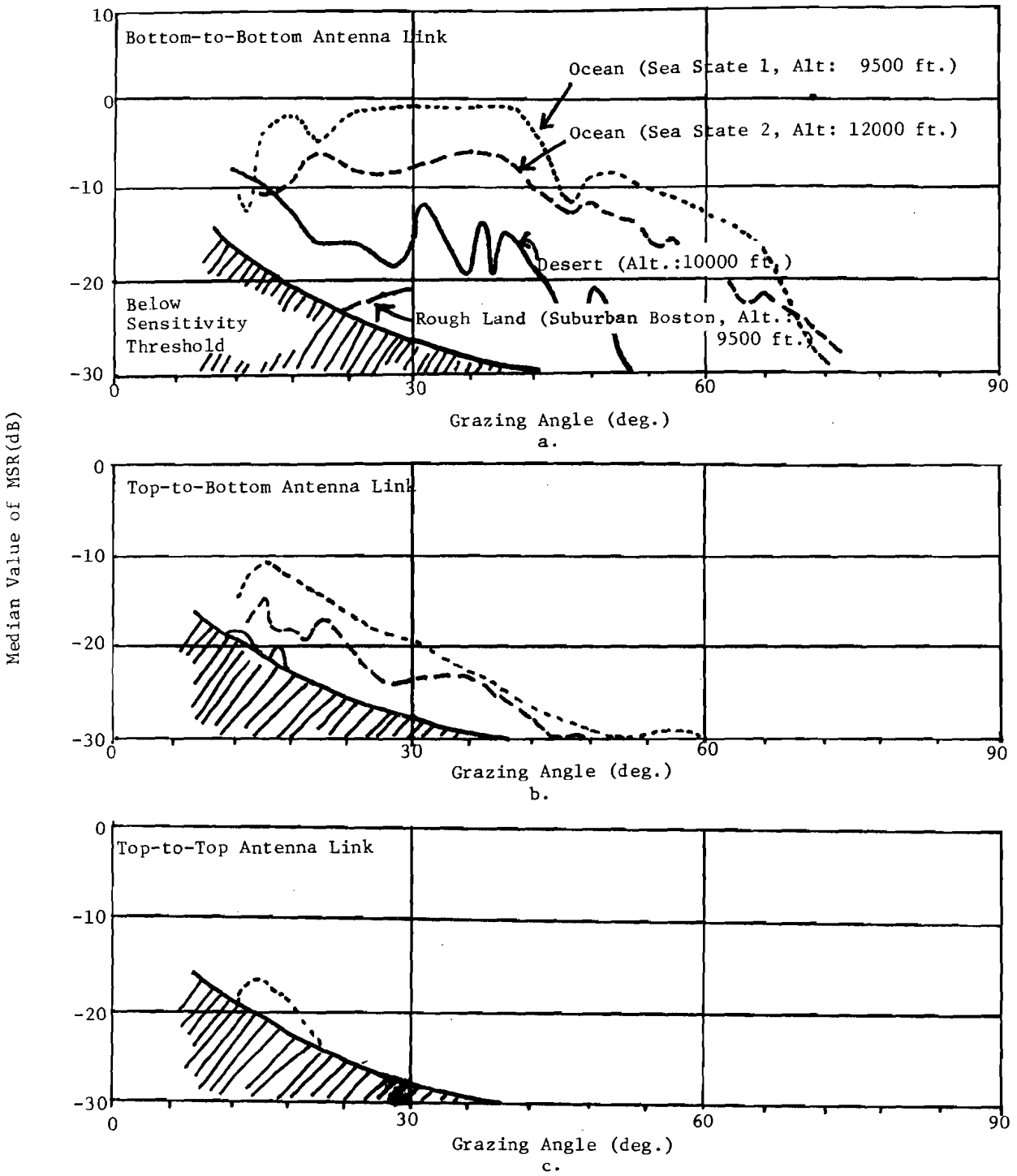


Fig. 2.1. Multipath-to-Signal Ratio Variation With Terrain.

of two components: a delayed slightly distorted pulselike replica of the direct pulse signal followed by a low-level noiselike waveform lasting tens of microseconds. In cases of flights over relatively smooth surfaces, such as ocean or desert, the pulselike component of multipath dominates the other component by many dB. For these surfaces the peak received multipath power is the strongest relative to the direct signal level. In other cases, i.e,. over more ordinary land regions which are relatively rough, the pulselike component is not present and the multipath waveform consists totally of a noiselike level of long duration which is slightly stronger than the noise level component associated with smooth surfaces, but still extremely small with respect to the direct signal.

Short-Term Variability. The multipath measurement was repeated at the rate of 20 per second. Multipath echos in successive measurements were compared to assess the short-term variability over 10-second periods (which is a short enough period that aircraft altitudes, orientations, and the air-to-air range are reasonably constant). In almost all cases the multipath power varied greatly during the 10 second period, with the span between 10 percentile and 90 percentile being 10 to 15 dB. The power distribution was analyzed and found to be in reasonable agreement with a "Rayleigh Model" (in most cases). The power distribution of the Rayleigh Model is that which results when amplitude A has a Rayleigh distribution and when received multipath power in dB is 20 log A. In this model, the span between 10 percentile and 90 percentile is 13.4 dB.

Statistical autocovariance calculations were carried out, and these showed that, in all cases agreeing with the Rayleigh Model, successive multipath samples are essentially uncorrelated. That is, the correlation time of the multipath variability is less than 50 ms (the measurement repetition period).

A few exceptions to this behavior were noted when flying over certain very smooth surfaces, such as small inland lakes on a windfree day or when frozen, or over larger bodies of water when frozen. In these cases the 10 to 90 percentile power variabilities were much lower -- on the order of 2 dB. Autocovariance calculations showed the correlation time to be on the order of 1 sec in these cases.

Power Level. The power levels of measured multipath echos are summarized in Fig. 2-1. The figure shows the median value of relative multipath power, given as the multipath-to-signal ratio (MSR), plotted as a function of grazing angle G. Evidently, under worst case conditions the median MSR can be as high as about 0 dB. In these cases, about 50% of multipath echos exceed the direct signal power, and about 10% of multipath echos exceed a level 5 dB above the signal.

Dependence on Grazing Angle. Figure 2-1 shows directly the dependence on grazing angle. Certain trends are evident. For example, as grazing angle increases above $30^{\circ}$, multipath power levels drop relative to the signal. As grazing angle decreases below $30^{\circ}$; and for a bottom-antenna-to-bottom-antenna link, ocean reflections and desert reflections exhibit opposite trends -- the former decreasing while the latter is increasing. Very low values of G, below about $10^{\circ}$, are relatively unimportant in the context of BCAS.

Dependence on Altitude. The multipath data have been analyzed to assess the dependence on altitude. Results show that MSR does have an altitude dependence, and that this consists primarily of the dependence on grazing angle discussed above, with very little additional dependence on altitude. Thus, for example, if aircraft A and B are both at one altitude and aircraft C and D are both at twice that altitude, then provided the range between C and D is twice the range between A and B, the two pairs of aircraft will experience approximately the same multipath-to-signal ratio. Because of this property, the format of Fig. 2-1 serves as a convenient summary of mulitpath effects over a range of altitudes.

Dependence on Aircraft Antennas. Aircraft antenna patterns play a major role in determining the relative level of received multipath since the effect of antenna pattern variations must be considered at both ends of the link. The data indicates that a bottom-to-bottom antenna link has gain variations that amplify the ground scattered multipath signal strength while reducing the direct signal strength, an expected result considering measured aircraft antenna patterns. The use of a single top mounted antenna in the link results in significant (15 dB) reductions in received multipath at high grazing angles ($10^{\circ} < G < 75^{\circ}$) with less multipath rejection observed at smaller grazing angles. The top-to-top antenna link reduces multipath levels still further for grazing angles above about $10^{\circ}$. For very low grazing angles, where multipath reduction would be especially beneficial, the additional MSR reduction due to the second top antenna is not very significant.

Dependence On Reflecting Surface. Figure 2-1 and Table 2-1 serve as a summary of the dependence on reflecting surface. The echos from land surfaces are, with few exceptions, found to be appreciably weaker than echos

from water. Multipath over the ocean is seen to depend on sea state, with stronger multipath occurring on calm days. Among the surfaces summarized in Fig. 2-1, the ocean in Sea State 1 generally stands out as being the worst-case producing strong echos with approximately 0 dB median MSR over a broad range of grazing angles.

## 3. CONCLUSIONS

1. Multipath scattered from smooth surfaces, especially water surfaces is a significant form of interference on the air-to-air channel.

2. Employment of top-mounted antennas appears to be warranted in preventing strong multipath from interfering with BCAS operation.

   a. A single top-mounted antenna in the link appears to provide significant multipath rejection for grazing angles above $\sim 10^{\circ}$ which includes almost all geometries of interest in BCAS.

   b. At lower grazing angles, the use of a top mounted antenna on each aircraft provides little additional multipath rejection.

# PART 2: EXPERIMENT DESCRIPTION AND RESULTS

# 4. DESCRIPTION OF THE EXPERIMENT

## 4.1 Flight Operations

In order to gather multipath data over a wide spectrum of scattering surface types, flights were conducted over several oceanic and CONUS regions. Table 4.1 lists the surface conditions and their locations which were investigated in the measurement program.

TABLE 4.1

SCATTERING SURFACES INVESTIGATED

| SURFACE TYPE | LOCATION |
|---|---|
| Ocean (sea state 1) | Massachusetts Bay |
| Ocean (sea state 2) | Massachusetts Bay |
| Frozen snow covered lake | Lake Champlain, Vermont; and Lake Cochituate, Massachusetts |
| Lake (sea state 0) | Lake Cochituate, Massachusetts |
| Desert | Mojave Desert, California |
| Flat Plain | Central Kansas |
| Rough Land surface | Massachusetts Suburbs |
| Snow covered rough surface | Massachusetts Suburbs |
| Forest covered mountains | White Mountains, New Hampshire |

These surfaces are typical of many that would be encountered on an air-to-air channel over which BCAS equipment would operate. Data gathered from these areas show marked differences in both received multipath signal strength and time structure.

Several data runs were flown at various altitudes over each surface. Most data runs consisted of two aircraft flying a V shaped divergent flight path. Both aircraft flew at the same altitude during each data run. As each pass was being flown, the headings of the aircraft were varied randomly. These random changes in heading tended to wash out the variations in multipath due to the fine structure of the antenna patterns associated with the antennas used. Several times during the flights large heading changes (> $10^{o}$) were made to determine the effect of aspect angle on the received multipath. During one flight, data was recorded as the two aircraft converged on each other.

## 4.2 Data Acquisition

### 4.2.1 Preliminary Flights

During the determination of a meaningful sampling scheme, several flights were conducted to gather data on the time structure of multipath signals scattered in response to pulse transmissions. During these flights two equal altitude aircraft were flown parallel to one another at a range of two nautical miles and at an altitude of 7500 feet. Pulses at a 63 dBm level and 1030 MHz frequency were transmitted from a bottom mounted L-Band blade antenna on one of the

aircraft. Direct and multipath signals were received via both top and bottom mounted antennas on the receiving aircraft. Photographs were taken of the analog signals at the outputs of log-video detectors.

The data from these flights indicated that the multipath signals in response to a pulse transmission can exist in one of two distinct forms depending on the roughness of the surface. Fig. 4.1 and Fig. 4.2 show log-video photographs taken during the flights. In all the photographs the pulse on the left is the direct pulse transmitted from a bottom mounted antenna. The captions indicate the location of the receiving antenna. The signal to the right of the direct pulse in each photo is the multipath scattered from the surface. Fig. 4.1 shows that the multipath from a smooth (Sea State 1) ocean surface had the appearance of a distinct and strong pulse with a width somewhat greater than that of the direct pulse. Later data verified that this was typical of signals scattered from smooth surfaces in general. Fig. 4.2 shows similar photographs taken over a rough land surface. Here the multipath signals were not pulselike but rather appeared as low level noise of long duration. Again, such signals proved to be typical of multipath scattered from a rough surface such as forest land or a residential area.

Fig. 4.3 shows log-video photographs taken during later flights illustrating the energy distribution of the multipath signal over long ($\sim$50 μsec) time intervals. During these flights an interrogation was sent from one aircraft to a second aircraft which responded with a four pulse reply.

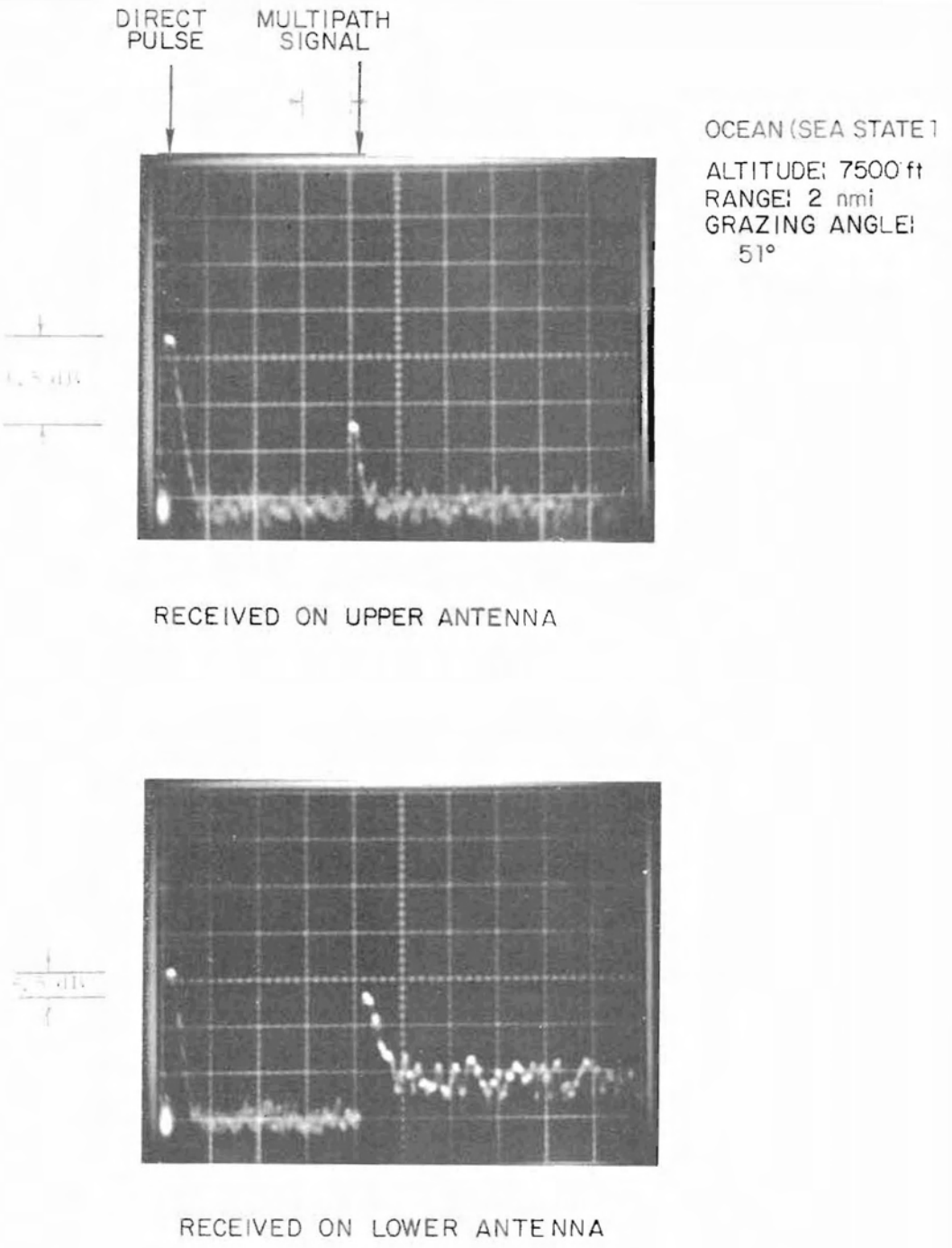


Fig. 4.1. Effect of Antenna Diversity on Ocean Scattered Multipath (Log-Video Photographs).

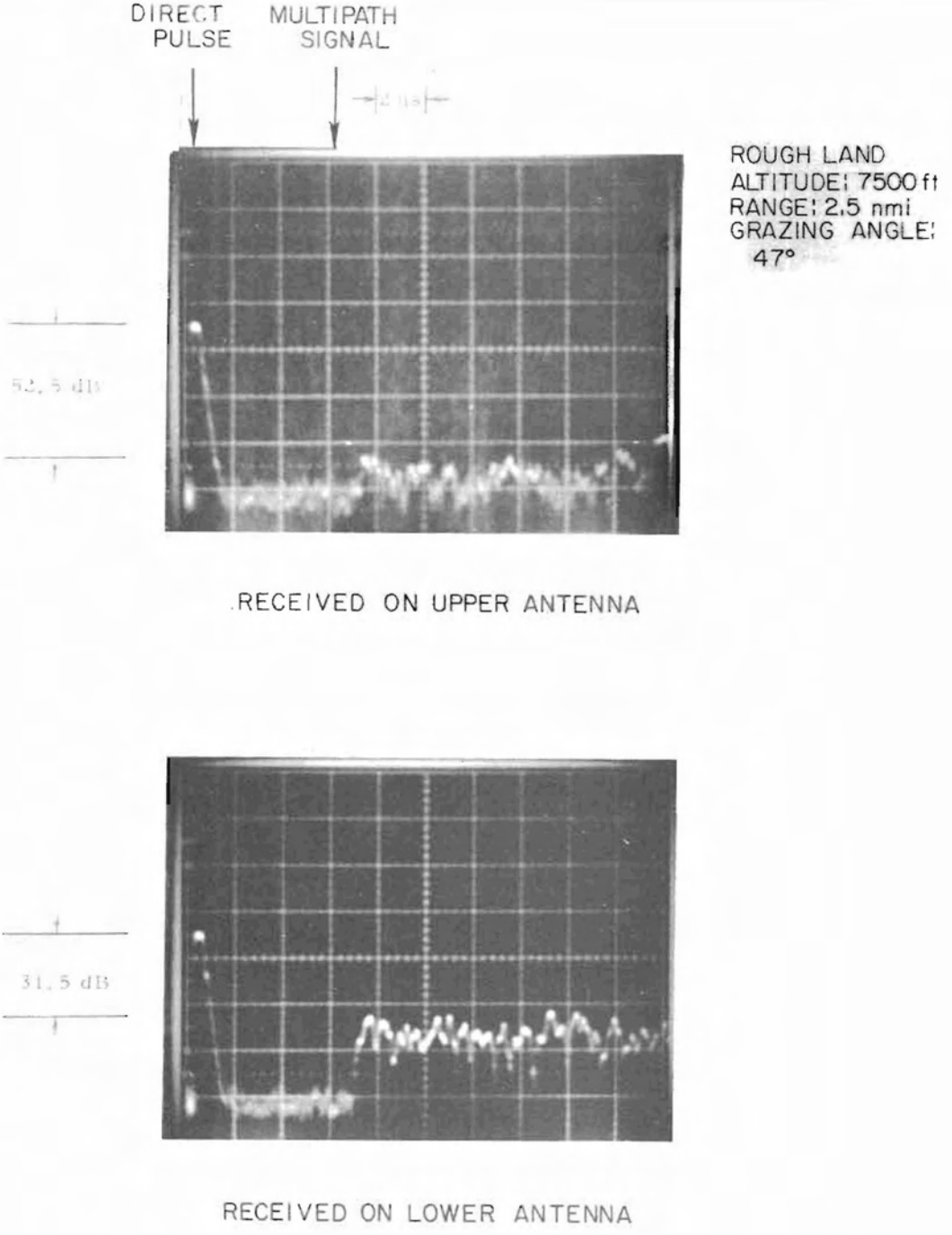


Fig. 4.2. Effect of Antenna Diversity on Land Scattered Multipath (Log-Video Photographs).

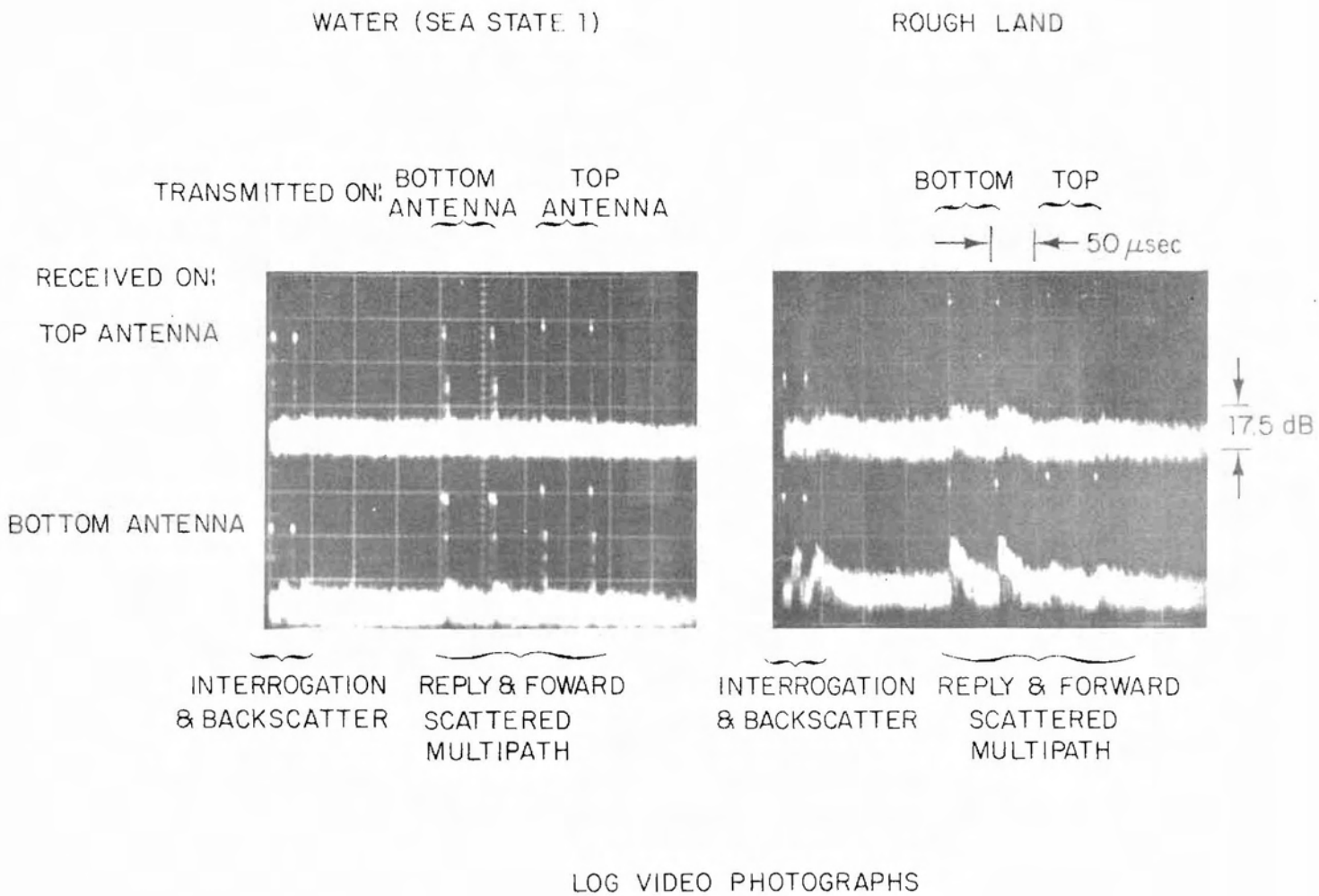


Fig. 4.3. Comparison of Land and Water Scattered Multipath (Log-Video Photographs With Long Time Scale).

The first two reply pulses were transmitted from a bottom antenna while the second two were transmitted from a top antenna. The bottom trace in each photograph shows signals received on a bottom antenna while the top trace shows signals received on the top antenna. The left most pulses in each trace represent the two interrogation pulses. On each bottom trace, back-scattered multipath was observed directly following each interrogation pulse. Note that the backscatter is stronger by approximately 6 dB for the rough land surface than for the relatively smooth water surface as would be expected. Scanning the pictures from left to right, the third and fourth pulses (spaced 55 μsec apart) are the first two direct pulses. Fig. 4.3a presents the multipath return from the water as a concentrated spike of energy (occurring shortly after the direct pulse), very strong (comparable in strength to the direct pulse) for the bottom-to-bottom antenna combination, but much weaker for the other antenna links. Fig. 4.3b shows that the multi-path return over land was much weaker than the water reflected multipath and much more dispersed in time. The bottom-to-bottom signals show that land scattered multipath can persist for as much as 35 to 40 μsec, although at a very low relative signal strength. The last two pulses in each trace show the direct pulses transmitted from a top antenna. The top-to-bottom and bottom-to-top antenna combinations exhibited much weaker multipath than the bottom-to-bottom link for both surfaces. Virtually no multipath was observed on the top-to-top combination for both surfaces.

### 4.2.2 System Description

The aircraft used in the program were a twin engine Navajo Chieftain and a single engine Beech Bonanza. The Navajo Chieftain was equipped with a set of top and bottom mounted L-Band antennas, a mode D interrogator unit, and the airborne subsystem of a digital processing/recording device known as the Airborne Measurement Facility (AMF). Fig. 4.4 is a photograph of the AMF (Ref. 1). This device was developed at Lincoln Laboratory for the purpose of gathering data on the RF environment at the ATC frequencies of 1030 MHz and 1090 MHz. The AMF records aircraft state data (heading, altitude, etc.) and navigation (VOR-DME) information as well as pulse data. Data from several data runs were recorded on a single high density instrumentation tape. The Mode D interrogator unit used a relatively low power (52 dBm) output stage. The interrogations were transmitted at a 20 Hz repetition rate.

The Beech Bonanza was equipped with a Crosslink Transponder Unit (CTU) and a set of top and bottom mounted L-Band antennas. The CTU was specially designed at Lincoln Laboratory for the multipath measurements. It used a modified King 76/78 Transponder RF receiver section and a high power (63 dBm) APX-76 transmitter. Defruiter logic was included so that the transponder could track the mode D interrogations from the Navajo. If the

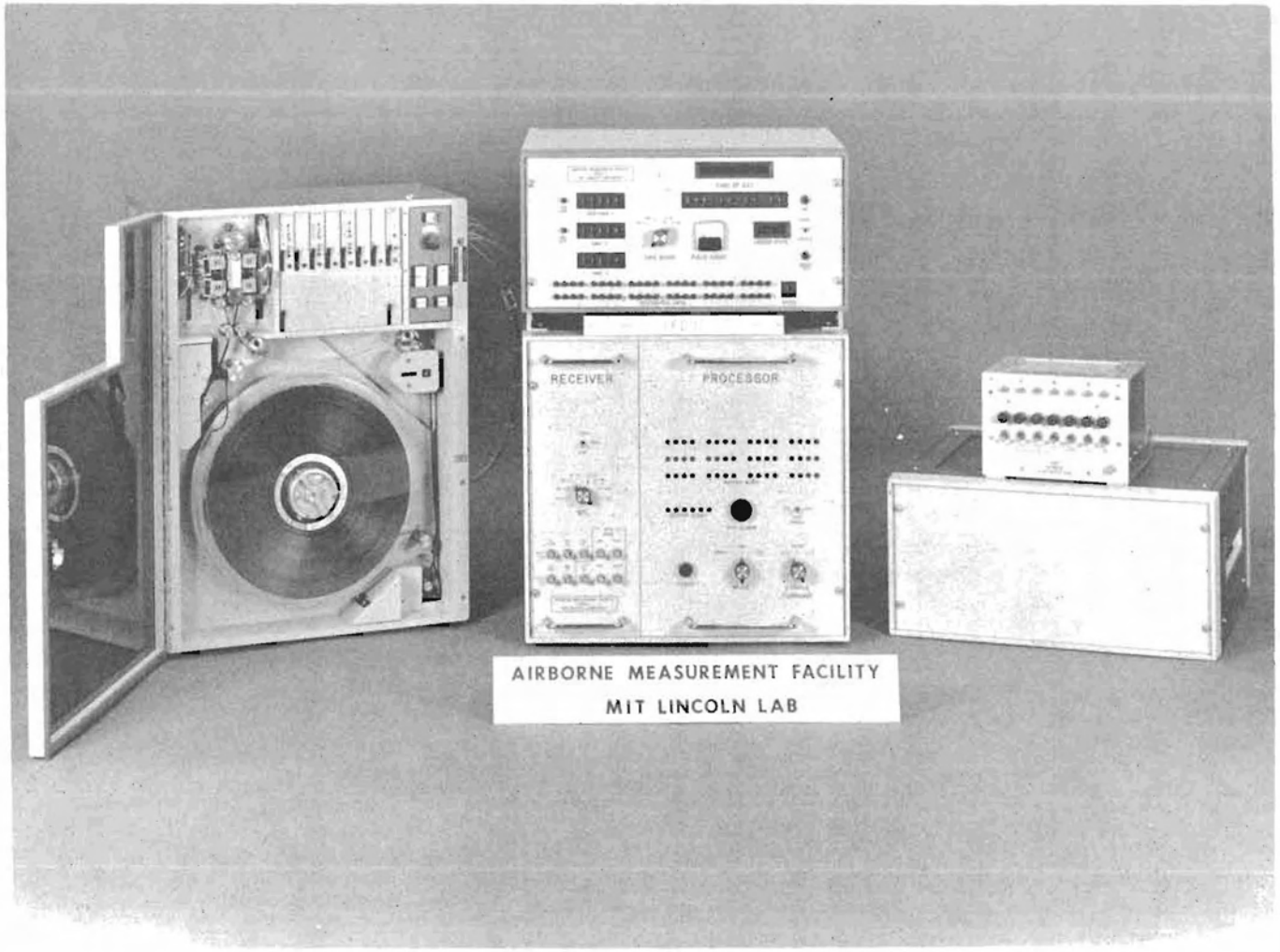


Fig. 4.4. Airborne Measurement Facility (AMF).

logic detected the absence of an interrogation, the transponder would still transmit a reply, but delayed in time by 30 μsec from its normal response time. The use of these contingency replies provided link reliability information while continuing to provide multipath data in the absence of a good interrogation link. If an interrogation was not received the CTU continued to "coast" the interrogation track and as long as interrogations were absent the transponder emitted the delayed contingency replies but when an interrogation reestablished the link, the CTU timing was resynchronized with the interrogation timing.

The signals used and their relative timing are illustrated in Fig. 4.5. Interrogation timing was derived from the AMF clock. Every 50 msec a mode D interrogation pulse pair was transmitted from the Navajo. An external trigger pulse was generated 150 μsec after the first pulse of the Mode D interrogation. The external trigger pulse caused interrogation time information to be recorded and enabled the recording circuitry to accept data for a 500 μsec window following the external trigger. The 150 μsec delay was required to prevent recording backscattered multipath generated by the interrogation as was observed in Fig. 4.3. During the recording window pulse data recording was initiated when a signal was received which was above the minimum triggering level (MTL) of either top or bottom receivers in the AMF. Once initiated, a series of data samples was taken in rapid sample fashion with a sample spacing of 0.25 μsec until the signal fell below the MTL. For each data sample, the AMF recorded the time of arrival and signal

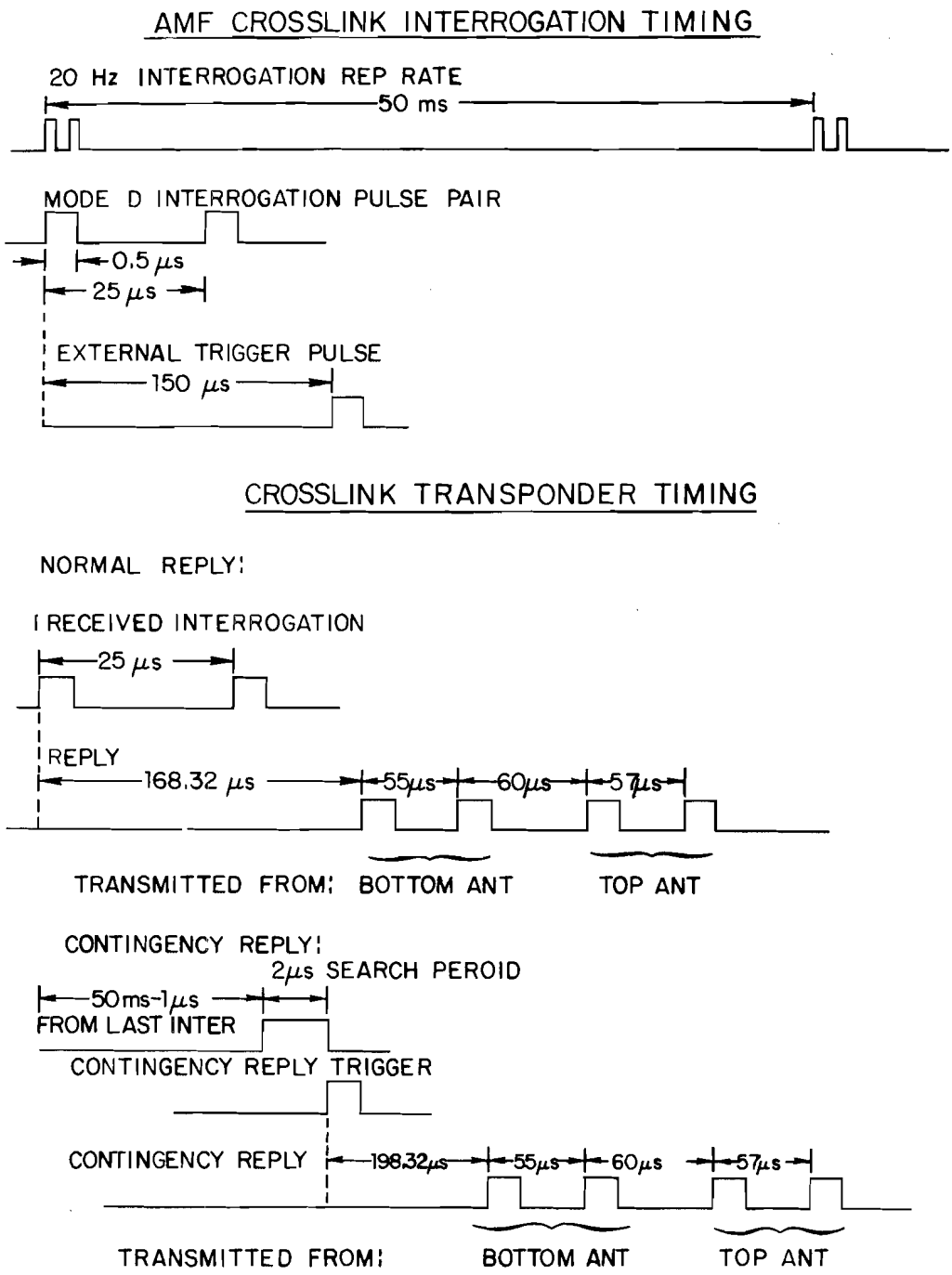


Fig. 4.5. Data Acquisition Crosslink Signals.

strength measured on both top and bottom antennas. Also, the analog log-video signals at the output of the detector were available for observation or photographing.

When the CTU on the Bonanza received a mode D interrogation in the proper time frame it waited for 168 μsec before responding. This delay corresponded to the 150 μsec external trigger delay previously mentioned. After the delay the four pulse reply was transmitted at 1030 MHz. As mentioned earlier the first two pulses were transmitted from the bottom antenna and the last two were transmitted from the top antenna.

Before collecting data, a short recording was made of calibrated pulse information. During a data flight the Mode D interrogations were continuously transmitted throughout the duration of each data run.

4.3 Data Reduction

The first step in the reduction of the multipath data was preliminary tape processing at the AMF ground playback facility. A Data General Nova minicomputer accepted data from the high density instrumentation tape and generated three types of output. The first type was an integrated data dump (ID dump) which presented the time of day, aircraft state, and navigation information associated with each second of recorded data for the entire instrumentation tape. This output made it possible to locate any given data block on the large instrumentation tape. The actual flight path of the Navajo can be reconstructed from the navigation data. The recorded AMF switch settings were also presented in the ID dump.

The second type of output was the AMF pulse data dump. This provided a look at the unprocessed data on an individual sample basis. Fig. 4.6 illustrates a section of such an output. The top line provides interrogation time information used in range calculations. The TOA column represents the pulse time of arrival. The receiver columns show the relative strength of the sampled pulses as received via top and bottom antennas. These values are linearly related to absolute power levels in dBm. The $\Delta T$ column represents the time between samples in 1/8th μsec clock increments. The last column provides sample identification numbers. The direct pulses can be identified by the proper spacing between the four pulses (see Fig. 4.5). The multipath pulses can be identified by examining the $\Delta T$ column and searching for a pair of samples with each sample delayed by the same amount following a direct pulse. For example, pulses 374 and 383 were separated by 55 μsec (440 clock counts) indicating that they were the first two direct pulses. Pulses 377 and 386 both occurred 129 clock counts after the direct pulses. Thus, these pulses were multipath signals. The time correlation between multipath pulses was necessary in order to filter out the multipath signals from uplink interference. Since the AMF operated in a rapid sample mode, a wide pulse had several data samples associated with it as illustrated for example by pulses i.e., samples 374, 375 and 376 which were all associated with the first direct pulse.

-4-10264

| | | Interrogation time reference | | TOA | | RECEIVER BOTTOM ANTENNA | | RECEIVER TOP ANTENNA | | | | ΔT | | | Sample Identification |
|---|---|---|---|---|---|---|---|---|---|---|---|---|---|---|---|
| 0 | 1 | 55442 | 60768 | | | | | | | | | | | | |
| 0 | 0 | 0 | 0 | 55442 | 61223 | | 56 | 0 | | 61 | 0 | 199 | 5415 | 454188514 | PULSE • 374 |
| 0 | 0 | 1 | 0 | 55442 | 61225 | $D_{BB}$ | 56 | 0 | $D_{BT}$ | 61 | 0 | 199 | 2 | 454188515 | PULSE • 375 |
| 0 | 0 | 0 | 0 | 55442 | 61227 | | 47 | 0 | | 54 | 0 | 109 | 2 | 454188515 | PULSE • 376 |
| 0 | 0 | 1 | 0 | 55442 | 61356 | | 36 | 0 | | 20 | 0 | 154 | 129 | 454188532 | PULSE • 377 |
| 0 | 0 | 0 | 0 | 55442 | 61358 | | 29 | 0 | | 20 | 0 | 109 | 2 | 454188532 | PULSE • 378 |
| 0 | 0 | 0 | 0 | 55442 | 61360 | $M_{BB}$ | 19 | 0 | $M_{BT}$ | 13 | 0 | 109 | 2 | 454188532 | PULSE • 379 |
| 0 | 0 | 0 | 0 | 55442 | 61364 | | 19 | 0 | | 16 | 0 | 75 | 4 | 454188533 | PULSE • 380 |
| 0 | 1 | 0 | 0 | 55442 | 61366 | | 13 | 0 | | 16 | 0 | 64 | 2 | 454188533 | PULSE • 381 |
| 0 | 1 | 0 | 0 | 55442 | 61376 | | 16 | 0 | | 17 | 0 | 64 | 10 | 454188535 | PULSE • 382 |
| 0 | 1 | 0 | 0 | 55442 | 61663 | | 56 | 0 | | 61 | 0 | 199 | 287 | 454188569 | PULSE • 383 |
| 0 | 0 | 1 | 0 | 55442 | 61665 | $D_{BB}$ | 56 | 0 | $D_{BT}$ | 61 | 0 | 199 | 2 | 454188570 | PULSE • 384 |
| 0 | 0 | 0 | 0 | 55442 | 61667 | | 47 | 0 | | 54 | 0 | 64 | 2 | 454188570 | PULSE • 385 |
| 0 | 0 | 0 | 0 | 55442 | 61796 | | 37 | 0 | | 17 | 0 | 177 | 129 | 454188586 | PULSE • 386 |
| 0 | 0 | 0 | 0 | 55442 | 61798 | $M_{BB}$ | 23 | 0 | $M_{BT}$ | 17 | 0 | 177 | 2 | 454188586 | PULSE • 387 |
| 0 | 0 | 0 | 0 | 55442 | 61804 | | 21 | 0 | | 14 | 0 | 64 | 6 | 454188588 | PULSE • 388 |
| 0 | 1 | 0 | 0 | 55442 | 61806 | | 13 | 0 | | 9 | 0 | 64 | 2 | 454188588 | PULSE • 389 |
| 0 | 1 | 0 | 0 | 55442 | 62143 | | 59 | 0 | | 63 | 0 | 199 | 337 | 454188630 | PULSE • 390 |
| 0 | 0 | 1 | 0 | 55442 | 62145 | $D_{TB}$ | 59 | 0 | $D_{TT}$ | 63 | 0 | 199 | 2 | 454188630 | PULSE • 391 |
| 0 | 0 | 0 | 0 | 55442 | 62147 | | 51 | 0 | | 55 | 0 | 64 | 2 | 454188630 | PULSE • 392 |
| 0 | 0 | 0 | 0 | 55442 | 62599 | | 60 | 0 | | 63 | 0 | 199 | 452 | 454188686 | PULSE • 393 |
| 0 | 0 | 1 | 0 | 55442 | 62601 | $D_{TB}$ | 59 | 0 | $D_{TT}$ | 63 | 0 | 199 | 2 | 454188687 | PULSE • 394 |
| 0 | 0 | 0 | 0 | 55442 | 62603 | | 51 | 0 | | 55 | 0 | 109 | 2 | 454188687 | PULSE • 395 |
| 0 | 0 | 1 | 0 | 55442 | 64590 | | 20 | 0 | | 19 | 0 | 334 | 1987 | 454188936 | PULSE • 396 |
| 0 | 0 | 1 | 0 | 55442 | 64595 | | 8 | 0 | | 5 | 0 | 87 | 5 | 454188936 | PULSE • 397 |

Fig. 4.6. Multipath Experiment Pulse Data Dump.

Since the time order of the direct pulses indicated the location of the transmitting antenna, it was possible to separate the signal strengths associated with the four possible antenna combinations. Thus, in Fig. 4.6, $M_{BT}$ designates the relative strength of a multipath signal received on the top antenna as a result of a pulse transmitted from a bottom antenna.

As well as providing a quick look at the unprocessed data, the pulse data dump allowed a visual inspection of the calibrated sections of recorded pulse information. Thus, the pulse data dump was extremely useful in verifying the validity of the data prior to analysis. Also, any given section of data which showed interesting behavior could be accessed via this output mode for detailed study.

The last type of output from the Nova computer was nine track IBM data tape. Each instrumentation tape was used to generate a number of nine track tapes corresponding to each data run. These tapes were then processed on an IBM 370 computer.

The analysis programs executed on the IBM computer extracted crosslink and multipath information and generated several kinds of plots and printouts which served to spotlight the multipath parameters of interest. Computer generated plots included the following:

1. Time-raster plot which showed signal tracks indicating the receipt of direct and multipath signals, the variation in multipath delay with range, and the multipath signal time dispersion.

2. Instantaneous signal power plot which showed the time variation of successive direct and multipath signal strengths over short (usually 10 second) time intervals.

3. Average signal strength plot* which showed direct and multipath signal strengths averaged over ten second intervals for the duration of an entire data run.

4. Signal-to-multipath ratio plot* which indicated the variation in the statistical distribution of the signal-to-multipath ratio as the grazing angle varied during the course of a data run.

Software was available to generate plot types 2 to 4 for each of the four possible antenna combinations. The plots will be described in greater detail as they appear in the data presentation.

In addition to the plots, the analysis program generated a printout which presented several types of statistical summaries of data averaged over ten second intervals for the duration of a data run. Probability distributions were generated for both the multipath signal strength and the signal-to-multipath ratio for each antenna combination. Mean and variance values of several multipath parameters were also computed for each antenna combination. The normalized autocovariance of the multipath signal received on the bottom-to-bottom antenna combination was computed for time lags up to two seconds.

---

*These figures are actually plotted versus time which increases linearly as the data evolves. Since the absolute time scales provide no insight into a physical understanding of the data the time scales have been suppressed.

## 5. EXPERIMENTAL RESULTS

### 5.1 Ocean Surface (Sea State 1)

The strongest multipath signals observed were reflected from smooth water surfaces and were received via a bottom-to-bottom antenna link. As mentioned earlier in the discussion of the multipath photographs, the multipath signals generated in response to RF pulse transmissions at L-Band were very pulselike in nature. The photographs in Fig. 5.1 show more structural detail than the previous photographs. Again the pulse on the left in each photograph is the direct pulse, the signal on the right is multipath. The leading edge of the multipath signals rose sharply following the leading edge of the direct pulse. Over a range of grazing angles from $15.2^{\circ}$ to $57.4^{\circ}$ the peak strength of the multipath signals varied over a range from 20 dB below the direct signal to as much as 8 dB above the direct signal strength (on the bottom-to-bottom antenna link). Across the top of the multipath signals the pulse was sometimes relatively flat probably indicating a uniformly smooth local reflecting surface for the duration of the incident direct pulse as in Fig. 5.1a. At other times the peak of the mulitpath signal was ragged as in Fig. 5.1b, taken a short time later, indicating a slightly rougher local scattering surface. Following the trailing edge of the direct signal the peak of the multipath signal dropped sharply. However, as indicated in Fig. 5.1b the trailing edge drop-off for an apparently rougher scattering area was not as sharp as in Fig. 5.1a.

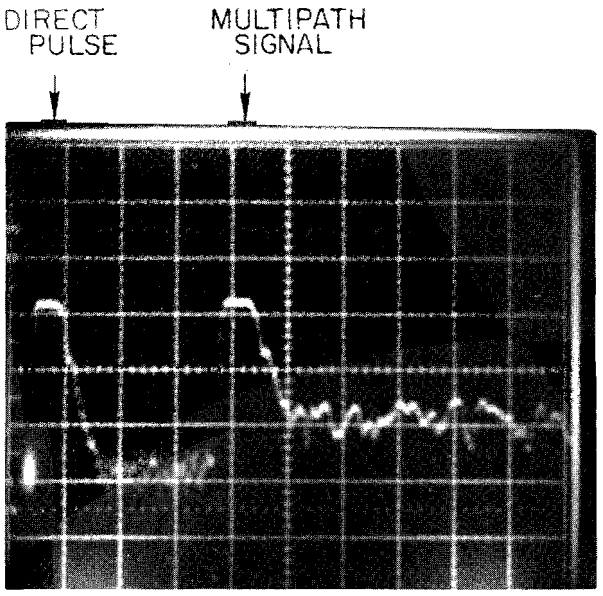


OCEAN (SEA STATE 1)
ALTITUDE: 5500ft
RANGE: 3 nmi
GRAZING ANGLE: 31°
BOTTOM TO BOTTOM ANTENNAS

UNIFORMLY SMOOTH SCATTERING AREA

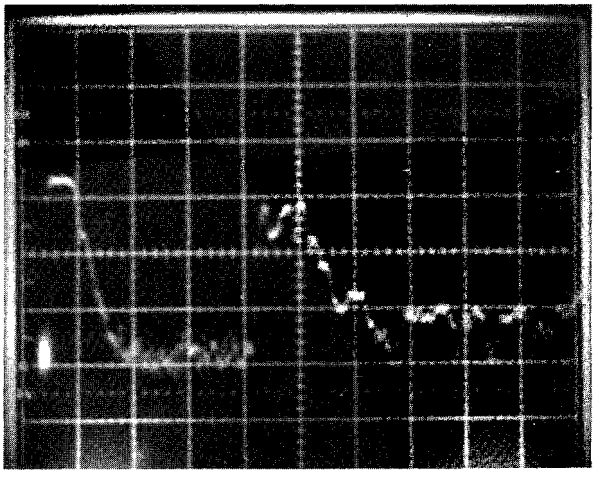

ROUGH SCATTERING AREA

Fig. 5.1. Ocean Scattered Multipath (Log-Video Photographs).

Fig. 5.2 is a time-raster plot showing multipath tracks from signals scattered from a calm ocean surface. The vertical scale shows the times of the external trigger pulses which enabled the recording circuitry for a 500 μsec period. Since the external trigger times and the interrogation times were related by a fixed time offset, the vertical axis also provides a scale of the interrogation times from the beginning of the flight, at the bottom of the figure, to the end of the flight at the top. The horizontal axis shows time in μsec as measured across the 500 μsec recording window associated with each external trigger. Each dot on the plot represents the occurrence of a pulse sample received by the AMF on the bottom antenna. Thus, for a particular external trigger time on the vertical scale, the dots viewed while scanning horizontally from left to right show the time distribution of pulses received during the associated recording window. The data evolves sequentially in time from left to right and bottom to top. The dots form four continuous pairs of pulse tracks representing four sets of direct pulses and associated multipath signals. As indicated in the figure the first two direct pulse tracks were due to bottom antenna transmissions while the last two were from top antenna transmissions. The tracks diverge from the vertical axis indicating the divergence of the aircraft flight paths. The variation of multipath delay with range is clearly indicated by the convergence of the direct and multipath trails as the aircraft range increases. Also, the width of the multipath trails illustrates the time dispersion of the multipath signals. (A comparison of Fig. 5.2 for the calm ocean with Fig. 5.34 for a rough land surface shows the variation in multipath dispersion with surface roughness).

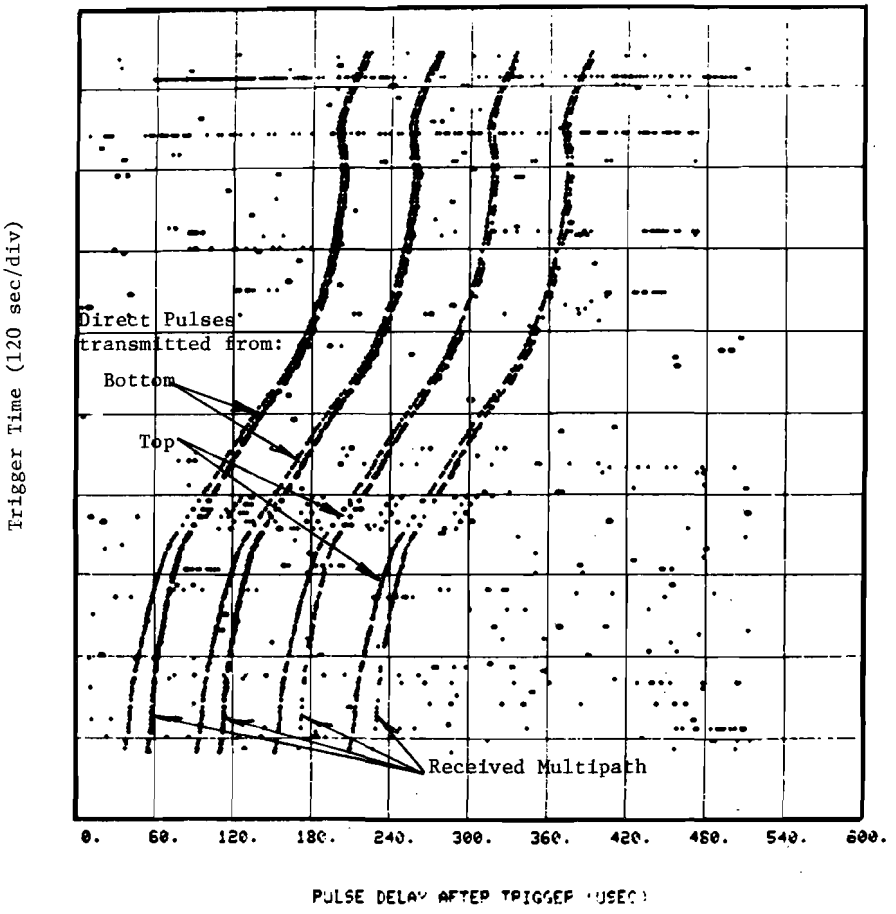


Ocean (sea state 1)
Alt: 9500 ft.
Receiving Ant: Bottom

Fig. 5.2. Ocean (Sea State 1) Multipath Time-Raster.

Since the receivers detected any signal of sufficient strength at a frequency of 1030 MHz there is a random background of pulses due to uplink interrogations and sidelobe suppression pulses from local ground stations.

In Fig. 5.2 the multipath trails were not much broader than the associated direct signal trails evidently indicating a relatively small scattering area. The multipath trails for the first two sets of pulse tracks, corresponding to a bottom-to-bottom antenna combination, were much stronger than for the last two sets of pulse tracks, corresponding to a top-to-bottom antenna combination. Also, at the beginning of the flight the last two sets of pulse tracks indicate that the multipath pulse trails were not well established until the aircraft had separated by about two miles indicating the reduced multipath rejection capability of the top antenna at lower grazing angles.

Still referring to Fig. 5.2, between trigger times from 420 seconds to 480 seconds there was a degradation of the interrogation link due to interference other than multipath. Contingency replies, as indicated by the delayed tracks, continued to provide multipath data during this period.

For the data shown in Fig. 5.2 the multipath delay was measured and the results are shown in Fig. 5.3. Also, shown is a theoretical curve that represents the delay of a simple specular multipath for equal altitude aircraft:

$$D = R\ (\text{secant}\ (G) - 1)/\ c \qquad (5.1)$$

where

D = multipath delay, R = range, c = speed of light, and G = grazing angle. Grazing angle G is given by:

$$G = \tan^{-1}\ (\frac{2A}{R}) \qquad (5.2)$$

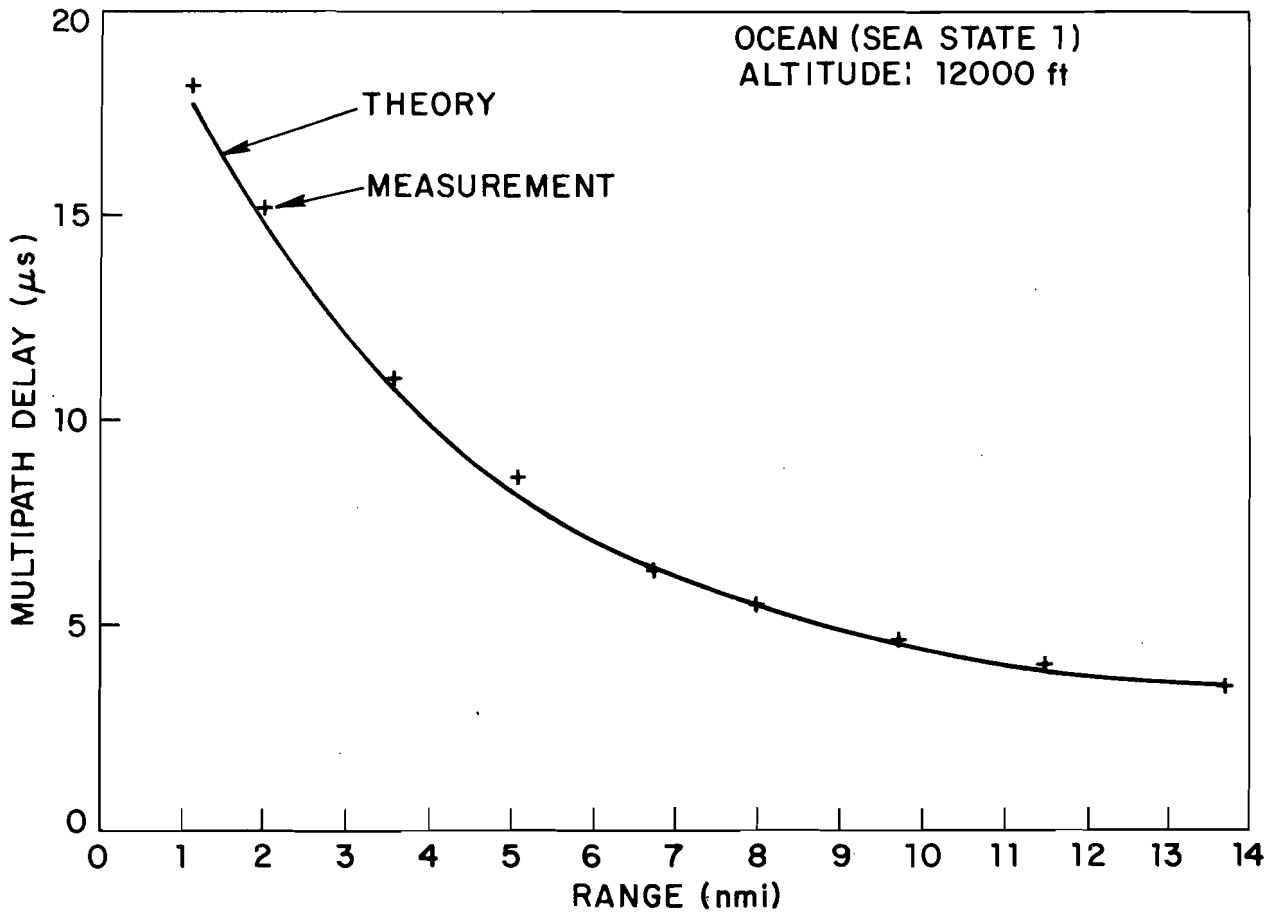


Fig. 5.3. Multipath Delay.

where A = altitude above ground level. As seen in Fig. 5.3 formula 5.1 agrees with the measurements quite accurately. This accurate predictability of multipath delay has been observed in all the data regardless of aircraft geometry or scattering surface.

One feature of the multipath scattered from the ocean which in fact was true of all but the very smoothest surfaces was the rapid variation in the multipath strength from sample to sample. Fig. 5.4 shows the instantaneous direct and multipath signal strengths for successive replies for a ten second period at different grazing angles. The signals in the figure were received via a bottom-to-bottom antenna combination. In both cases successive multipath values changed by as much as 25 dB over a 50 msec time interval. Such variability in the multipath seems to imply that a significant portion of the multipath is not due to purely specular multipath. In conducting this experiment interest was focused on the total multipath signal received. No attempt was made to separate the coherent and incoherent components of the multipath signal.

Fig. 5.5 shows normalized autocovariance plots corresponding to the data in Fig. 5.4. Both curves confirm in a quantitative way that there is very little correlation between successive multipath samples. Such lack of correlation further indicates that even a relatively calm sea gives rise to a large incoherent component in the multipath at large grazing angles.

Several features were observed in the data which are illustrated in the signal-to-multipath ratio (SMR) cumulative distribution curves in Fig. 5.6. The curves have a shape similar to the exponential distribution curve corresponding to Rayleigh amplitude statistics associated with diffuse multipath (see Ref. 2). The Rayleigh property was commonly observed in the data at all

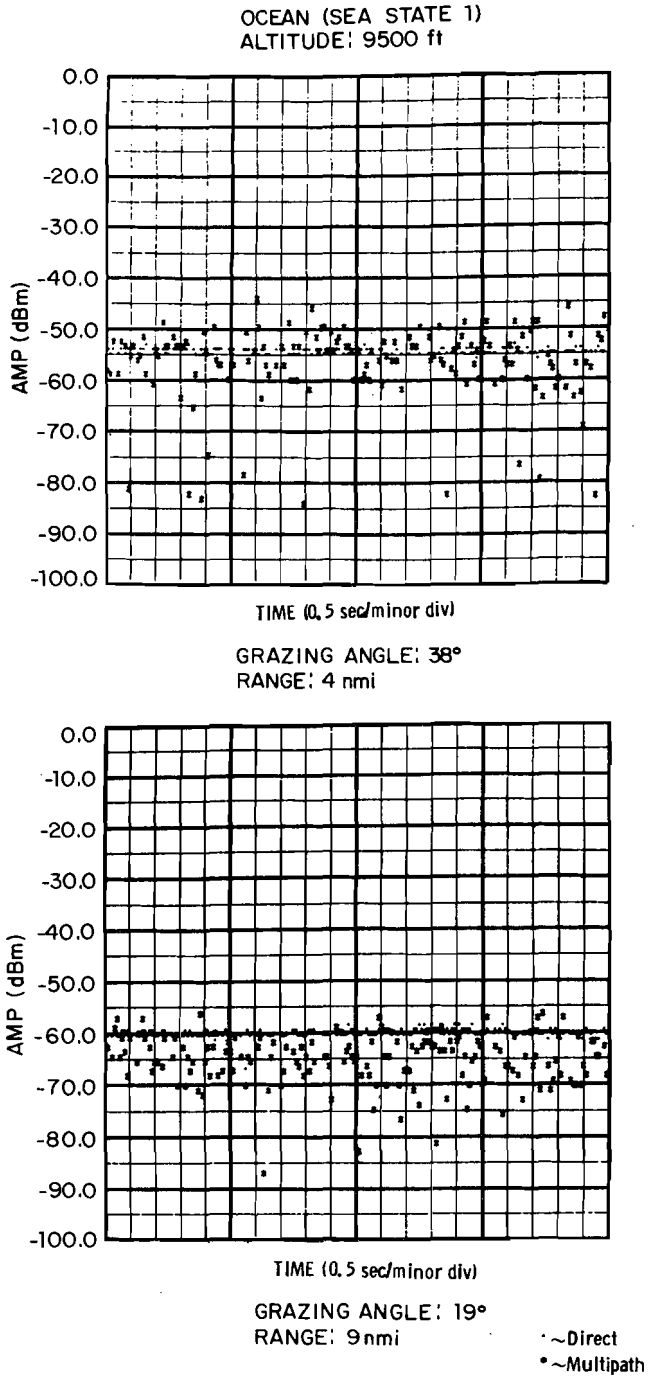


Fig. 5.4. Ocean (Sea State 1) Multipath Instantaneous Signal Strength.

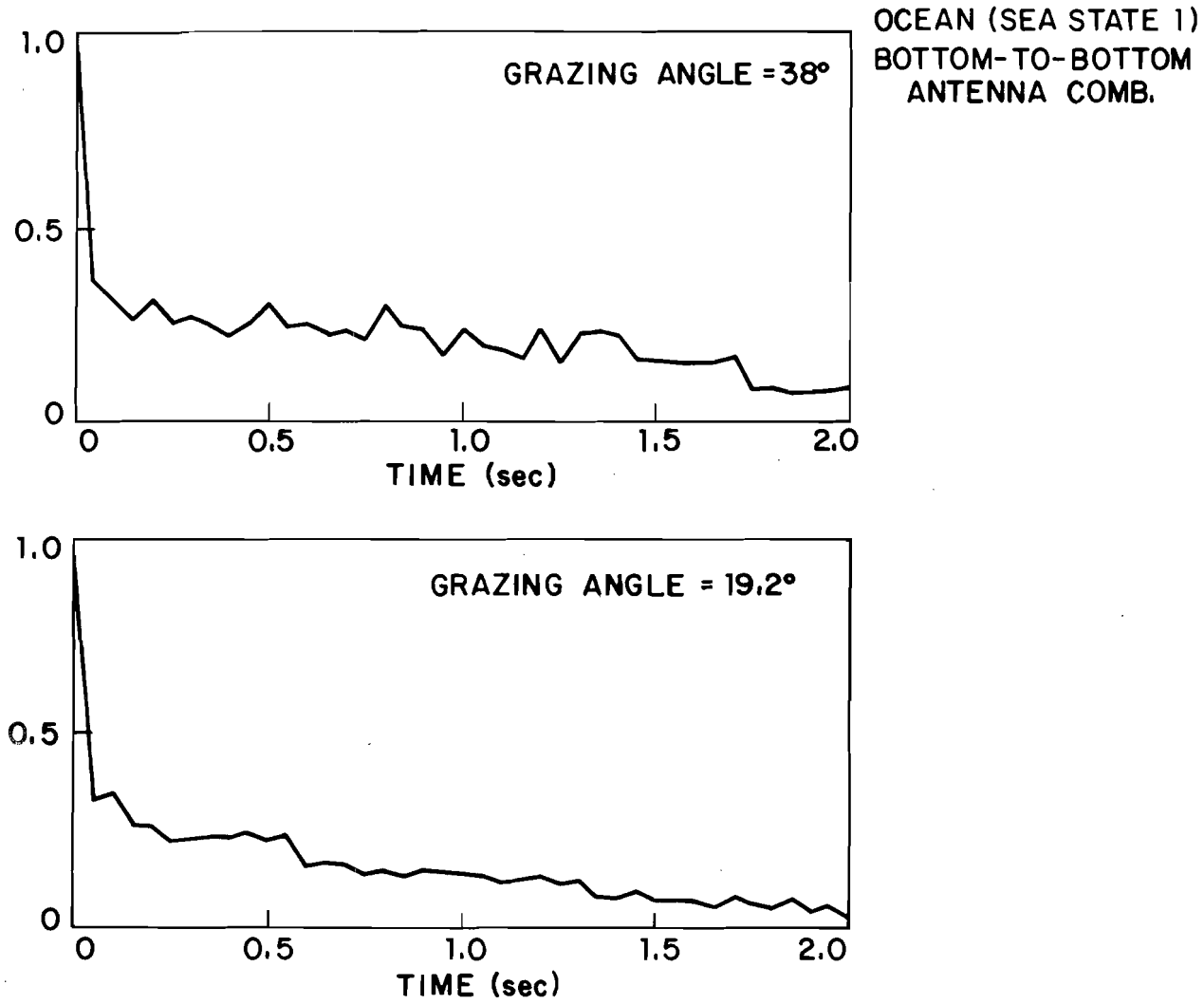


Fig. 5.5. Normalized Autocovariance (Ocean Sea State 1).

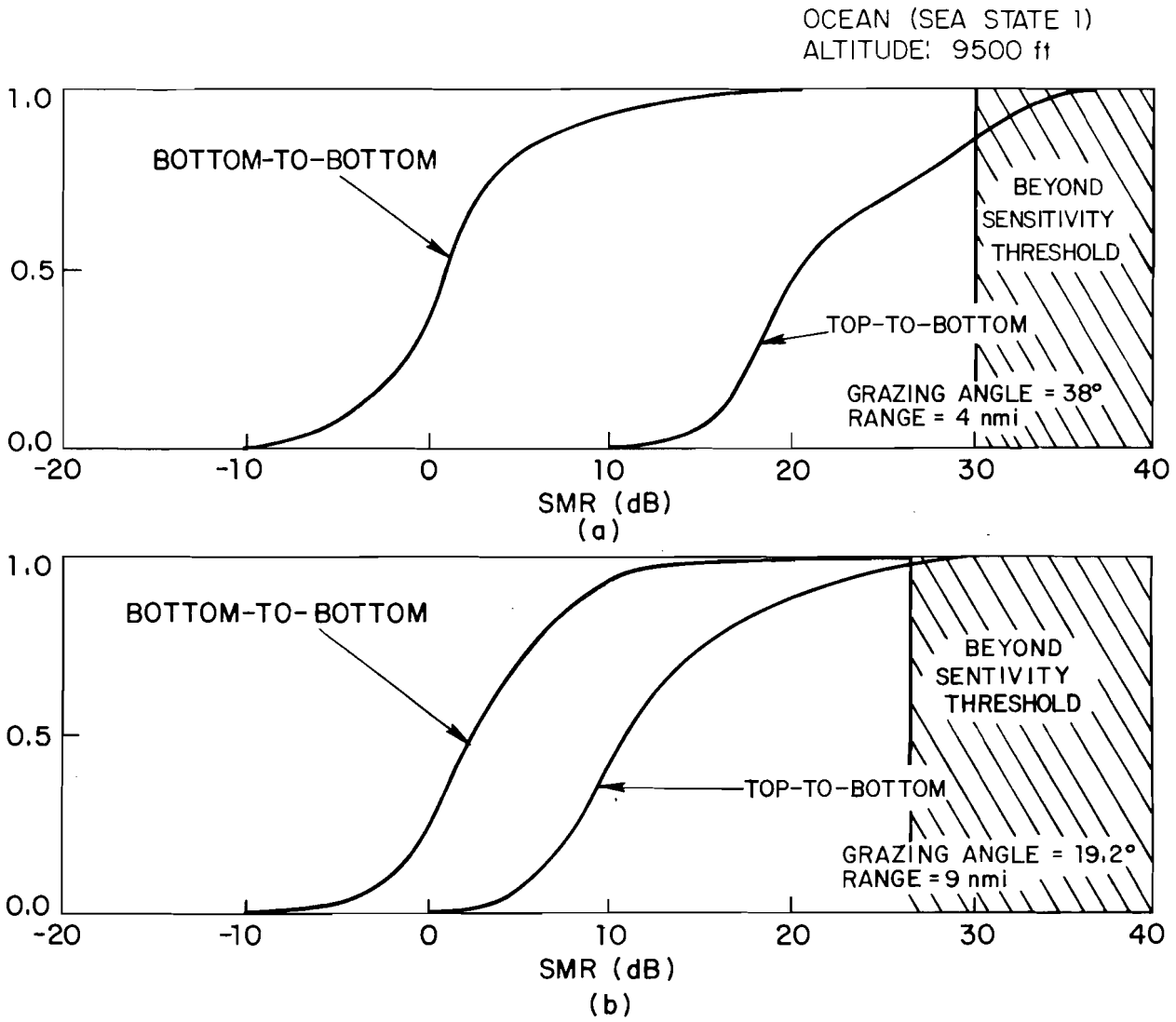


Fig. 5.6. Signal-to-Multipath Ratio Cumulative Distribution (Ocean Sea State 1).

ranges, altitudes, antenna combinations and all surfaces with the exception of the very smoothest surfaces. For the bottom-to-bottom link curves, the probability of SMR $\leq$ 6 dB was 0.86 at the higher grazing angle and 0.76 at the lower grazing angle. At both grazing angles the top-to-bottom curves were shifted to the right from the bottom-to-bottom curves indicating an improvement in SMR due to the shielding of the top transmitting antenna from the active scattering surface. However, the degree of improvement was reduced from 20 dB at the higher grazing angle to 9 dB at the lower grazing angle. At lower grazing angles the two distributions continued to converge to a single limiting curve with a median SMR of ~10 dB. Two mechanisms could contribute to the reduced SMR improvement at the lower grazing angle. The bottom-to-bottom curve in Fig. 5.6b has shifted slightly to the right of its position in Fig. 5.6a indicating slight reductions in both antenna gain in the multipath direction and scattered multipath strength. The primary reduction in SMR improvement was due to the shift of the top-to-bottom curve to the left at the lower grazing angle since the top antenna was less shielded from the scattering area.

Distribution curves for the bottom-to-top and top-to-top antenna combinations followed the same trends as the top-to-bottom curve. The bottom-to-top antenna link behavior was slightly less sensitive to grazing angle than the top-to-bottom link. The asymmetry in the top-to-bottom and bottom-to-top links was probably due to slight differences in aircraft size and antenna locations.

The strong multipath reflected from the ocean is rather dramatically illustrated in Fig. 5.7 which shows the average direct and multipath signal

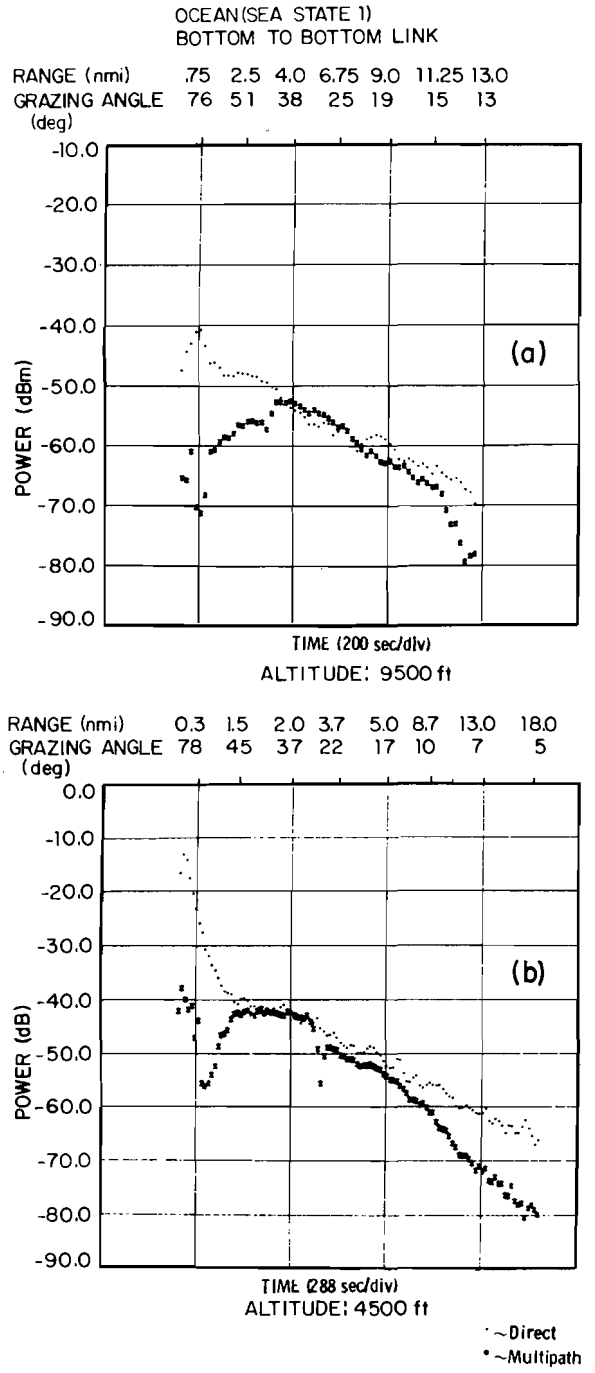


Fig. 5.7(a-b). Ocean (Sea State 1) Multipath Average Signal Strength.

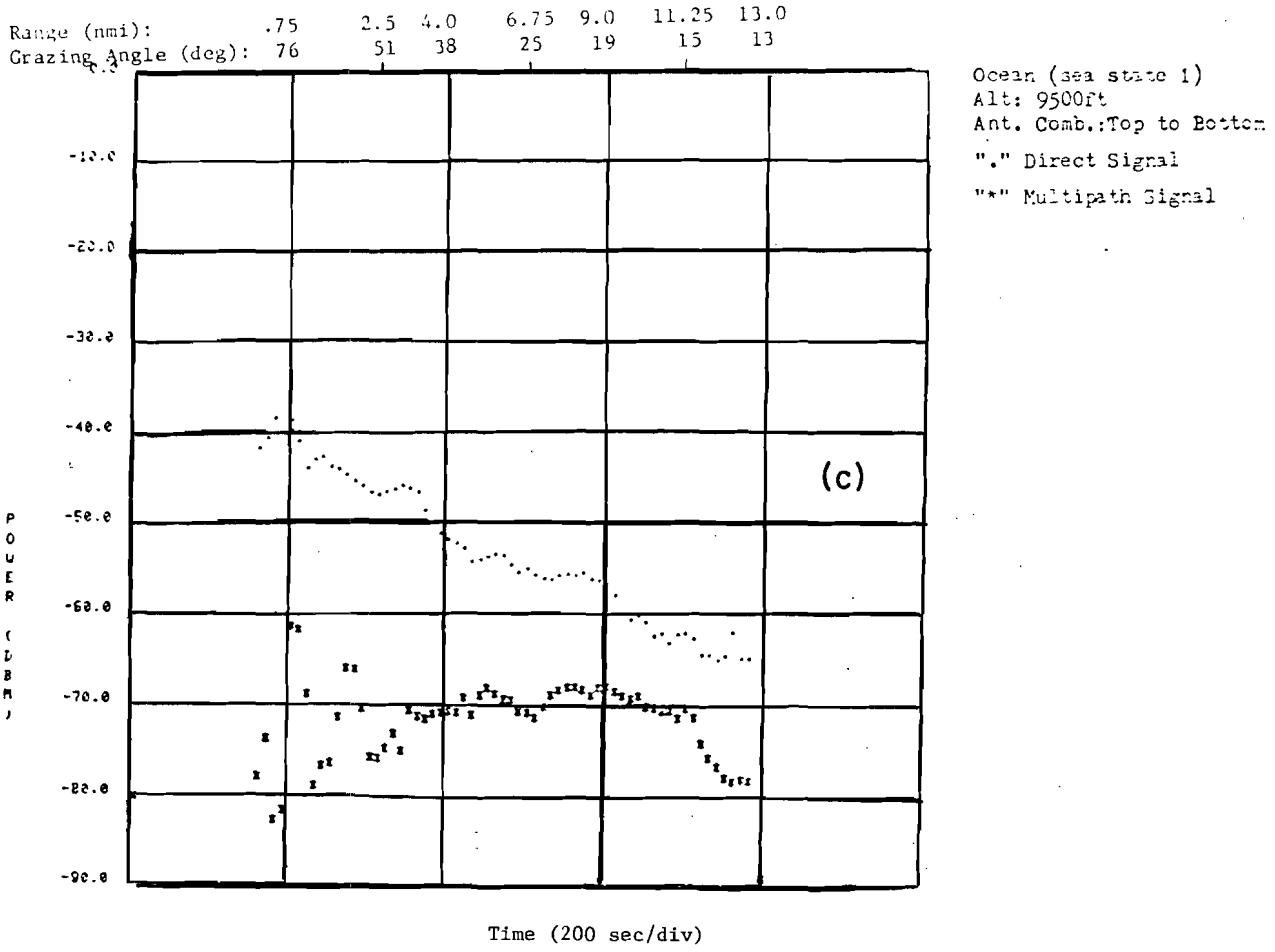


Fig. 5.7(c). Ocean (Sea State 1) Multipath Average Signal Strength.

strength as a function of time into a data run. For grazing angles from $15^{\circ}$ to $57^{\circ}$ the multipath signals were very strong. The reflections were strong enough so that for grazing angles between $25^{\circ}$ and $40^{\circ}$ the differential antenna gains consistently increased the average multipath signal strength to a level greater than or equal to the average direct signal strength.

Fig. 5.7c showing average signal strengths for a top-to-bottom antenna link illustrates a very significant multipath feature regarding the effectiveness of antenna diversity. For grazing from $14^{\circ}$ to $40^{\circ}$ the average multipath was nearly constant. The phenomenon appears to be due to two competing mechanisms. If the top antenna had not been shielded from the scattering surface the multipath would initially increase and then decrease with range as in Fig. 5.7a. The shielding of the top antenna reduces the received multipath level but by an amount that decreases with increasing range. The variations in multipath strength and top antenna shielding with range evidently offset each other producing the relatively constant level of average received multipath. This phenomenon was observed on antenna links employing one or two top mounted antennas. Also, this phenomenon was observed in all the data associated with smooth surfaces i.e., desert, flat plain, and lake surfaces.

The drop in multipath signal strength at the higher and lower grazing angles was apparently due to two mechanisms as indicated in Fig. 5.8. This figure shows the measured signal-to-multipath ratio at several grazing angles for the data in Fig. 5.7a. Also, shown are the total differential antenna gain and the reflection loss. The differential antenna gain is the total

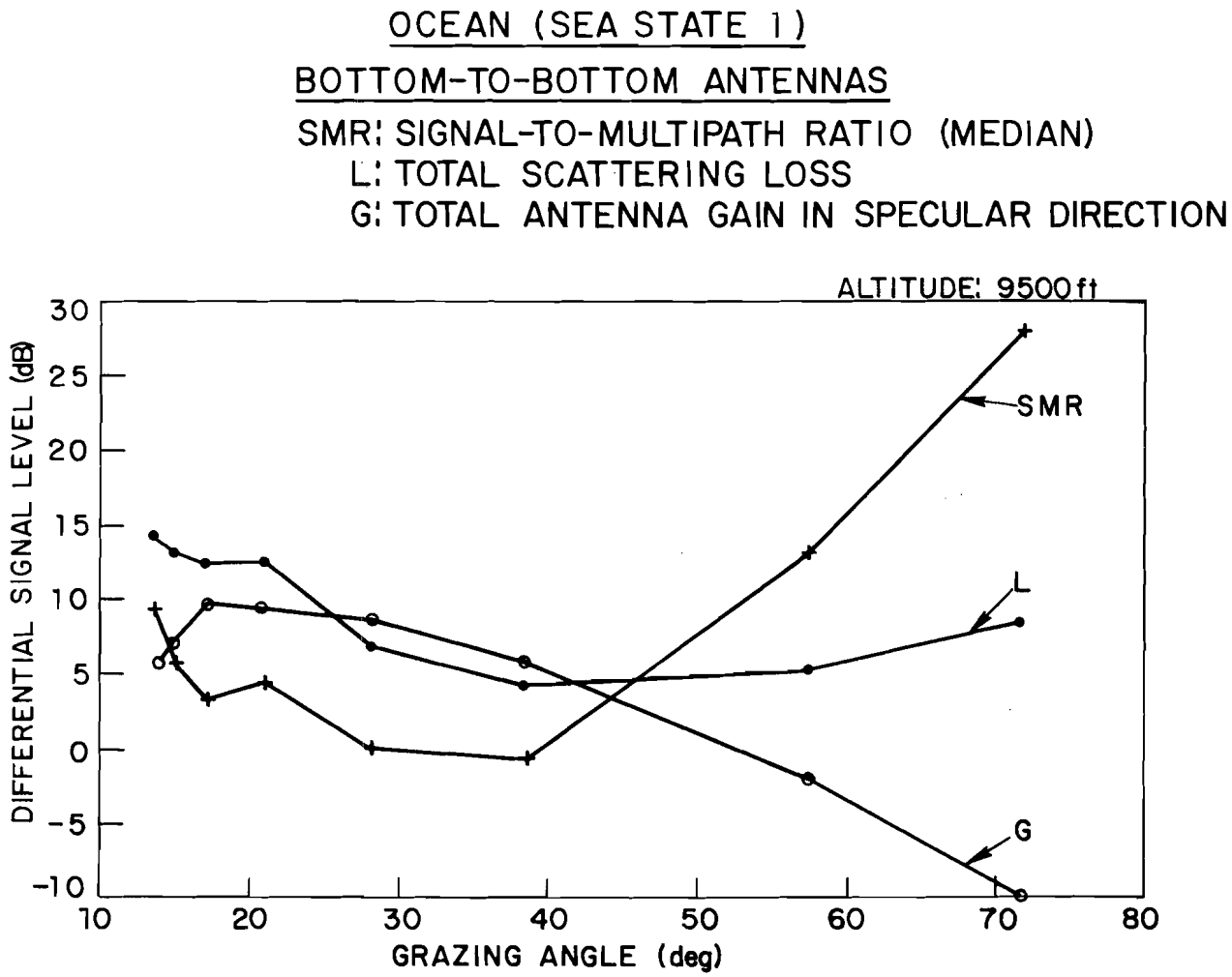


Fig. 5.8. Signal-to-Multipath Ratio, Antenna Gain, and Total Scattering Loss (Ocean Sea State 1).

gain in the specular multipath direction over that of the crosslink direction taking into account the gains of both transmitting and receiving antennas. The antenna data was taken from Ref. 3 *. The loss curve represents the total reflection loss (absorption and scattering loss) computed from the measured signal strengths and the antenna gain variations.

From Fig. 5.8 it is seen that for these grazing angles, the variations in signal-to-multipath ratio were primarily dependent on antenna gain variations rather than on variations in the scattering loss.

For this data the reflection loss increased at the lower grazing angles. This is most likely because of the surface roughness. The "Rayleigh criterion" states that a surface is considered smooth if the height of the surface irregularities, h, satisfies:

$$h < \frac{\lambda}{8 \sin \gamma}$$

where $\lambda$ is the signal wavelength and $\gamma$ is the grazing angle. The waveheights encountered exceeded the Rayleigh smoothness factor even at the lower grazing angles at which data was recorded. Hence, the surface was electrically rough and scattered less energy in the direction of the receiving antenna. This qualitative behavior was anticipated by theoretical analyses of rough surface scattering (see for example Ref. 2 ). At lower grazing angles, shadowing also becomes an important factor in reducing the energy scattered in the specular direction.

Fig. 5.9 shows plots of signal-to-multipath ratio (SMR) distribution variations versus time, range and grazing angle. Each figure corresponds to one of the four possible antenna combinations. In evaluating the performance

---

*Crude antenna patterns were measured for the actual aircraft used in the multipath measurements and were found to agree with the more detailed patterns in Ref. 3 to first order.

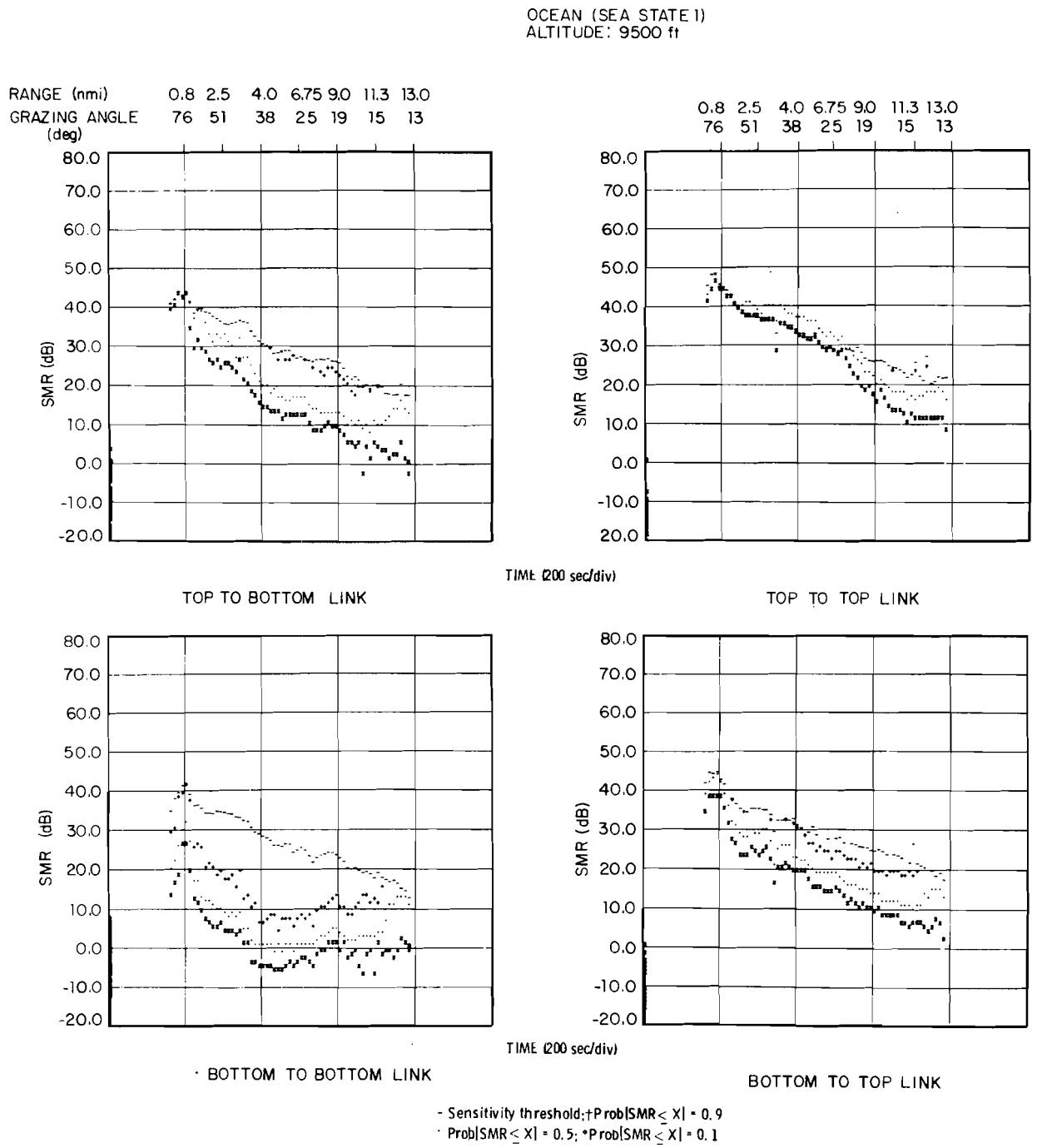


Fig. 5.9. Signal-to-Multipath Ratio Distribution Variations (Ocean Sea State 1).

of the top antennas in rejecting multipath, the angle of flight divergence (nominally $30^{o}$ for the data under consideration) plays an important role in determining the degree of top antenna shielding from the scattering region by the aircraft structure. A $30^{o}$ divergence provided a nearly minimum wing shielding of the top antennas. In constructing these figures the cumulative distribution of the signal-to-multipath ratio was accumulated over successive ten second intervals for each antenna combination and certain points of each distribution were plotted. In each figure the "+" corresponds to the SMR value below which 90% of the SMR values measured during a ten second interval fell. The "." corresponds to the median SMR value while the "*" corresponds to the 10% point on the SMR distribution. The "-" represents the limiting measurement threshold imposed by the minimum triggering level reflecting the instrumentation sensitivity. Points above the MTL symbol do not represent valid data.

The effects of antenna combination on the SMR are evident from the plots in Fig. 5.9. In comparing the median SMR curve for the bottom-to-bottom antenna link with the median SMR curves associated with antenna links which include at least one top antenna there was a substantial improvement at grazing angles greater than $19^{o}$. At $38^{o}$ the top-to-bottom link caused a 20 dB improvement in mediam SMR link while the top-to-top antenna link provided a 32 dB improvement in median SMR. As the grazing angle descreased there was a reduction in the ability of the top antennas to discriminate against multipath signals. This is evident in Fig. 5.9 from a comparison of SMR improvements at various grazing angles. For instance, at $38^{o}$ the top-to-bottom link afforded a 20 dB improvement while at $19^{o}$ there was a 10 dB improvement over the bottom-to-bottom case.

The overall effect of the top antennas was to increase the minimum SMR value and to cause it to occur at a lower grazing angle, i.e., at a greater range for a given altitude. While the top antennas always produced an increase in SMR over the bottom-to-bottom case, the degree of improvement at lower grazing angles depended strongly on the roughness of the surface since the top antennas were more exposed to the active scattering area. The data in Fig. 5.9 show that the minimum SMR improvement was provided by the top-to-bottom antenna combination which shifted the bottom-to-bottom minimum median SMR of -2 dB at $35^{\circ}$ to 8 dB at $15^{\circ}$. This amounted to raising the minimum average SMR by 10 dB and causing it to occur at a range six nautical miles greater than for the bottom-to-bottom antenna link.

Another feature of the data is that for all antenna links the 10% to 90% spread in SMR distributions was somewhat constant for grazing angles from $17^{\circ}$ to $76^{\circ}$ having values from 10 dB to 15 dB depending on the antenna combination. For grazing angles lower than $17^{\circ}$ the spread tended to increase as the grazing angle decreased for all antenna combinations. This was possibly due to sampling irregularities at low multipath signal levels.

Fig. 5.10 shows a comparison of median SMR curves for two different altitudes. Two features are evident in the curves. First, both curves varied somewhat inversely to the antenna gain plot as is also indicated in Fig. 5.8 for the higher altitude. Also, for higher grazing angles (above $45^{\circ}$) where the antenna gain was rapidly dropping below its peak and for lower grazing angles (below $25^{\circ}$) where the scattering loss seemed to be increasing, the SMR for the lower altitude was several dB less than for the

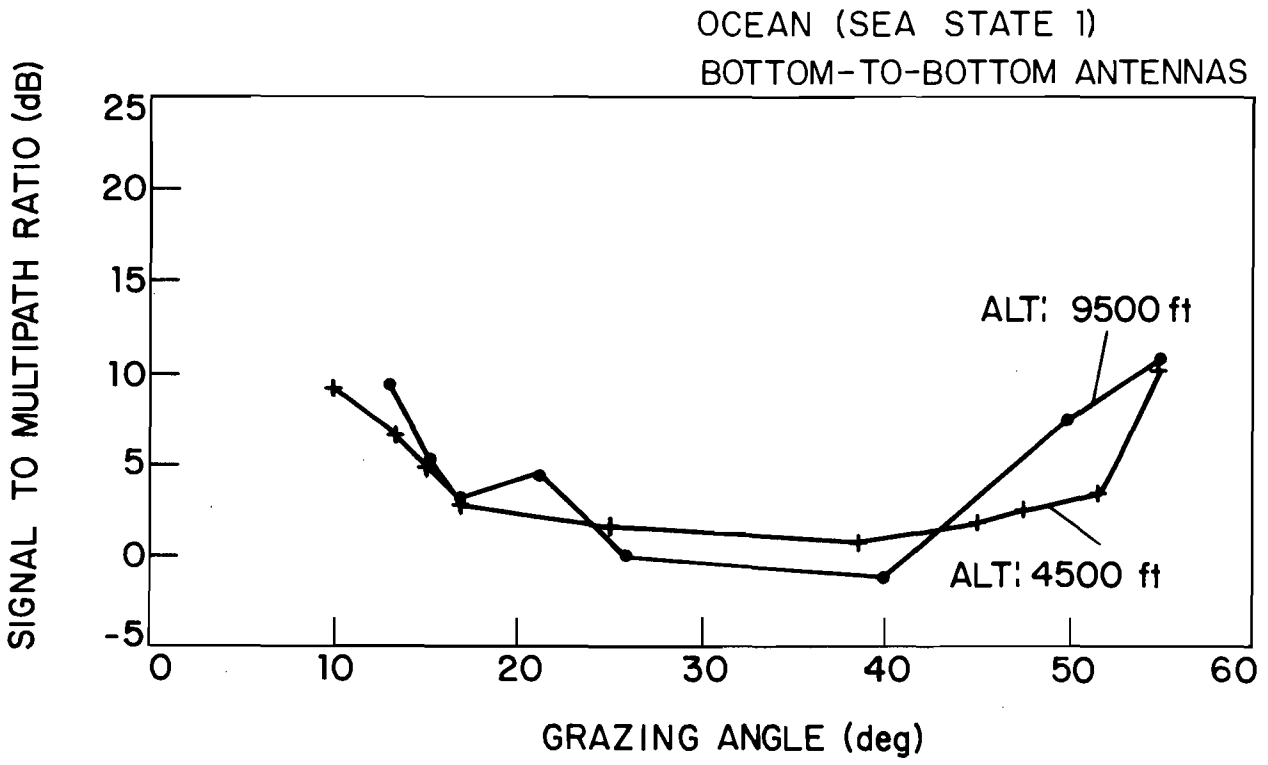


Fig. 5.10. Altitude Variations in Signal-to-Multipath Ratio (Ocean Sea State 1).

higher altitude. This might be attributed to the increased size of the active scattering area at the higher altitude. Since the scattering area was presumably larger at the higher altitude, the multipath energy was probably more dispersed than for the lower altitude. Hence, the higher altitude might be expected to have a slightly higher SMR than the lower altitude. For intermediate grazing angles from $25^{\circ}$ to $45^{\circ}$ this effect was swamped out by the combined effects of strong antenna gain and any reduction in scattering loss indicating that variations in SMR due to altitude variations were second order effects. Thus, multipath has a definite dependence on grazing angle, as would be expected. The additional dependence on altitude is minor with no significant change in the worst-case multipath, and with a small change in the grazing angle at which the worst-case multipath occurs.

The SMR variations in Fig. 5.11 summarize the Sea State 1 ocean multipath data. The main features are that a bottom-to-bottom antenna link over the calm ocean surface experienced a severe multipath environment over a large variation in grazing angle and over an altitude variation of at least 5000 ft. The use of top antennas in the link provided substantial multipath rejection at high grazing angles but the multipath discrimination capability of top antennas decreased with decreasing grazing angle. The minimum SMR for a link employing a top antenna was 8 dB for the top-to-bottom link. The top antennas caused the minimum SMR to occur at a greater range than for the bottom-to-bottom case. The amount of the range shift in the SMR minimum point varied directly with altitude.

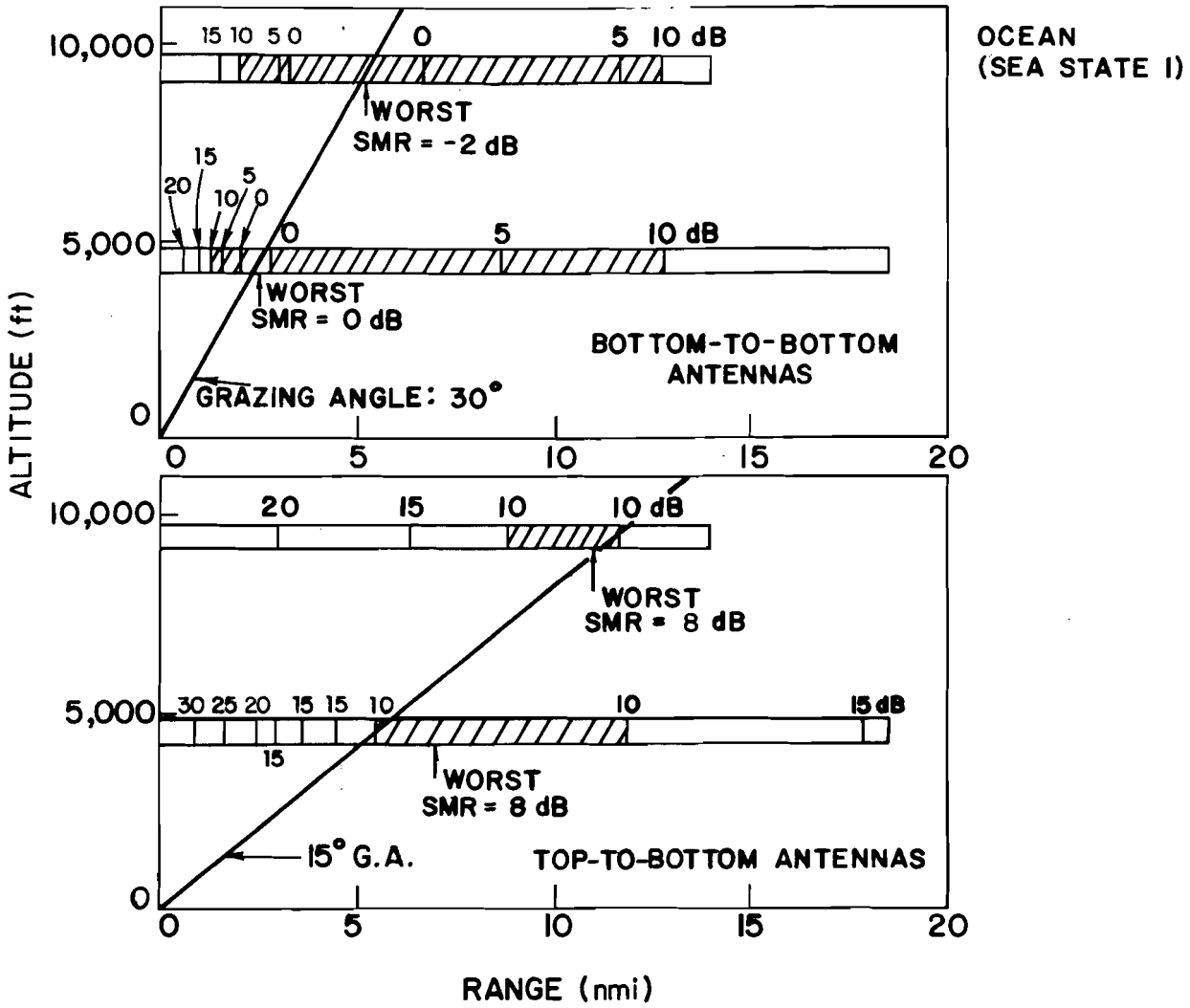


Fig. 5.11. Geometrical Dependence of Signal-to-Multipath Ratio (Ocean Sea State 1).

## 5.2 Ocean Surface (Sea State 2)

Photographs taken of multipath returns from a sea state 2 ocean indicated that the signals for this slightly rougher surface were still well defined pulses. While the increased surface roughness tended to reduce the average level of multipath signals by several dB from the Sea State 1 level, occasionally multipath pulses were observed which equalled or exceeded the direct signal in strength. The envelopes of the received multipath signals generally were more ragged than for the smoother Sea State 1 ocean as in Fig. 5.1b. Also, as in Fig. 5.1b the bases of the main portion of the multipath signals were somewhat broader than that illustrated in Fig. 5.1a. The peak multipath levels tapered down more slowly indicating the increased time dispersion indicative of a slightly larger scattering area associated with a rougher surface.

A raster-plot of multipath data recorded at an altitude of 1200 ft. exhibited the same temporal characteristics illustrated by the multipath trails in Fig. 5.2. The multipath trails were quite thin indicating a relatively small scattering area but were slightly broader than the direct pulse trails. Instantaneous signal strength plots showed rapid variations over a 20 dB range in the strength of successive multipath samples in Fig. 5.4. The autocovariance computed from the Sea State 2 data indicated that successive multipath samples were slightly less correlated than was the Sea State 1 case in Fig. 5.5b. There was very little variation in the multipath correlation over the range of grazing angles for which data was recorded ($14^{\circ}$ to $75^{\circ}$).

Fig. 5.12 shows several signal-to-multipath ratio cumulative distribution curves. As in Fig. 5.6 a decrease in grazing angle was accompanied by a slight (~2 dB) improvement in the median SMR for the bottom-to-bottom antenna link indicating a slight drop in the total antenna gain in the multipath direction and possibly a slight increase in the scattering loss at the lower grazing angle. There was only a very slight reduction in the median SMR for the top-to-bottom link at the lower grazing angle unlike the curves in Fig. 5.6. The primary reason for the slight shift in top-to-bottom distribution is that at a grazing angle of $38^{\circ}$ the top-to-bottom link SMR distribution was at a lower SMR range than was the case for Fig. 5.6a. This degradation in SMR was caused by increased multipath reception via two possible mechanisms. When the aircraft were at a grazing angle of $38^{\circ}$, their flight paths were diverging at an angle of $\sim 35^{\circ}$ allowing a relatively high exposure of the top antennas to the scattering surface due to the absence of wing shielding thus increasing the level of received multipath. In addition to the increased top antenna exposure to the scattering surface, the larger scattering area associated with the rougher sea tended to expose the top antennas to multipath contributions from the outer portions of the scattering area at higher grazing angles than would be the case for a smaller scattering area associated with a smoother surface. The latter mechanism was probably a second order effect.

In comparison with the Sea State 1 data in Fig. 5.6, the bottom-to-bottom SMR distributions at both grazing angles were shifter to higher SMR values (by $\sim 7$ dB at $38^{\circ}$; $\sim 4.5$ dB at $19^{\circ}$) indicating the effect of increased

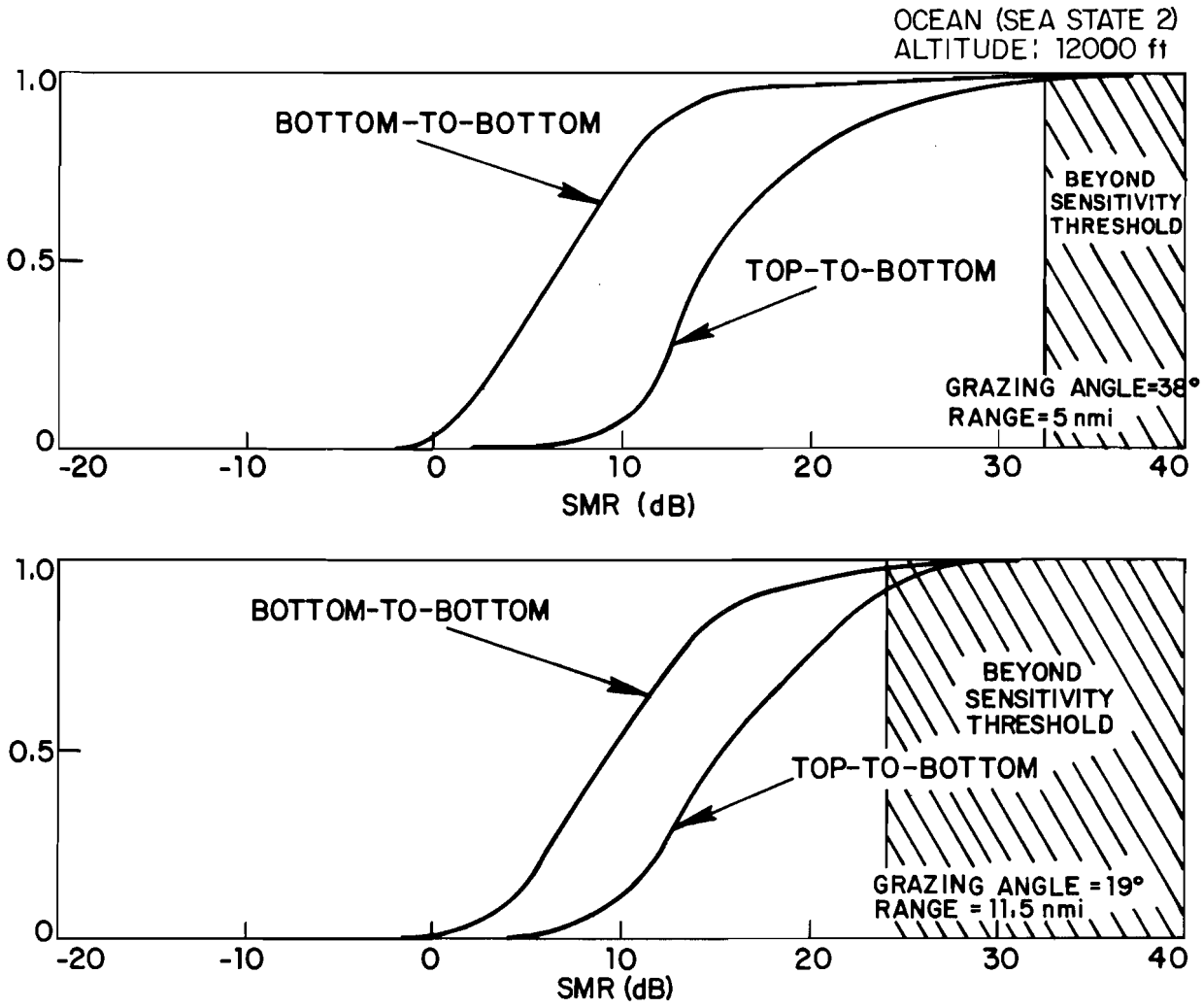


Fig. 5.12. Signal-to-Multipath Ratio Cumulative Distribution (Ocean Sea State 2).

surface roughness on received multipath strength. Thus, the improvement in the bottom-to-bottom SMR distribution due to the rougher surface and the degradation in the top-to-bottom distribution apparently caused a significant decrease in the SMR improvement at the higher grazing angle. In spite of the premature reduction in the effectiveness of top antennas in rejecting multipath at closer ranges the top antennas still provided substantial multipath rejection. The SMR improvement at the lower grazing angle of Fig. 12b was not significantly different from that shown in Fig. 5.6b since flight conditions were such that top antennas were exposed to approximately the same scattering area in both cases.

At the lower grazing angle the bottom-to-bottom link curve shifted to higher SMR values as rough surface scattering loss evidently increased as in the Sea State 1 data. The bottom-to-bottom and top-to-bottom curves tended to converge toward a single limiting curve with a median SMR approaching ~17 dB at lower grazing angles as the top antennas viewed an increasing portion of the scattering area "seen" by the bottom antennas.

The average signal strength plots in Fig. 5.13 bear out the median SMR variations in Fig. 5.12. A comparison of Fig. 5.13b with the Sea State 1 data in Fig. 5.7a clearly indicates the reduction in received multipath due to increased scattering loss. The variation in average multipath strength in Fig. 5.13a indicates another rough surface effect in that the relative constancy of the average multipath signal strength range observed over smooth surfaces (as in Fig. 5.7c) is absent for the top antenna links.

The antenna gain and scattering loss curves in Fig. 5.14 again indicate that over most grazing angles the variations in SMR were due to antenna gain

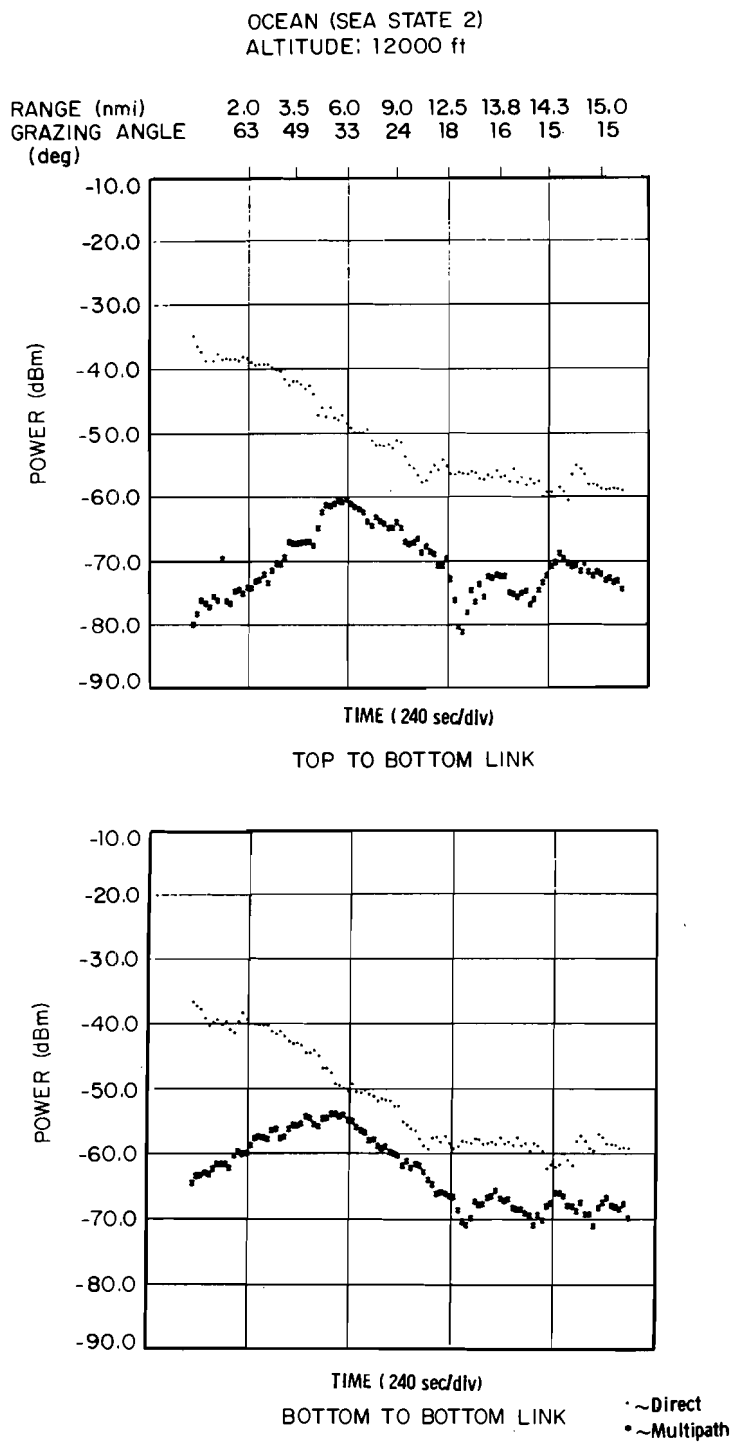


Fig. 5.13. Ocean (Sea State 2) Multipath Average Signal Strength.

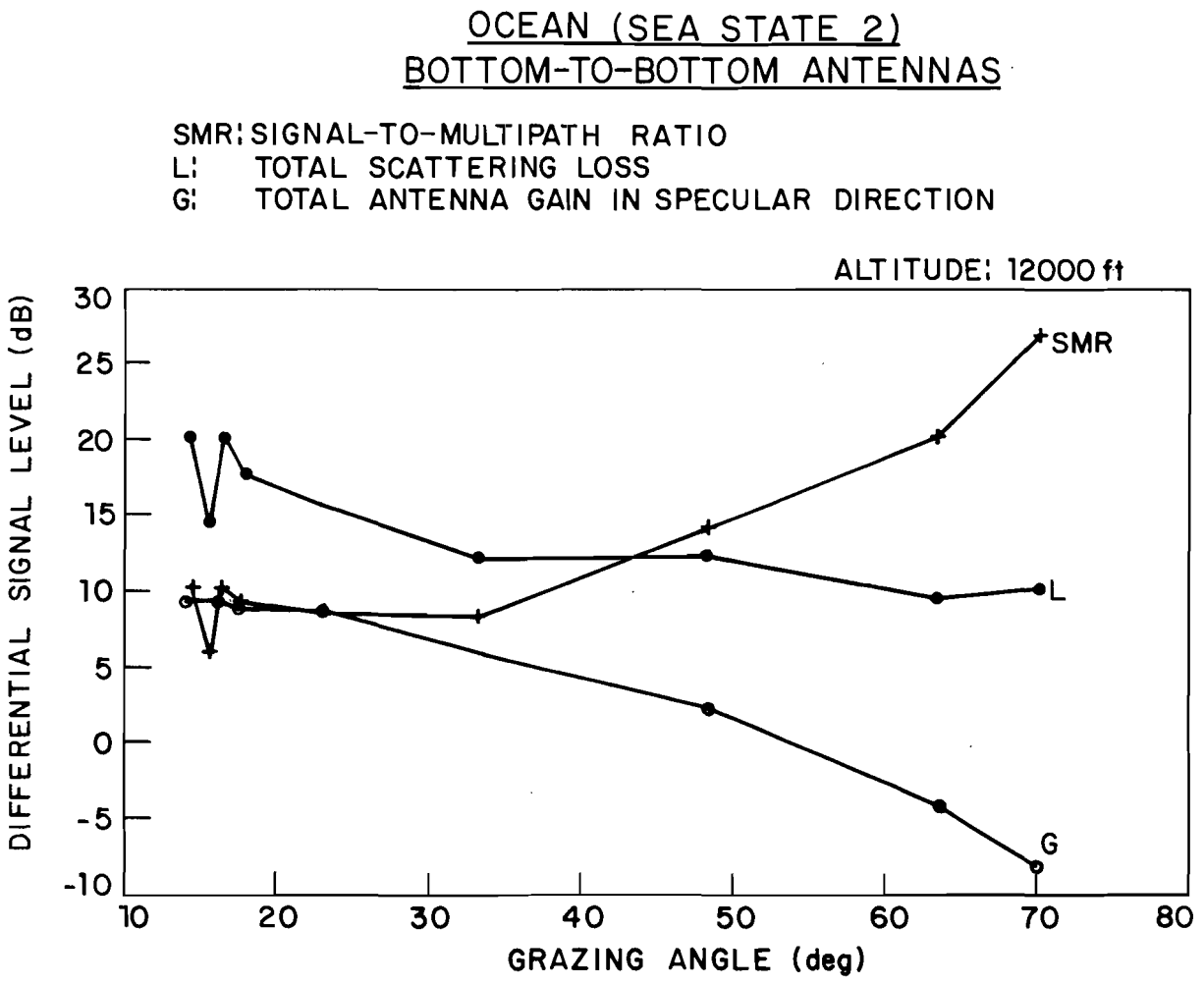


Fig. 5.14. Signal-to-Multipath Ratio, Antenna Gain, and Total Scattering Loss (Ocean Sea State 2).

variations rather than scattering loss variations. While the total loss curve did not vary greatly over most grazing angles (i.e., $20^{\circ}$ to $70^{\circ}$) its average value was raised by ~7 dB over that in the Sea State 1 data in Fig. 5.8 consequently improving the SMR curve. Again, the increased scattering loss at the lower grazing angles indicates the rough surface scattering of less energy in the direction of the receiving aircraft.

The signal-to-multipath ratio curves of Fig. 5.15 illustrate the SMR improvement due to different levels of antenna diversity as the grazing angle varied. A comparison of Figs. 5.15a and 5.15c with Figs.5.9a and 5.9c indicates that for grazing angles higher than $40^{\circ}$ the reduction in SMR improvement was probably due mostly to a decrease in the multipath level raising the SMR curves for the bottom-to-bottom link above the level shown in Fig. 5.9c. This was during a period when the aircraft flight paths diverged at the same angle for both data sets. The sharp drops in the SMR curves in Figs. 5.15a and 5.15b at $\sim 40^{\circ}$ indicate that the SMR improvements was apparently further reduced by a change in aircraft heading which increased the exposure of the top antenna on the transmitting aircraft. All top antenna links had a minimum median SMR $\geq$ 10 dB.

The median SMR curves in Fig. 5.16 show the same trends at all altitudes. At high grazing angles the SMR increased due to antenna nulls in the multipath direction in addition to scattering loss. At low grazing angles the SMR increased presumably due to increased scattering loss rather than a reduction in antenna gain. The minimum SMR of the lower altitudes was

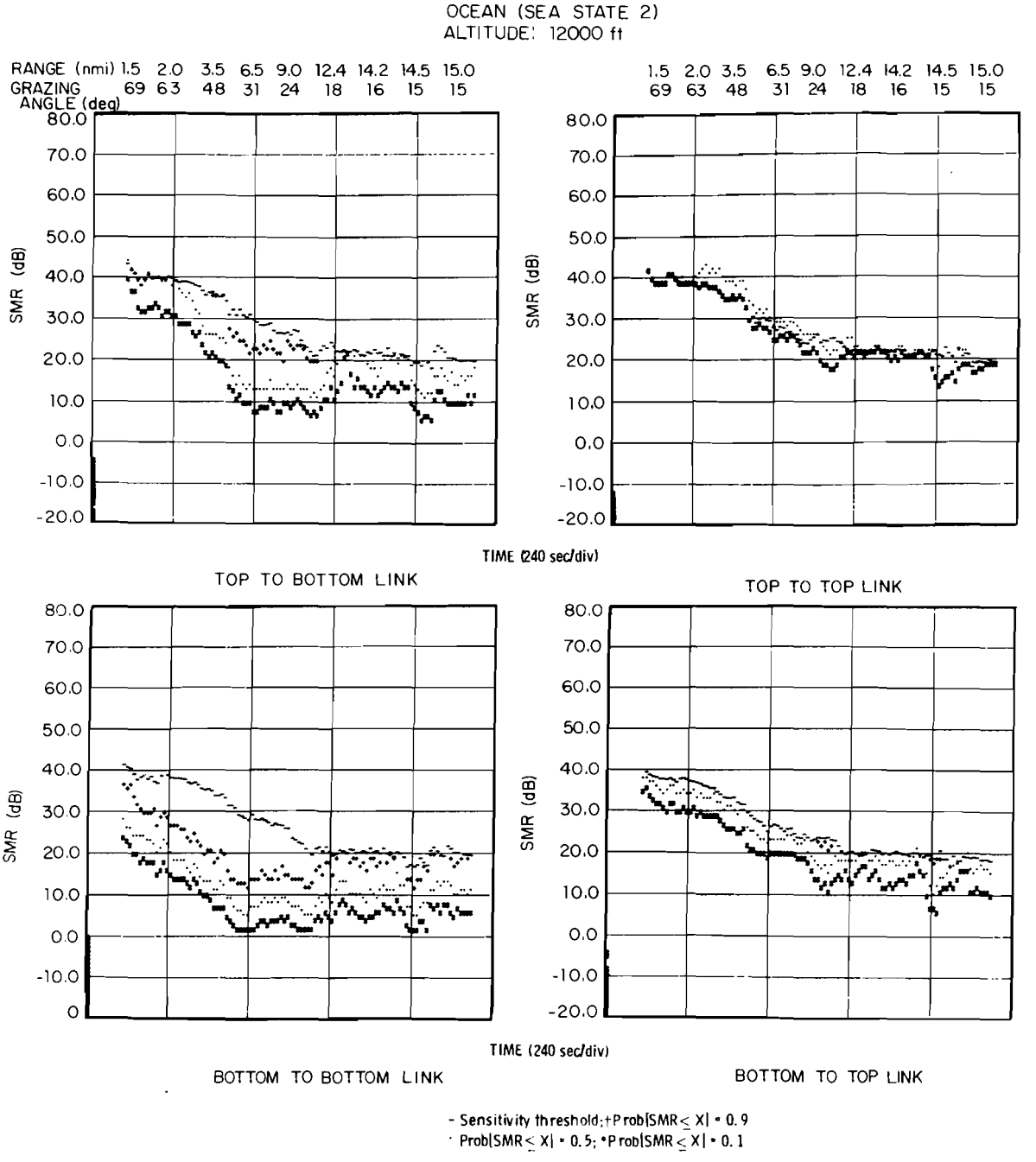


Fig. 5.15. Signal-to-Multipath Ratio Distribution Variations (Ocean Sea State 2).

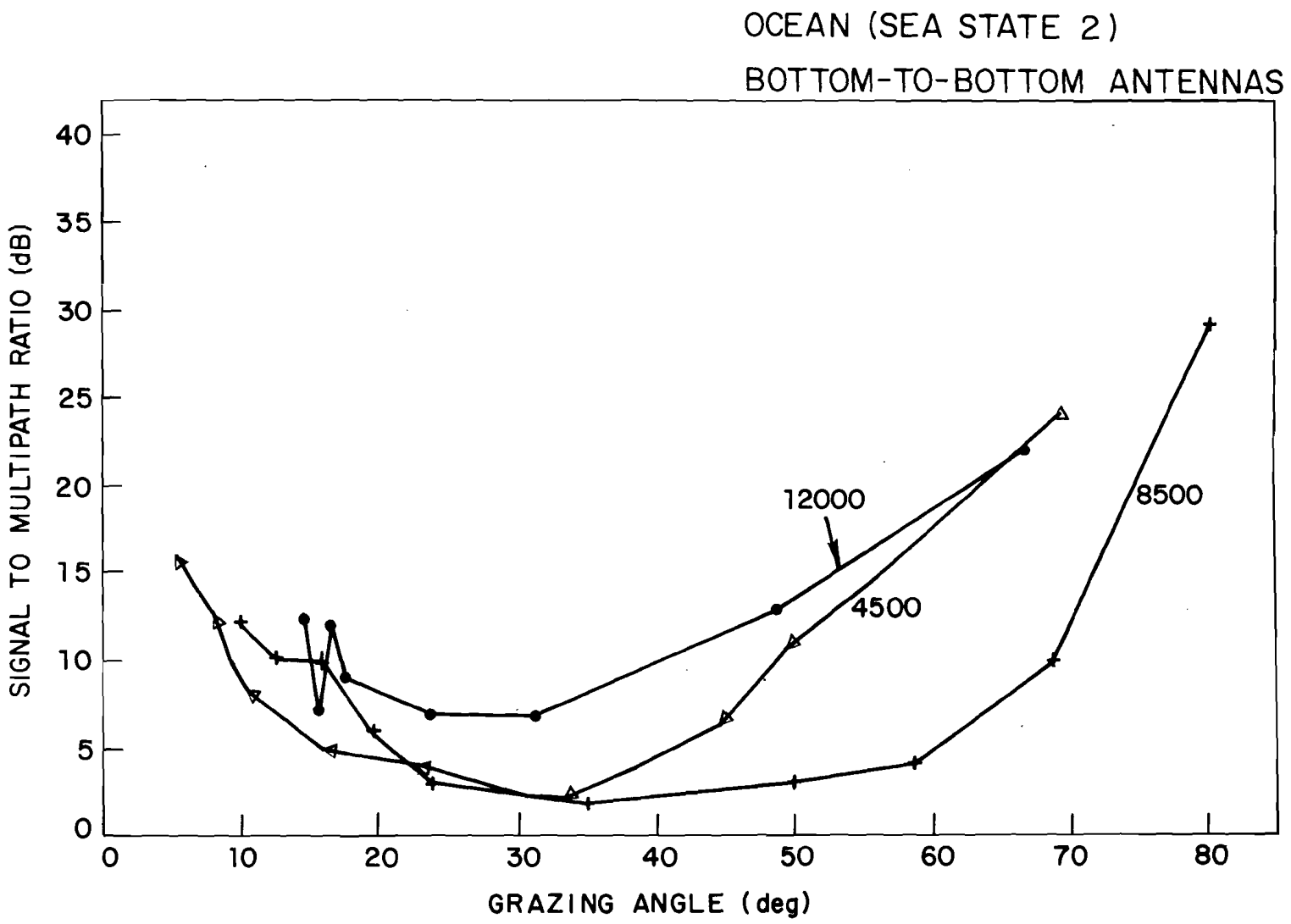


Fig. 5.16. Altitude Variations in Signal-to-Multipath Ratio (Ocean Sea State 2).

reduced by 4 dB compared to the higher altitude curve possibly since multipath signals were detected from a larger scattering area than at the high altitude. Other than small downward shift in minimum SMR the curves exhibited no significant altitude dependence.

The graphs in Fig. 5.17 indicate the SMR improvement with a top antenna link over the airspace for which data was obtained. While the bottom-to-bottom link was susceptible to relatively strong multipath interference over a wide volume of airspace, links which used at least a single top mounted antenna did not experience a high level of multipath intensity over any portion of the airspace investigated.

## 5.3 Frozen Lake Surface

While very strong multipath was scattered from the Sea State 1 ocean as described above, the surface was still rough enough to render the multipath samples taken 20 msec apart essentially uncorrelated as shown in Fig. 5.5. Data from flights over two frozen lakes indicated that not only was the multipath very strong but it was much more correlated than for rougher surfaces.

Fig. 5.18 shows the instantaneous multipath measured over a small lake (Lake Cochituate) at a grazing angle of $33^{\circ}$. When the scattering area was primarily over the frozen lake the multipath level at times exceeded the direct signal level by as much as 9 dB on the bottom-to-bottom antenna link. As indicated in Fig. 5.18a the use of a top transmitting antenna provided significant reduction in the multipath.

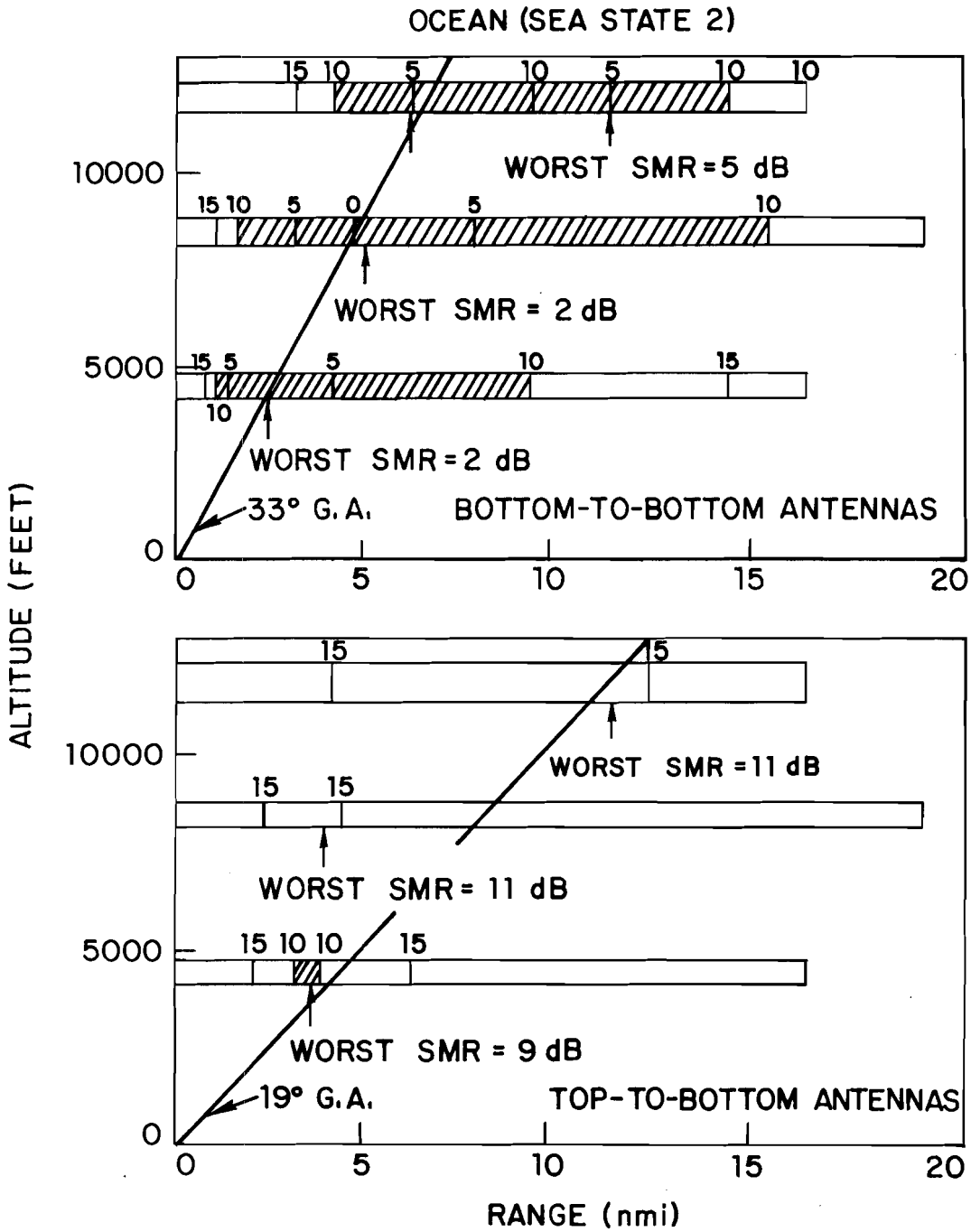


Fig. 5.17. Geometrical Dependence of Signal-to-Multipath Ratio (Ocean Sea State 2).

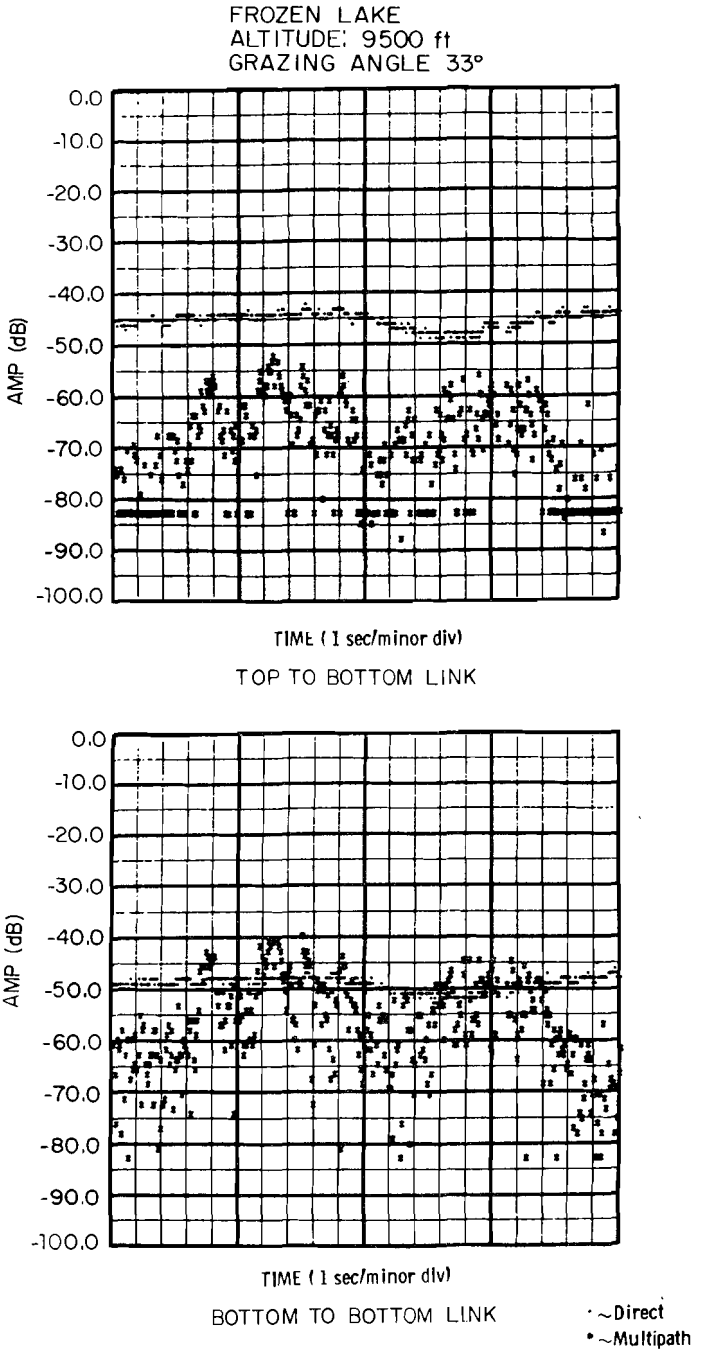


Fig. 5.18. Frozen Lake (High Grazing Angle) Multipath Instantaneous Signal Strength.

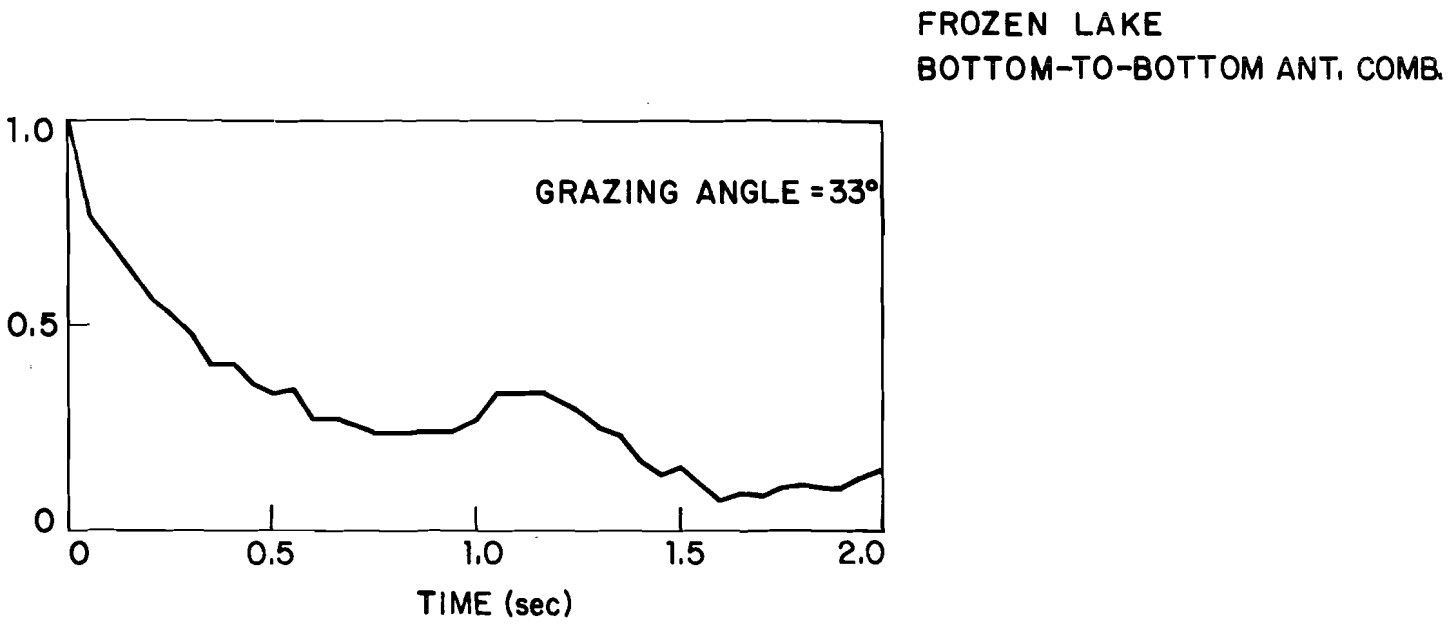


Fig. 5.19. Normalized Autocovariance (Frozen Lake).

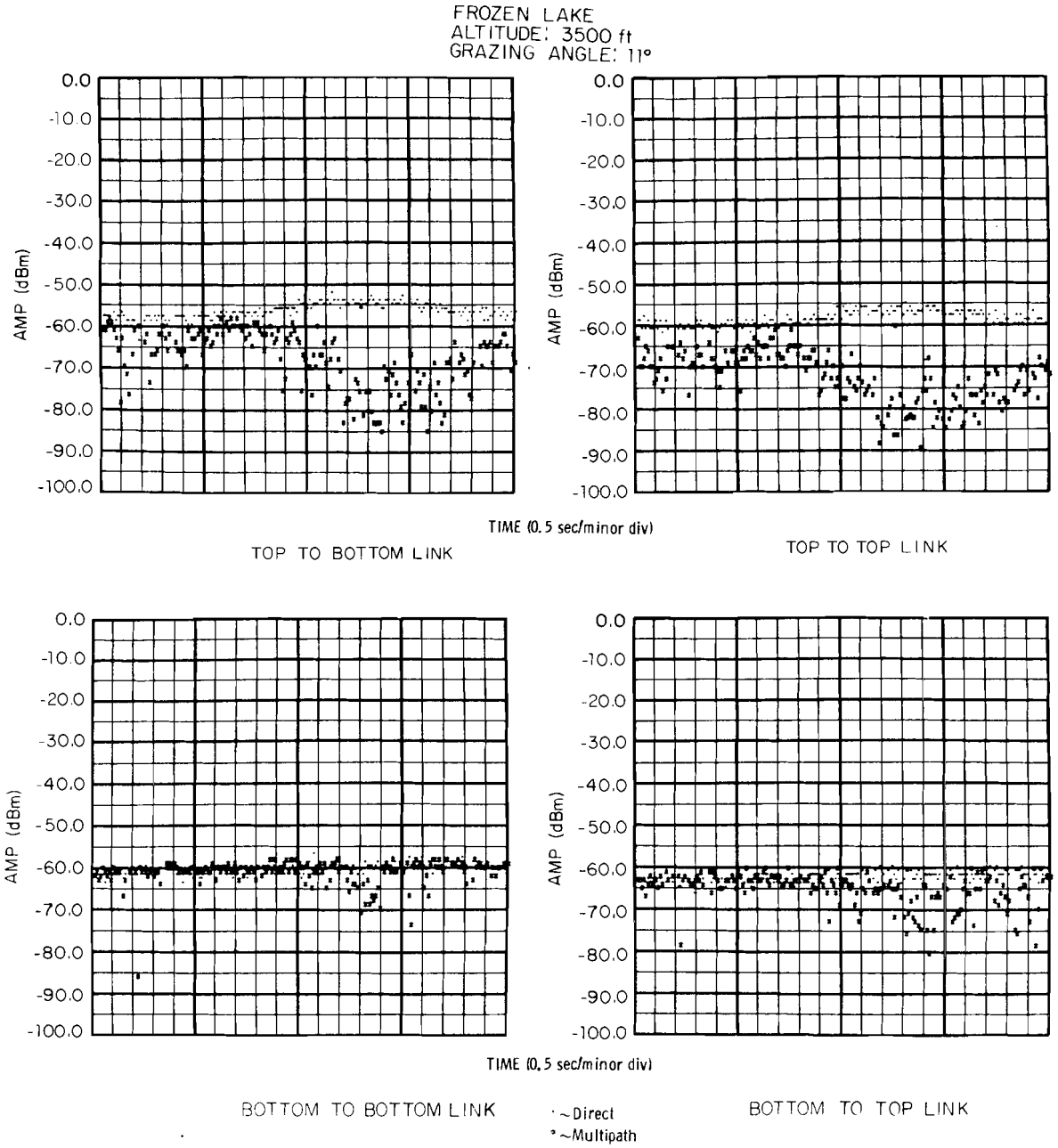


Fig. 5.20. Frozen Lake (Low Grazing Angle) Multipath Instantaneous Signal Strength.

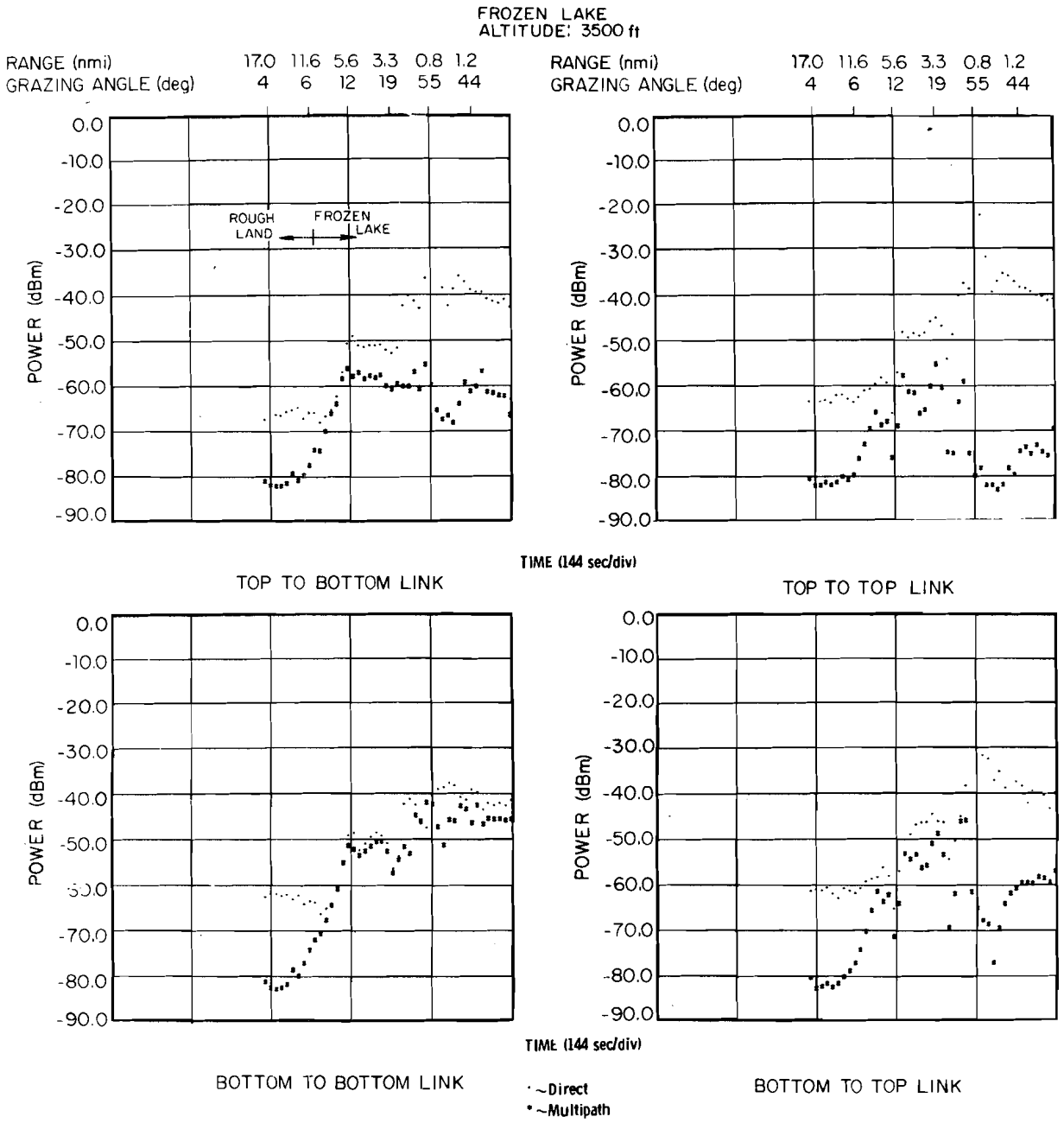


Fig. 5.21. Frozen Lake (Low Altitude) Multipath Average Signal Strength.

Fig. 5.19 shows the correlation observed between the multipath samples shown in Fig. 5.18. Multipath samples taken 1.25 seconds apart were somewhat correlated. A comparison with the Sea State 1 data in Fig. 5.5 indicates the degree of increased correlation as surface roughness decreased from waves 1.5 feet high peak-to-peak to a nearly flat surface.

The lower grazing angle data in Fig. 5.20 was collected at an altitude of 3500 feet over Lake Champlain. Again, a high degree of correlation was observed between successive multipath samples received over the bottom-to-bottom antenna link. The poor performance of the top antenna in rejecting the multipath illustrates the degree to which the top antennas were exposed to the scattering area at a grazing angle of $11^{\circ}$. The drop in received multipath during the last 5 seconds of Figs. 5.20a and 5.20b was most likely due to a slight change in heading of the transmitting aircraft which caused the top antenna to be more shielded, by the aircraft structure, from the active scattering surface.

The effect of aircraft heading on antenna shielding is shown in Fig. 5.21. The aircraft were initially converging at $\sim 63^{\circ}$ until a range of 5.6 nmi when a heading change reduced the angle of convergence to $\sim 40^{\circ}$. At a range of roughly 1.2 nmi the aircraft heading changed such that they were diverging at $19^{\circ}$. Also, during the first portion of the flight up to $\sim$300 seconds the aircraft were over land accounting for the very low multipath observed initially. As soon as the scattering area was primarily over the frozen lake surface the multipath level rose sharply. The low grazing angle and large converging aspect angle caused a significant degrada-

tion in the performance of the top antenna links in rejecting multipath. The first heading change caused the top transmitting antenna to become slightly more shielded resulting in a noticable reduction in the multipath for the top-to-bottom and top-to-top antenna links. As the aircraft approached and departed from the closest point the high grazing angles reduced the multipath received on all four antenna links. After diverging slowly to 3 miles the aircraft flew a nearly parallel flight. The increased multipath reduction for the small diverging angle is very evident in the significant increase in SMR for the top antenna links in Fig. 5.21. This was most likely due to increased wing shielding of the top antennas.

Data was also collected at an altitude of 1200 feet over a frozen (Lake Champlain). Again, strong multipath was observed on the bottom-to-bottom link as shown in Fig. 5.22b, but since the grazing angles were higher (minimum $11^{o}$) the top antenna links performed much better in reducing the received multipath level as indicated in Fig. 5.22a. The top-to-bottom and bottom-to-top links had minimum average SMR values of 7 dB and 8 dB respectively. While the top-to-top link had a minimum average SMR value of 17 dB. The top antennas were not particularly well shielded by the wings during this flight as a result of aircraft aspect angle since they were diverging at an angle of $\sim 54^{o}$.

5.4 Calm Lake Surface

During a portion of a flight which was intended to be primarily over a rough land surface a small lake was straddled which had a very smooth surface. As the location of the active scattering surface moved from perdominantly

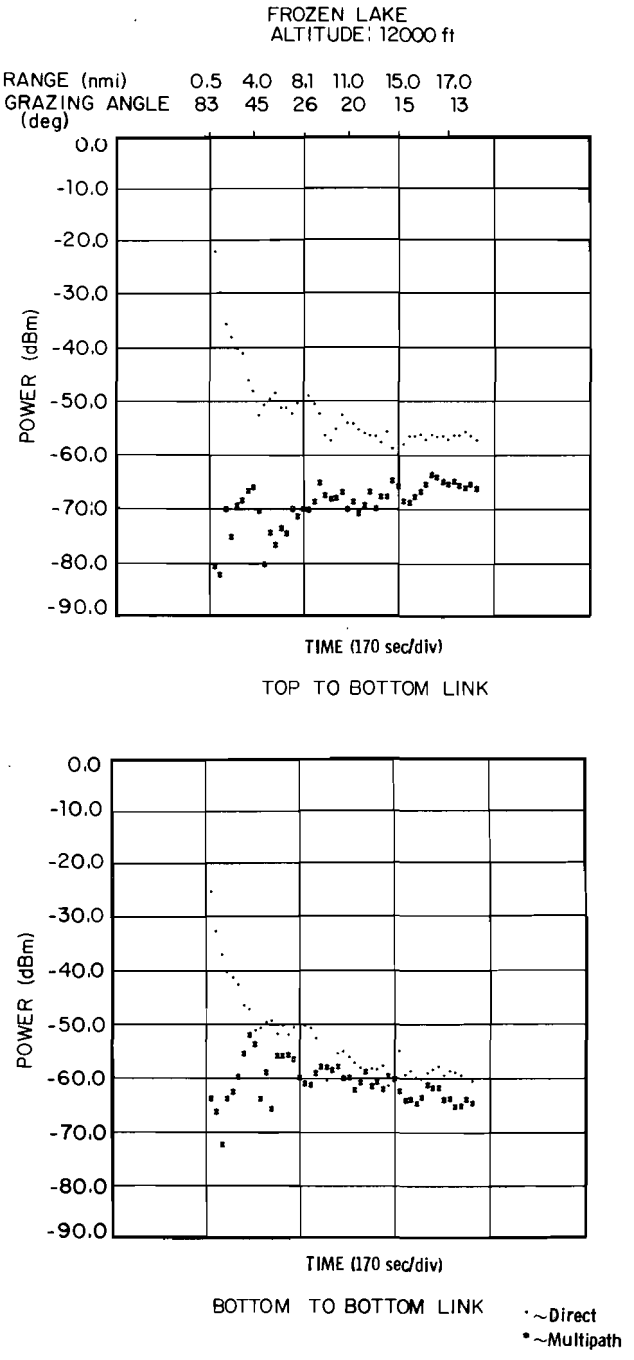


Fig. 5.22. Frozen Lake (High Altitude) Multipath Average Signal Strength.

land to predominantly water and back again very sharp changes took place in the nature of the multipath as shown in Fig. 5.23. When the active scattering surface was over the water, not only did the average multipath level rise by ~15 dB, but the samples became much more correlated exhibiting slightly weaker correlation than for the frozen lake shown in Fig. 5.19, but still significant for 1.25 seconds. Since the grazing angle was relatively high ($33^{o}$) the top antennas were very effective in reducing the received multipath. The lowest median SMR observed on a link using a top antenna was observed on the top-to-bottom link and was 17 dB, a 12 dB improvement in the average SMR value over the bottom-to-bottom antenna link. Since the data in Fig. 5.23 was taken from the same lake as the data in Fig. 5.18, it is interesting to observe that in the frozen lake multipath of Fig. 5.18b there was a ~10 dB increase in the multipath level over the calm lake multipath in Fig. 5.23 due most likely to the smoother surface afforded by the frozen lake.

## 5.5 Smooth Land Surfaces

Data collected over the Mojave Desert in California and the flat plain of central Kansas exhibited very similar properties. For an altitude of 14,500 feet (12,000 feet above the surface) the desert time-raster plot is shown in Fig. 5.24a while at 7,500 ft the plot in Fig. 5.24b was observed. At the high altitude the multipath tracks were similar to those observed for the Sea State 1 ocean surface in Fig. 5.2 except that they were much weaker

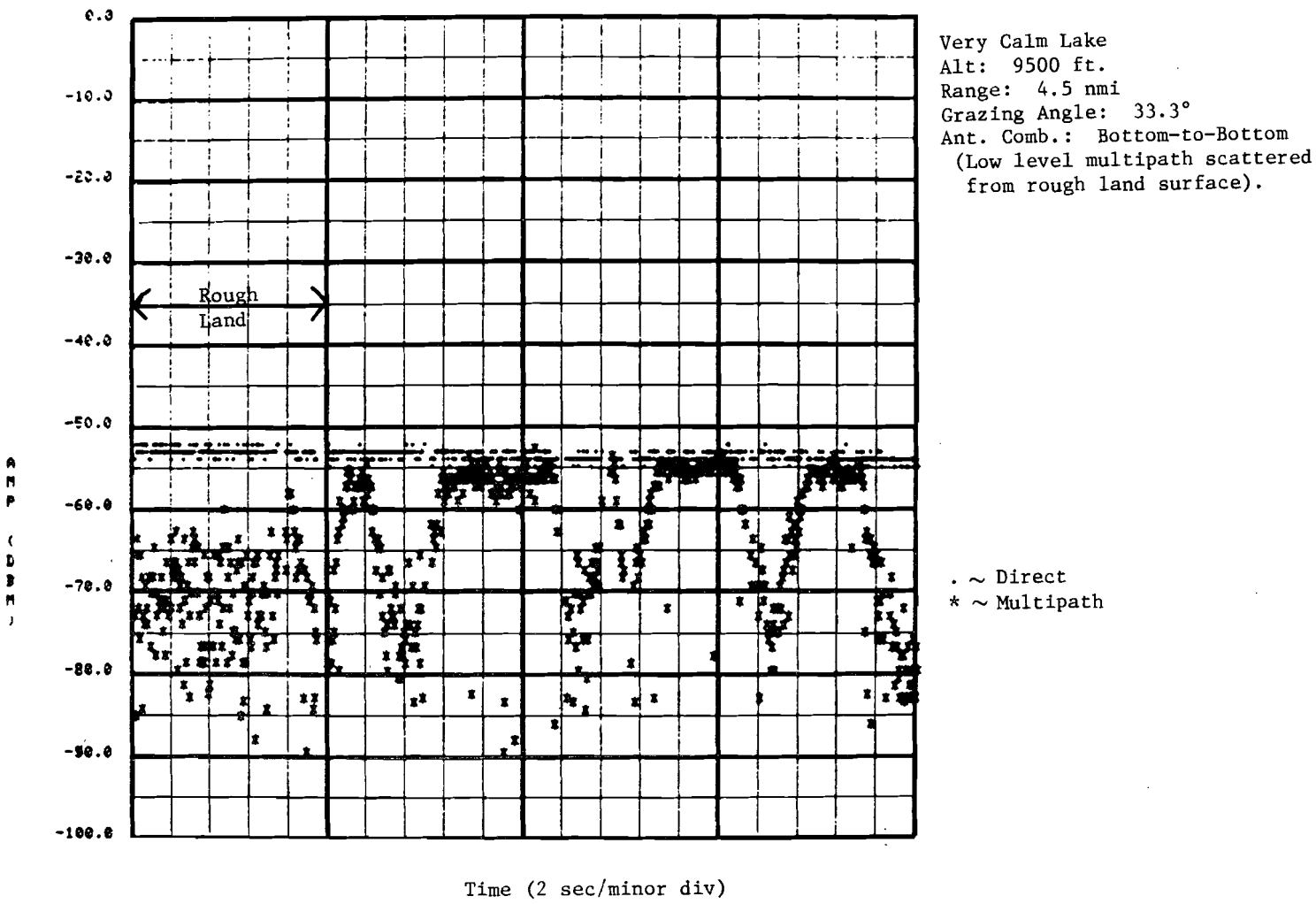


Fig. 5.23. Calm Lake Multipath Instantaneous Signal Strength.

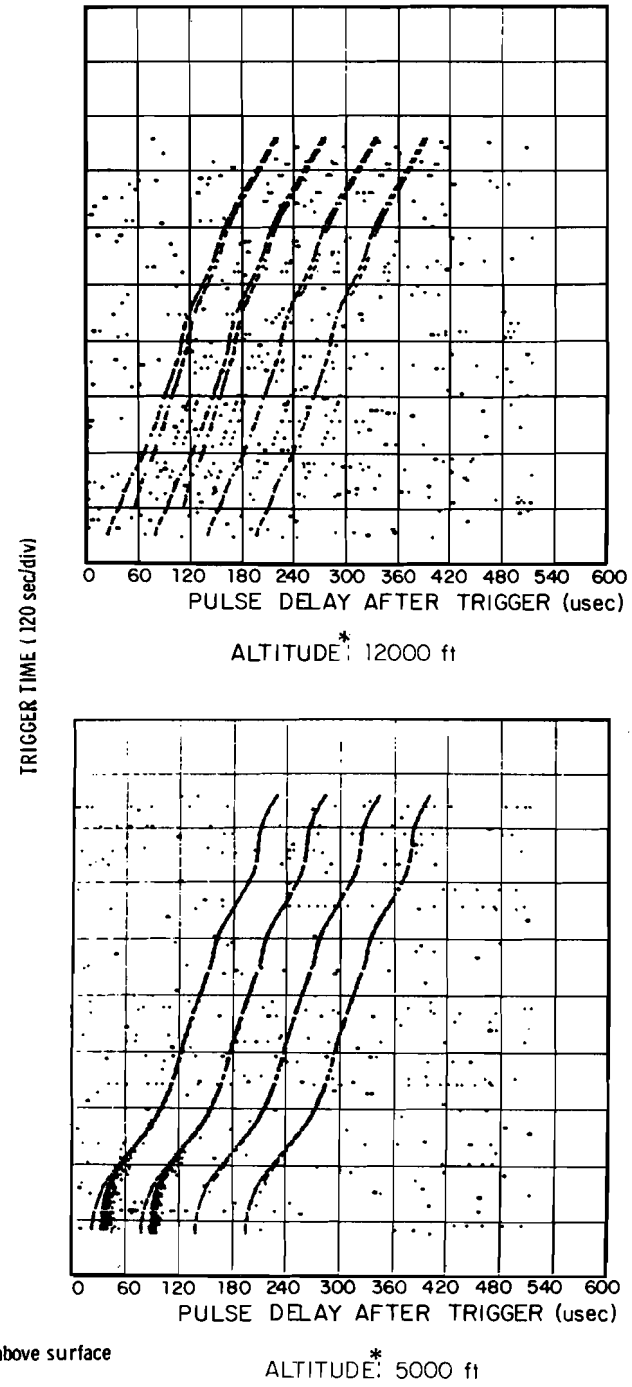


*Height above surface

Fig. 5.24. Desert Multipath Time-Raster.

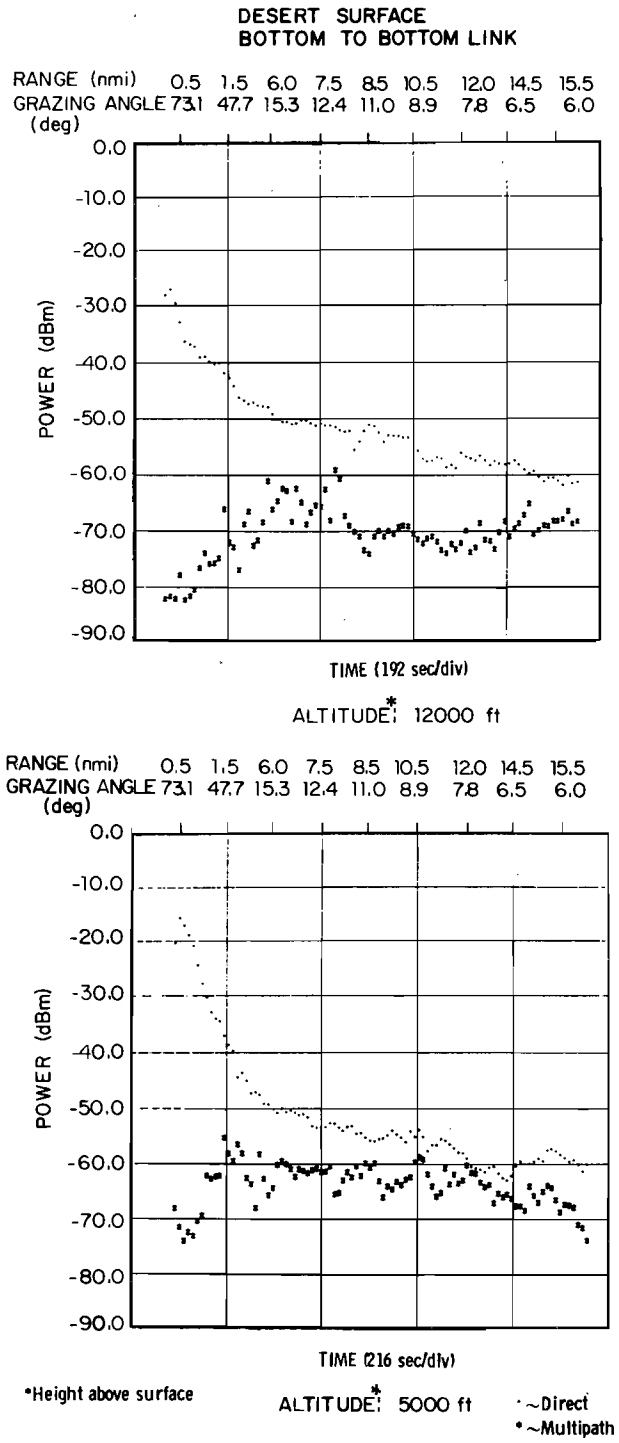


Fig. 5.25. Desert Multipath Average Signal Strength.

at the high grazing angles near the beginning of the flight. Also, the tracks for the top-to-bottom link did not become significant until the aircraft were much further apart. At the lower altitude the multipath tracks were no longer narrow tracks as in the higher altitude case but during the early portion of the flight were quite broad persisting for as much as 20 μsec. This indicated that although the multipath detected was very low level as subsequent data will show, signals were detected which were scattered from a larger area. While such tracks were indicative of multipath scattered from a rough surface, the rapidity with which the tracks became narrow as the aircraft diverged indicates that the surface was relatively smooth.

The average signal strength plots in Fig. 5.25 indicate that at higher grazing angles ($> 16^{\circ}$) the desert scattered multipath though not negligible was still relatively weak. However, at the lower grazing angles the multipath became relatively strong with respect to the direct signal, i.e., within 10 dB.

The SMR and scattering loss curves in Fig. 5.26 show that the total scattering loss was much higher than for the water surfaces in Figs. 5.8 and 5.14. The increased reflection loss was due most likely to increased absorption loss by the sandy desert surface since the smooth surface would not scatter much incident energy away from the specular direction toward the receiving aircraft. Furthermore, aircraft aspect angle cannot account for the reduced multipath strength since the aircraft were diverging at the same angle as in the previous flights. A higher absorption loss is consistent with theoretical considerations (Ref. 2).

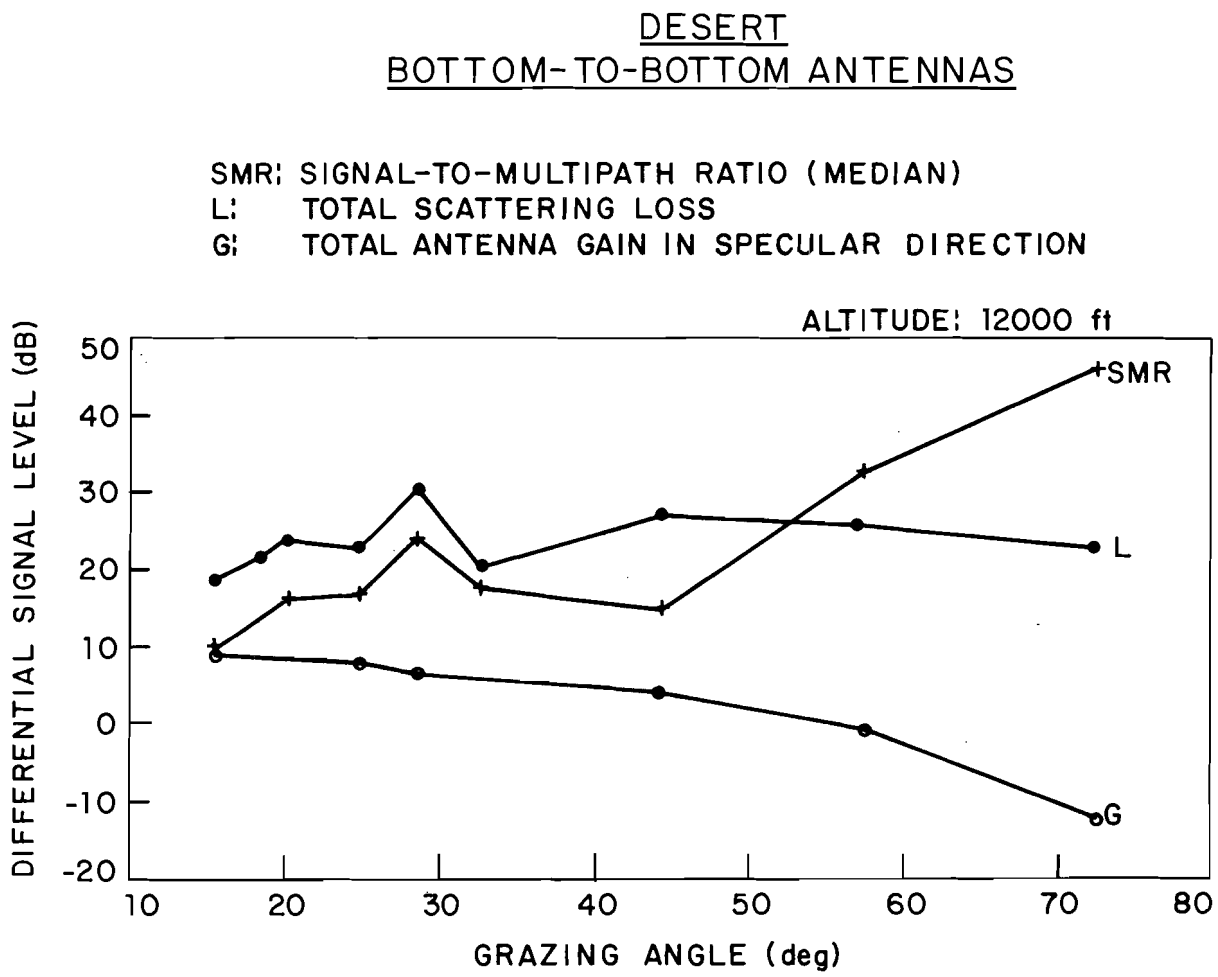


Fig. 5.26. Signal-to-Multipath Ratio, Antenna Gain, and Total Scattering Loss (Desert).

As in the previous data the SMR decreased with decreasing grazing angle at the higher grazing angles reflecting the increase in antenna gain in the multipath direction. However, unlike the previous data the SMR and scattering loss decreased at lower grazing angles. This was probably due to the smooth surface which scattered more energy in the direction of the receiving aircraft at the lower grazing angles than the rougher surfaces previously considered.

Figs. 5.27 and 5.28 summarize the measured SMR data for all antenna combinations over a wide range in grazing angle. In Fig. 5.27c the median SMR was relatively high (i.e., > 10 dB) for grazing angles greater than $\sim 16^{\circ}$ while Fig. 5.28c indicates predominantly low SMR values at lower grazing angles for the bottom-to-bottom antenna link. While the top antenna link curves in Fig. 5.27 all indicate very high multipath rejection, the top antenna link curves in Fig. 5.28 show median SMR values below the 10 dB level for grazing angles lower than $9^{\circ}$.

The SMR curves in Fig. 5.29 show relatively little dependence on altitude. These curves differ from previous curves in that the SMR continued to decrease at lower grazing angles due to the smoothness of the scattering surface as noted earlier.

The data collected over the flat plain of central Kansas exhibited scattering properties very similar to the data from the desert except that the level of multipath was slightly higher as shown by comparing the average signal strength curves in Figs. 5.25a and 5.30. There was probably less absorption loss over Kansas plain due to the moisture in the foliage present. Altitude dependence was similar to the desert case shown in Fig. 5.29.

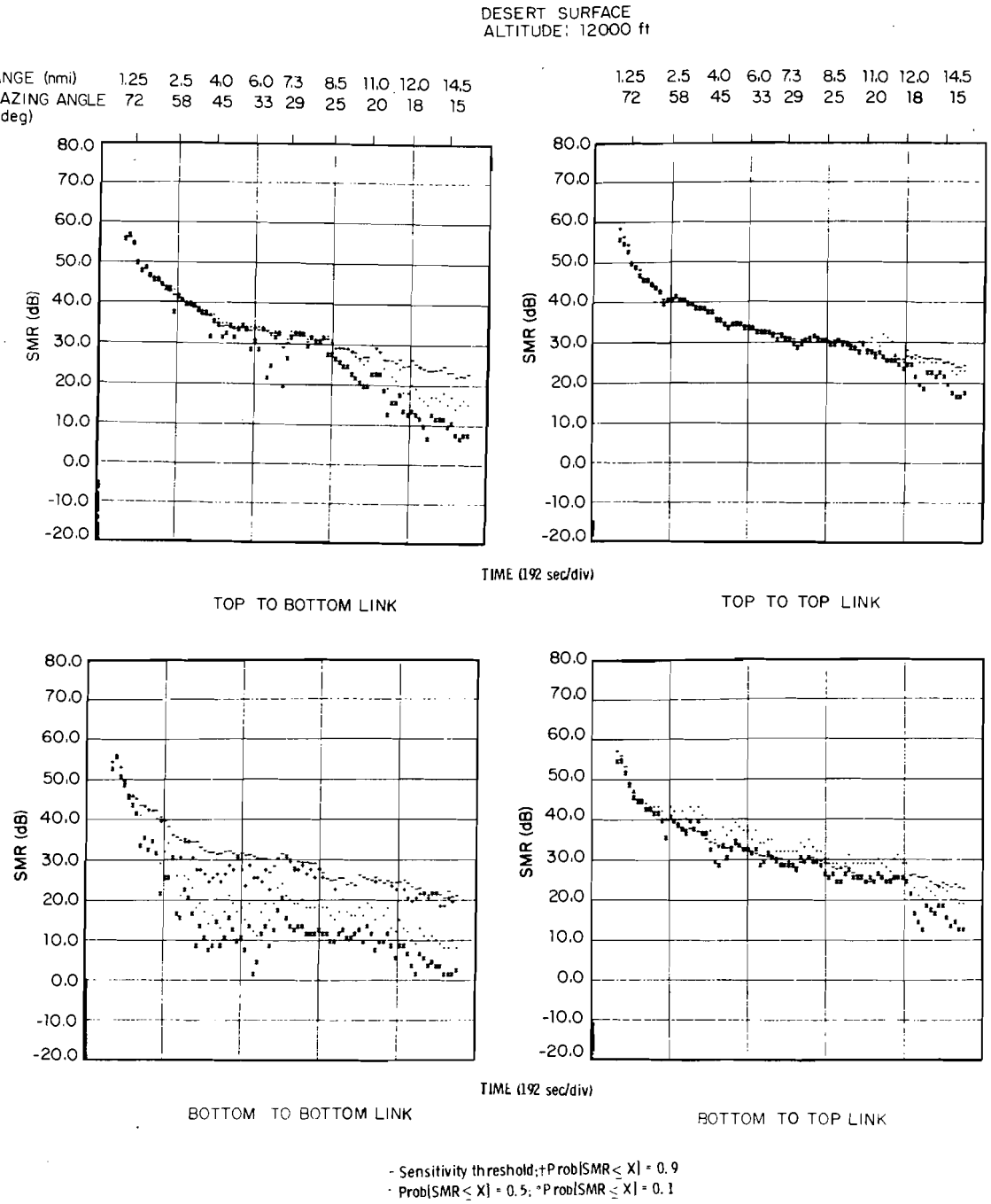


- Sensitivity threshold; †Prob[SMR ≤ X] = 0.9
· Prob[SMR ≤ X] = 0.5; *Prob[SMR ≤ X] = 0.1

Fig. 5.27. Signal-to-Multipath Ratio Distribution Variations (Desert, High Grazing Angles).

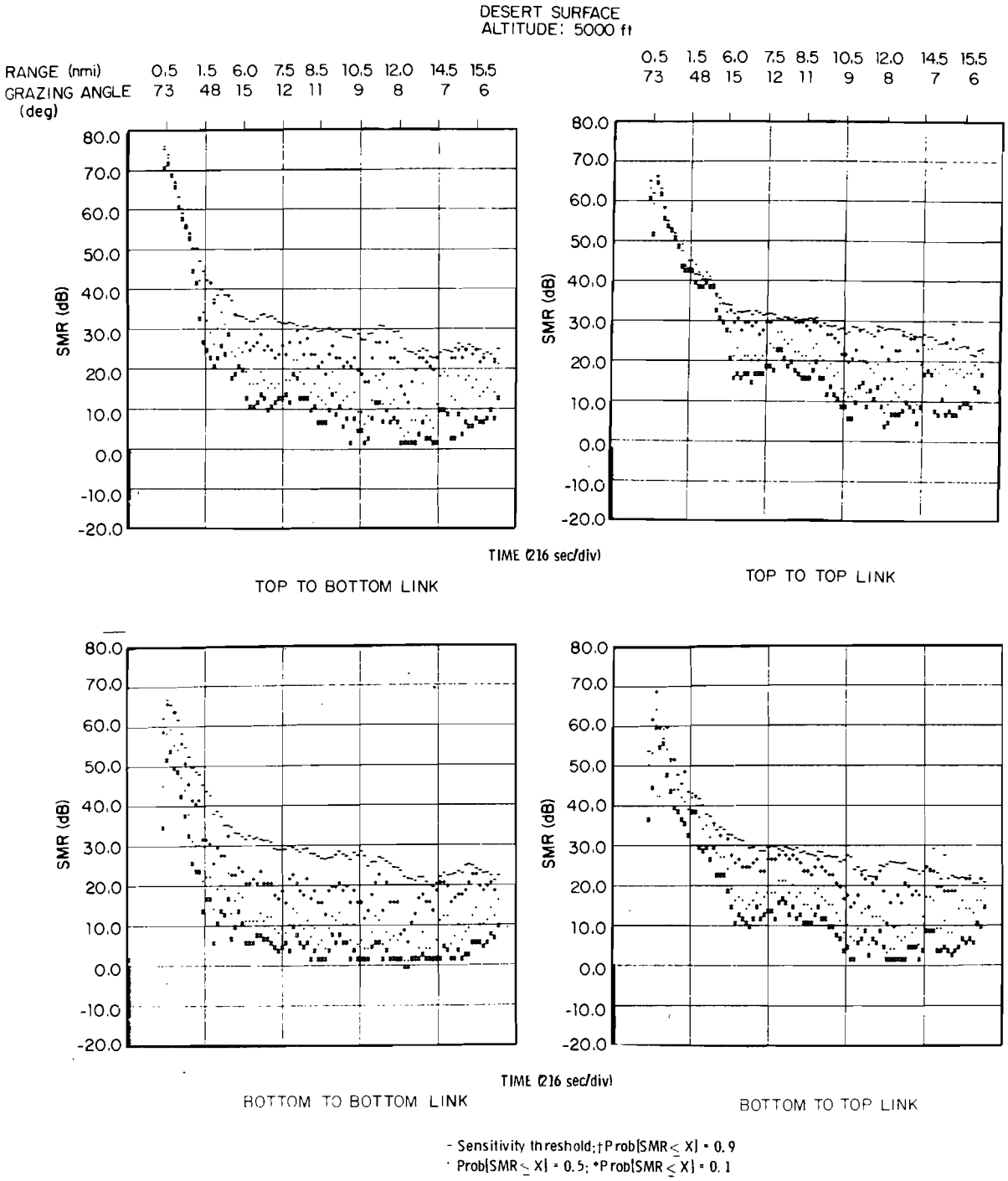


Fig. 5.28. Signal-to-Multipath Ratio Distribution Variations (Desert, Low Grazing Angles).

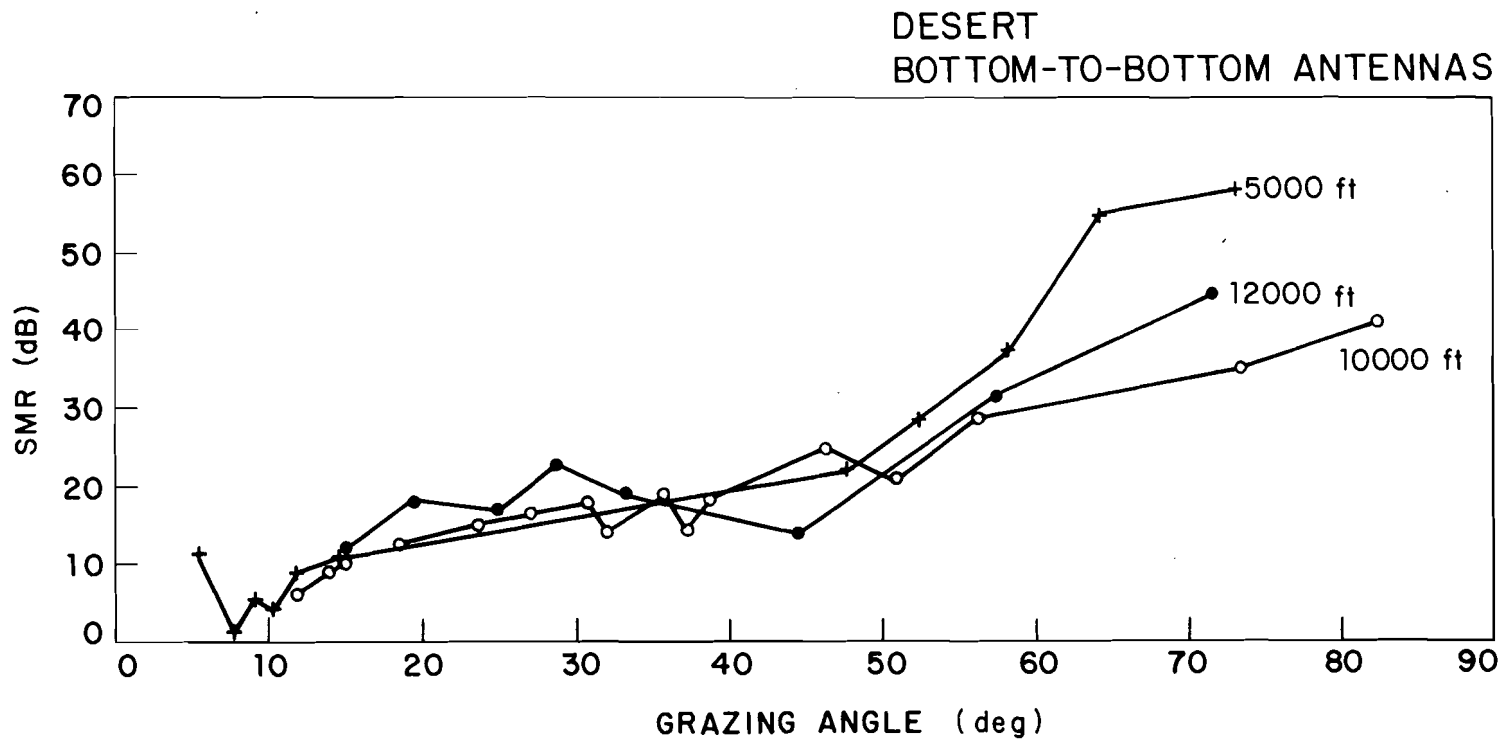


Fig. 5.29. Altitude Variations in Signal-to-Multipath Ratio (Desert).

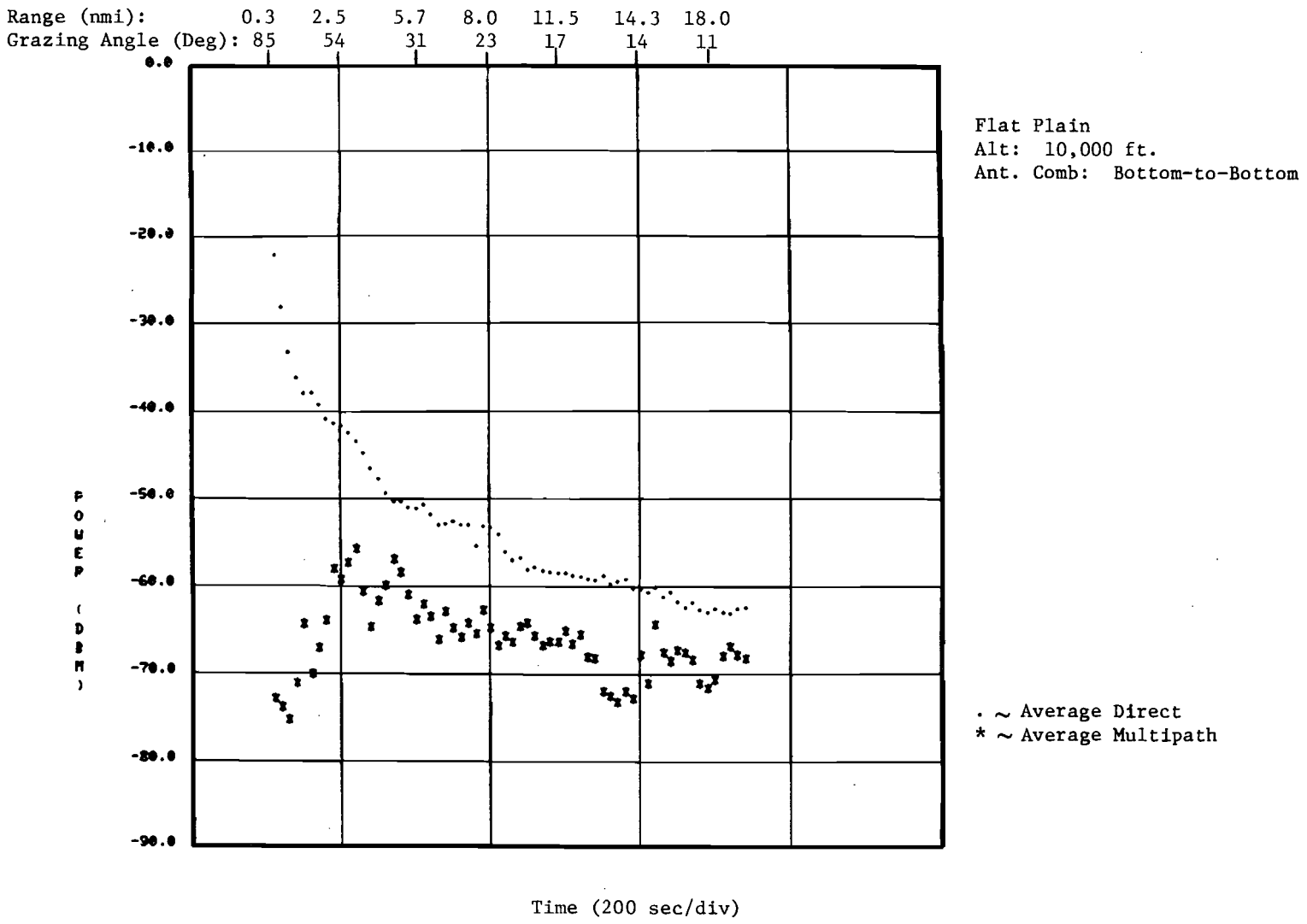


Fig. 5.30. Flat Plain Multipath Average Signal Strength.

The multipath signals scattered from the surface of both the desert and the flat plain were well defined pulses as in Fig. 5.1a with the multipath pulse generally several dB lower than the direct pulse.

The correlation properties of data from both terrains are summarized in Fig. 5.31. Most of the multipath pulse sequences were weakly correlated as shown by the lower curve. Occasionally, bursts of multipath pulses were observed which showed very strong correlation as indicated by the upper curve. Such instances were most likely due to locally very smooth areas over which the active scattering area passed.

Figs. 5.32 and 5.33 summarize the variations in SMR as explicit functions of aircraft geometry and antenna combination for the desert and flat plain surfaces respectively.

5.6 Rough Land Surfaces

In this section multipath data for very rough scattering surfaces is presented. Flights were conducted over the suburban Boston area and the White Mountains of New Hampshire. In all of these flights the multipath observed was not pulselike but rather appeared as weak noise level of long duration which eventually decayed as pictured in Figs. 4.2 and 4.3b. The dispersed nature of the multipath is clearly brought out in Fig. 5.34 where the multipath tracks for the bottom-to-bottom link were much broader than for smooth water or land surface as in Figs. 5.2 or 5.24a. Successive multipath samples varied rapidly over a 20 dB range as in the first ten seconds of Fig. 5.23. The samples were essentially uncorrelated exhibiting less correlation than shown in Fig. 5.5b.

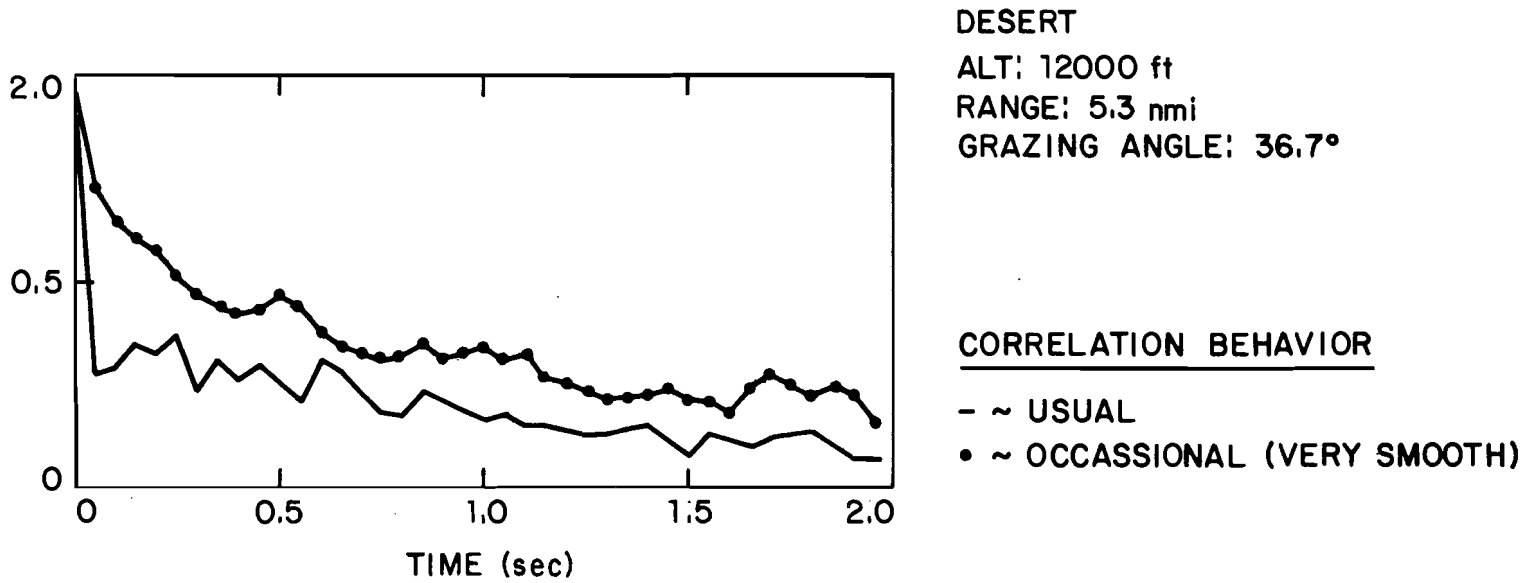


Fig. 5.31. Normalized Autocovariance (Smooth Land).

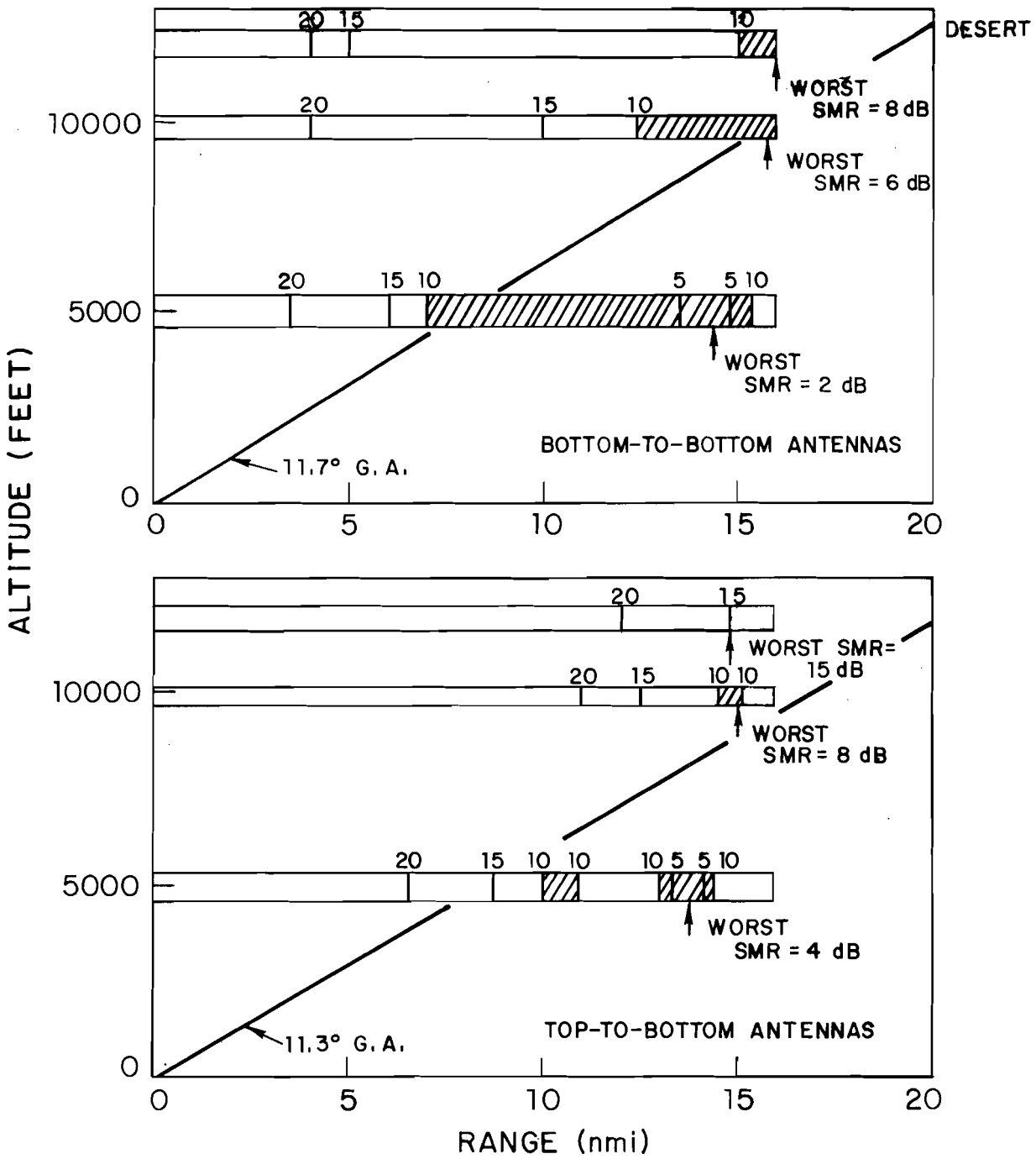


Fig. 5.32. Geometrical Dependence of Signal-to-Multipath Ratio (Desert).

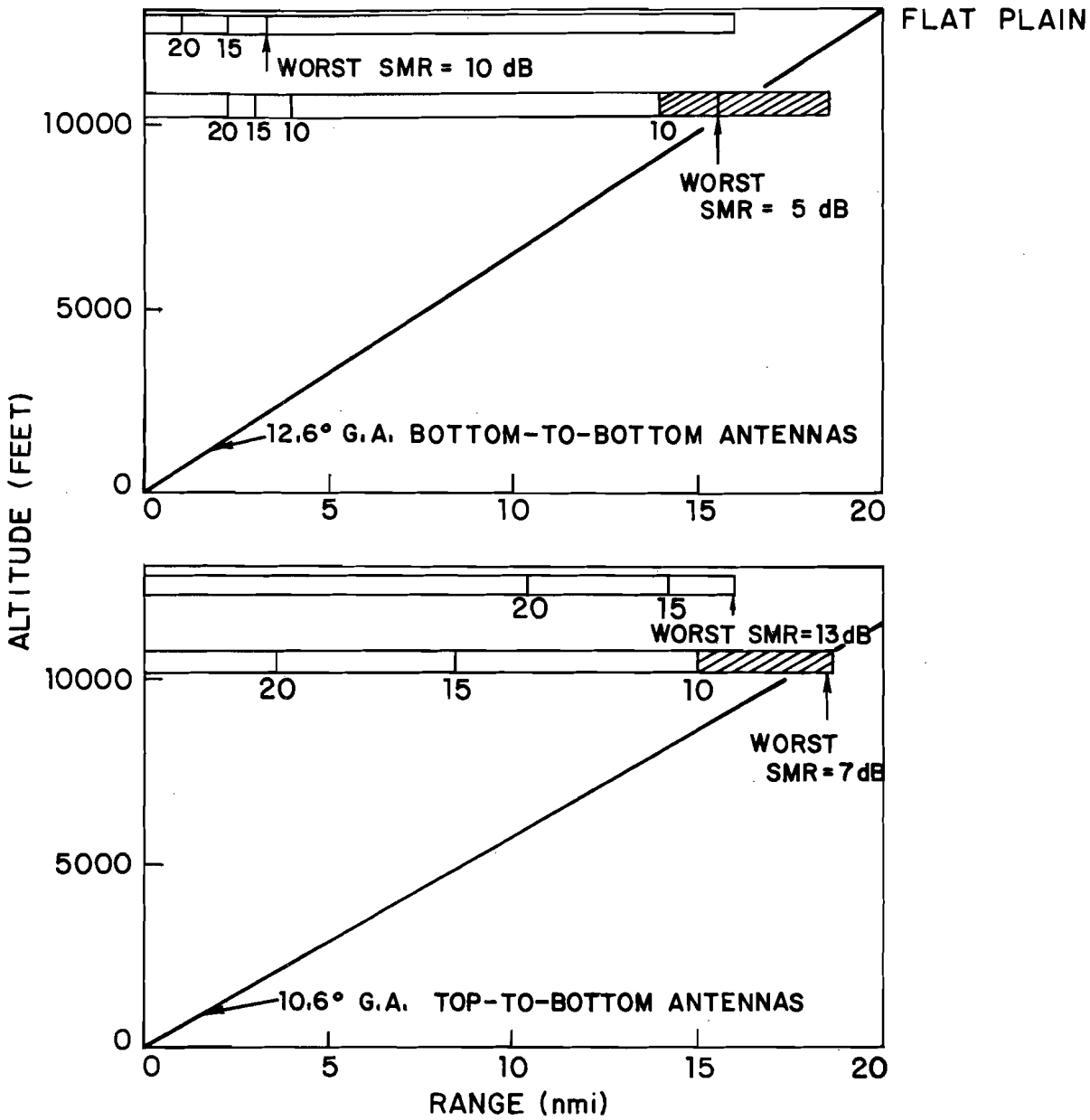


Fig. 5.33. Geometrical Dependence of Signal-to-Multipath Ratio (Flat Plain).

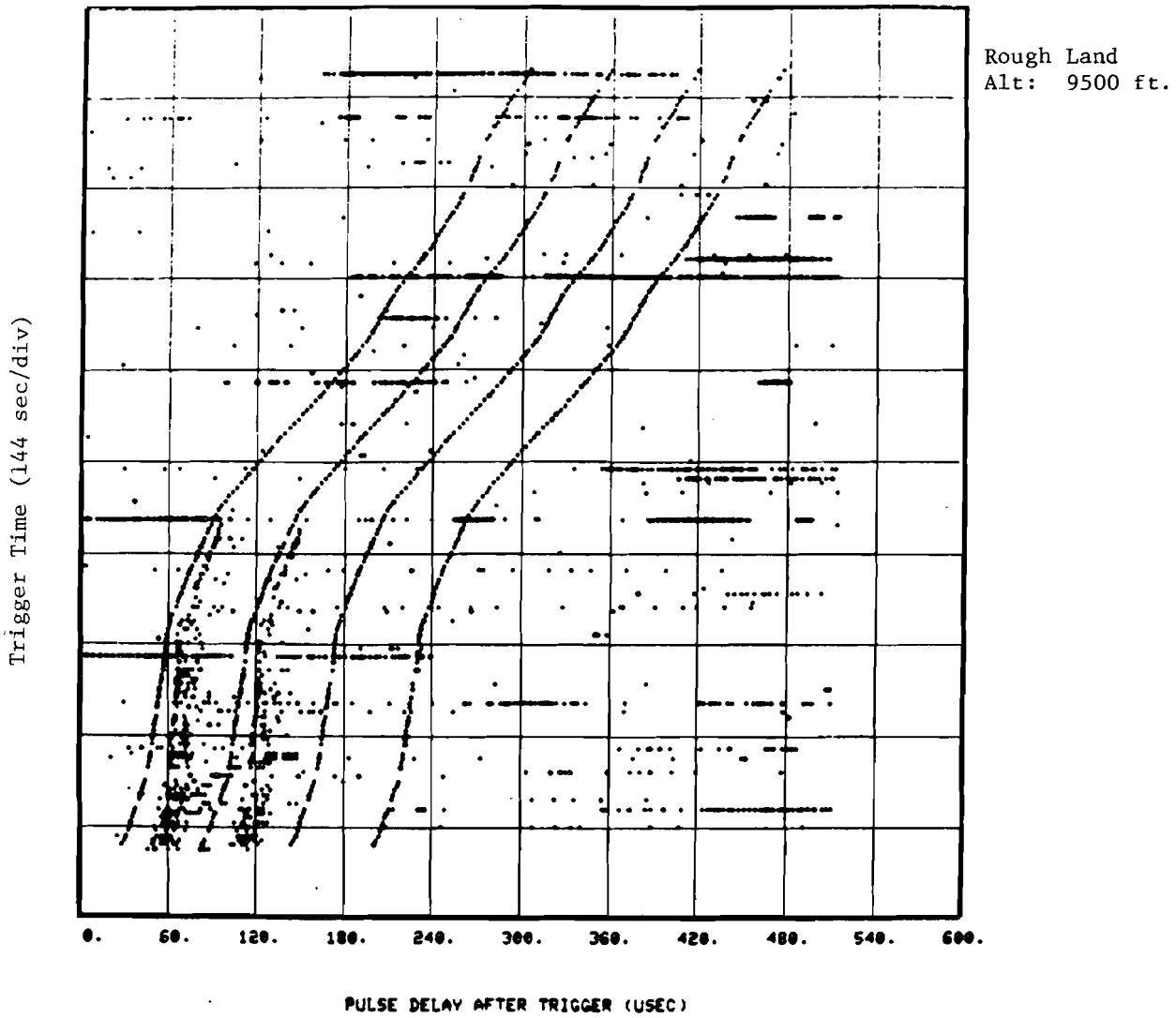


Fig. 5.34. Rough Land Multipath Time-Raster.

Fig. 5.35 shows SMR distribution variations for one of the suburban flights. Fig. 5.36 shows an average signal strength plot for the same flight. Except for the indicated lake and ocean regions, the multipath was essentially negligible. (At the high grazing angle in the lake region the top-to-bottom antenna link provided a 10 dB SMR improvement while at the lower grazing angle of the ocean section there was only a 5 dB improvement). The data in Fig. 5.37 was gathered over the same area covered with snow. While the multipath from the snow covered land was about 7 dB stronger than in Fig. 5.36 it was still very weak with respect to the direct signal.

In Figs. 5.36 and 5.37 the multipath level changed very rapidly when a water surface was encountered. The lake straddled (Lake Cochituate) was quite small. The stronger multipath signals received under these conditions were discussed above in Sections 5.3 and 5.4 in connection with Figs. 5.18 and 5.23 (which correspond respectively to the lake regions in Figs. 5.36 and 5.37).

The average signal strength plot in Fig. 5.38 indicates that negligible multipath was scattered from a forest covered mountain area. The data in this section implies that multipath scattered from rough land surfaces is not a significant form of interference.

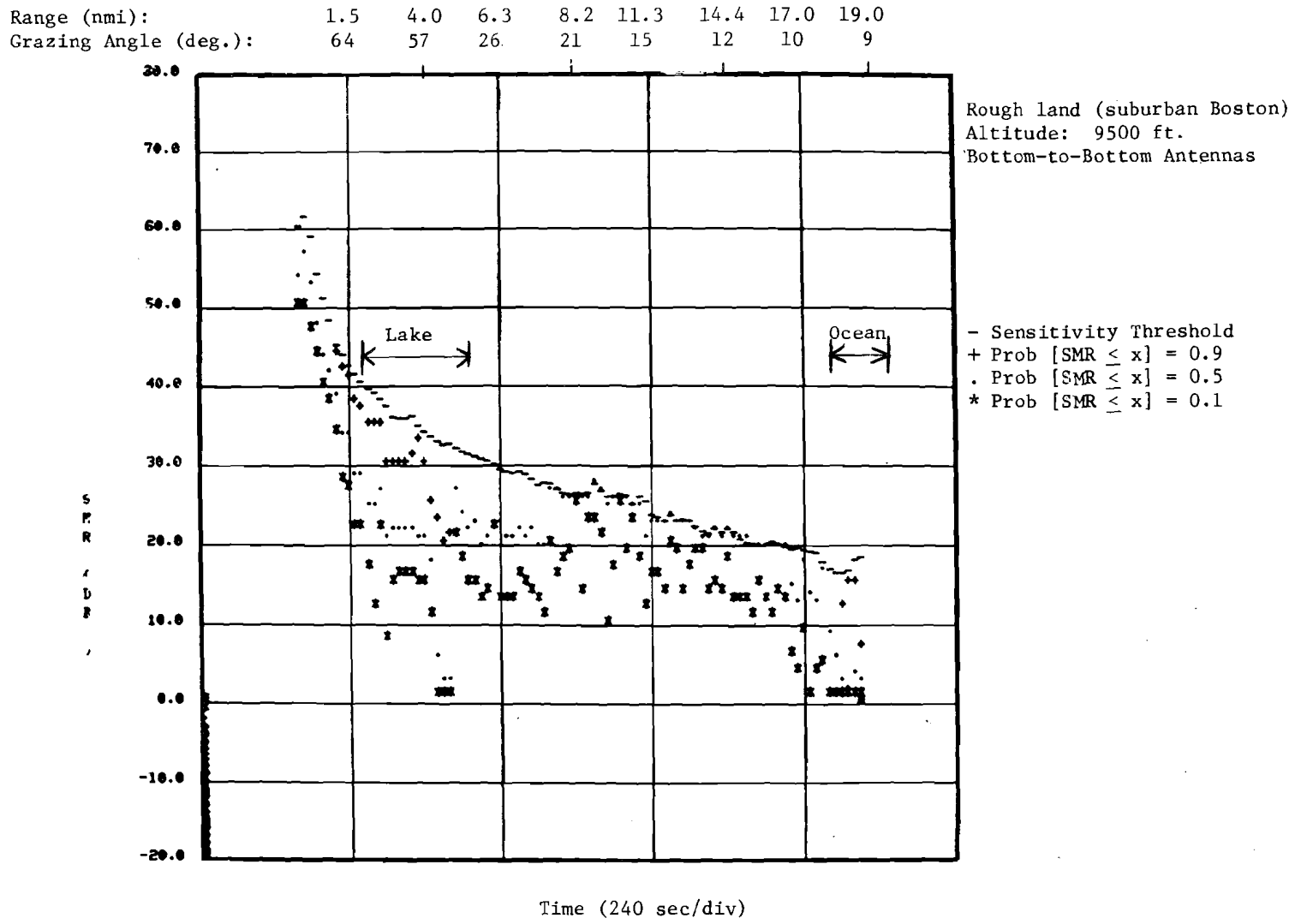


Fig. 5.35. Signal-to-Multipath Ratio Distribution Variation (Rough Land).

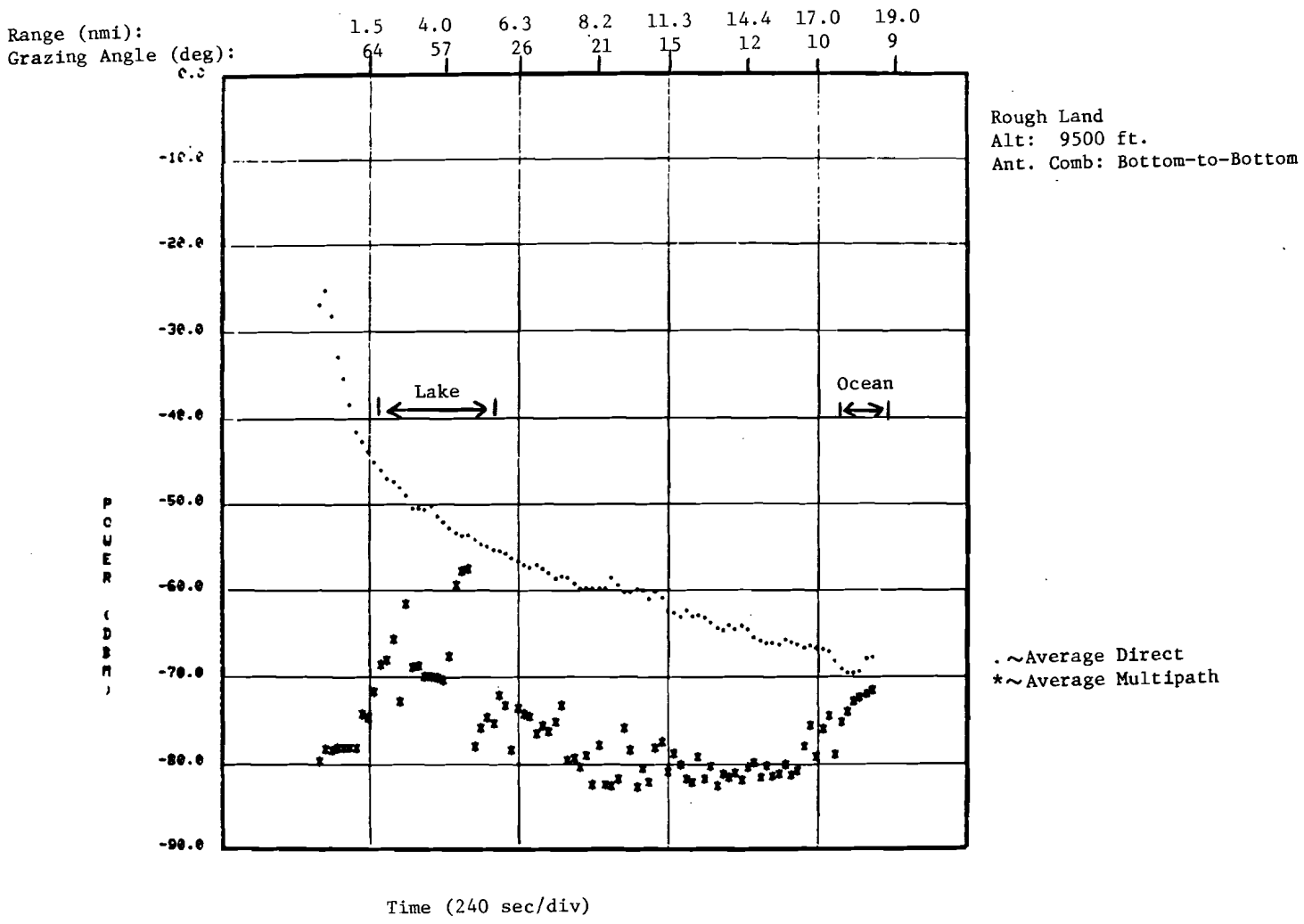


Fig. 5.36. Rough Land Multipath Average Signal Strength.

| | | | | | | | | |
|---|---|---|---|---|---|---|---|---|
| Range (nmi): | 1.2 | 3.5 | 6.2 | 8.1 | 10.0 | 11.4 | 13.2 | 14.0 |
| Grazing Angle (deg): | 69 | 42 | 27 | 21 | 17 | 15 | 13 | 12 |

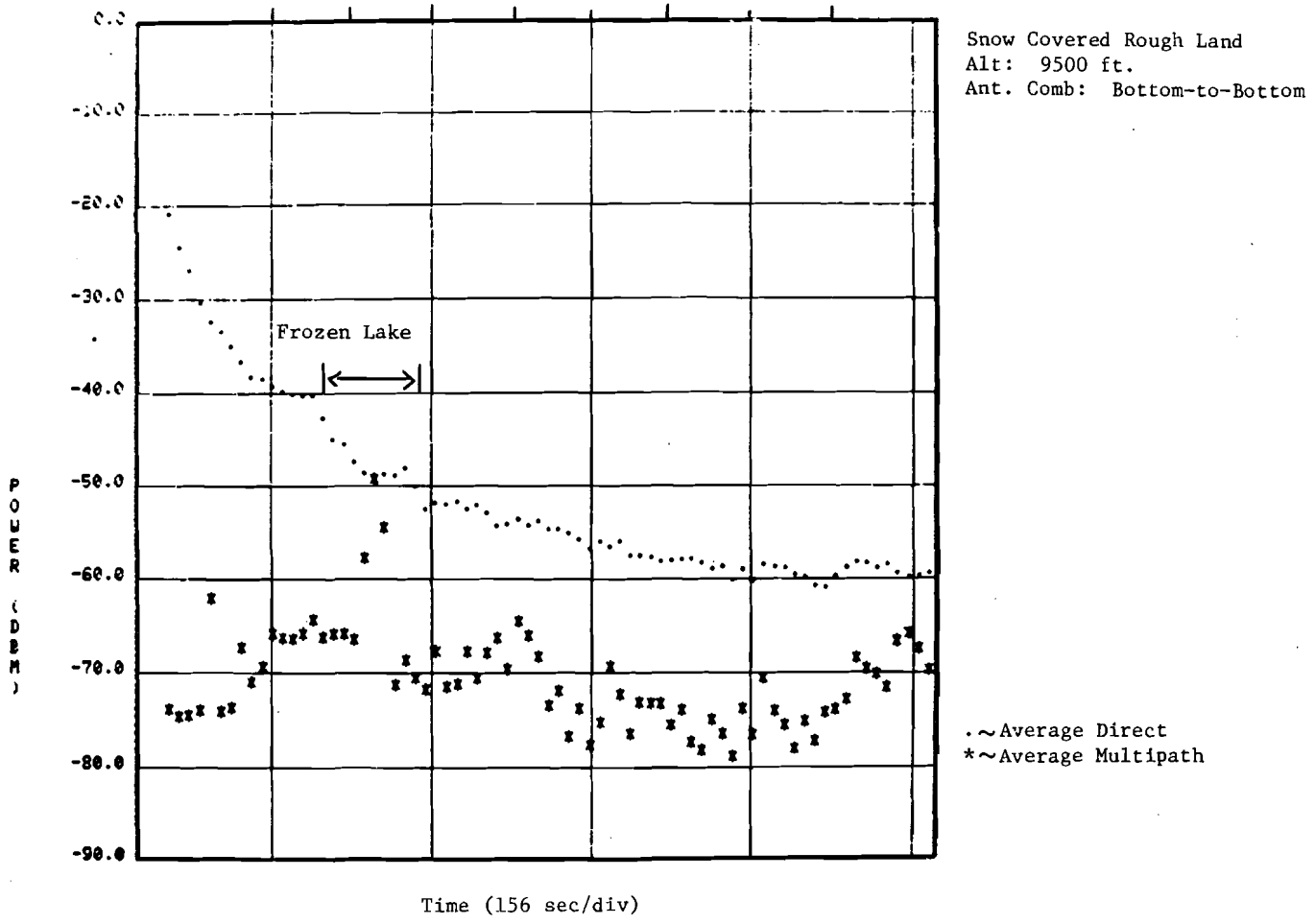


Fig. 5.37. Snow Covered Rough Land Multipath Average Signal Strength.

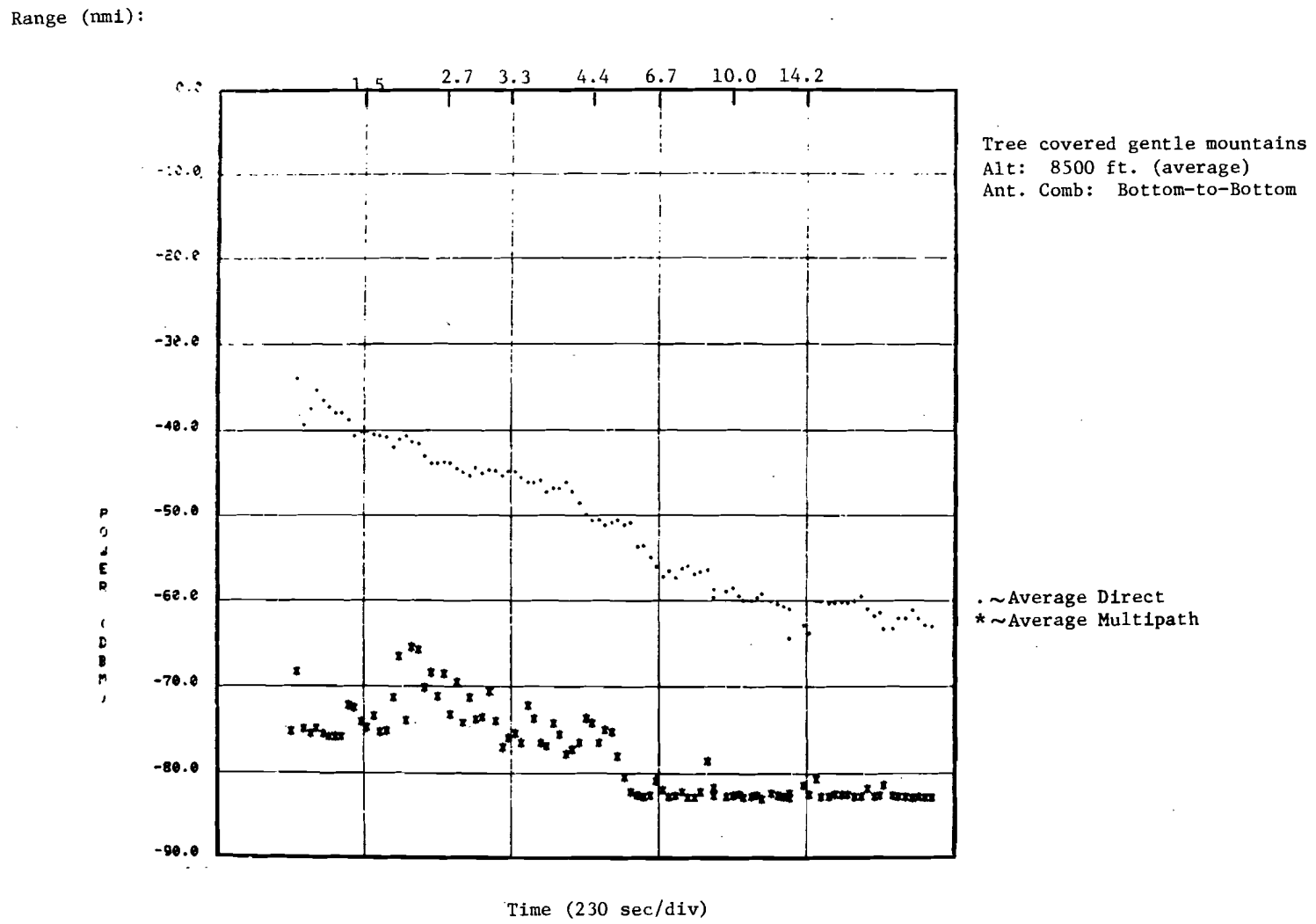


Fig. 5.38. Forested Mountain Multipath Average Signal Strength.

## 5.7 Banking Over Ocean Surface

In order to investigate the sensitivity of the various antenna combinations to banking maneuvers, a flight was conducted over an ocean surface in a Sea State 2 condition. The aircraft followed a roughly parallel flight path with a nominal separation of three nautical miles at an altitude of 5000 feet. During the flight the receiving aircraft continuously banked alternately $30^{\circ}$ away from the transmitting aircraft (indicated by $-30^{\circ}$ in Fig. 5.39 then $30^{\circ}$ toward the transmitting aircraft (indicated by $+30^{\circ}$). Fig. 5.39 shows average signal strength curves for each antenna combination for a portion of the flight.

Multipath received on the bottom antenna experienced small variations as the aircraft banked while multipath received on the top antenna experienced large variations in signal power. Direct signals received on the top antenna experienced smaller signal strength variations than those received on the bottom antenna. Direct and multipath signals were out of phase on the top-to-bottom link while they were in phase on the bottom-to-top link. Even though the aircraft were at a high grazing angle it is evident that banking degraded the SMR improvement of the top-to-bottom link when banking toward each other. The bottom-to-top link also suffered a slight degradation in SMR improvement from the level flight condition since banking away from each other evidently tended to shield the top receiving antenna from the direct signals while allowing slightly more exposure to the multipath signals. The top-to-top link continued to provide high SMR values at all bank angles.

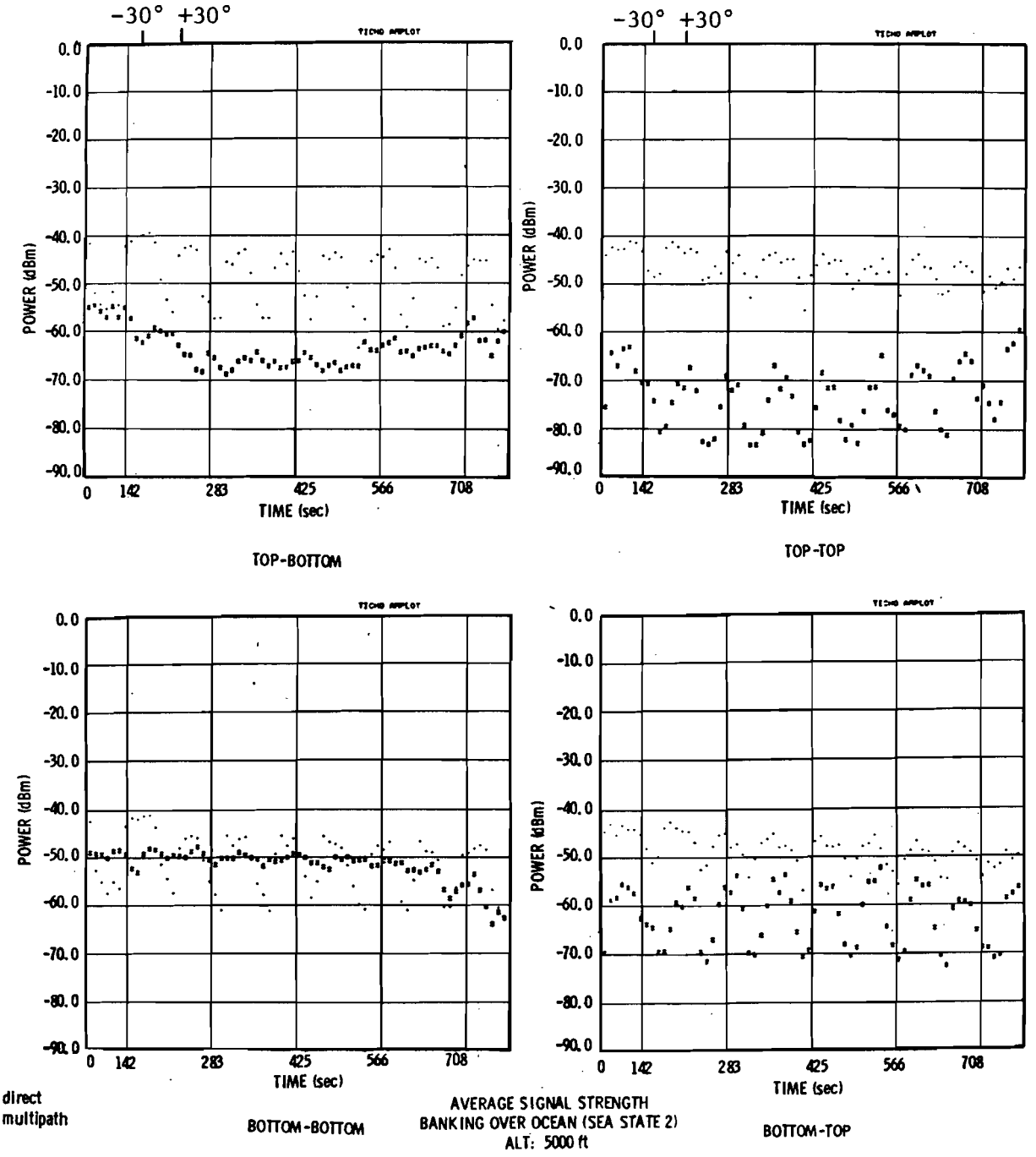


Fig. 5.39. Multipath Sensitivity to Banking.

Acknowledgment

A great many people who were involved in conducting the Air-to-Air Measurement Program have my appreciation for their cooperation. The successful completion of the operational aspects of the program was due in large part to the efforts of Everett A. Crocker and Joseph V. Gagnon. The insights and encouragement from William H. Harman and Jerry D. Welch throughout the project have also been greatly appreciated.

## REFERENCES


[1] G.V. Colby, "The Airborne Measurement Facility (AMF) System Description," "Project Report ATC-60, Lincoln Laboratory, M.I.T. (25 March 1976), FAA-RD-75-233.

[2] P. Beckmann and A. Spizzichino, "The Scattering of Electromagnetic Waves from Rough Surfaces," Pergamon Press Inc. NY 1963.

[3] K.J. Keeping and J.C. Sureau, "Scale Model Pattern Measurements of Aircraft L-Band Beacon Antennas," Project Report ATC-47, Lincoln Laboratory, M.I.T. (4 April 1975), FAA-RD-75-23.